Modeling Sea Ice as a Multiscale Composite Material

Kenneth M. Golden
Department of Mathematics
University of Utah

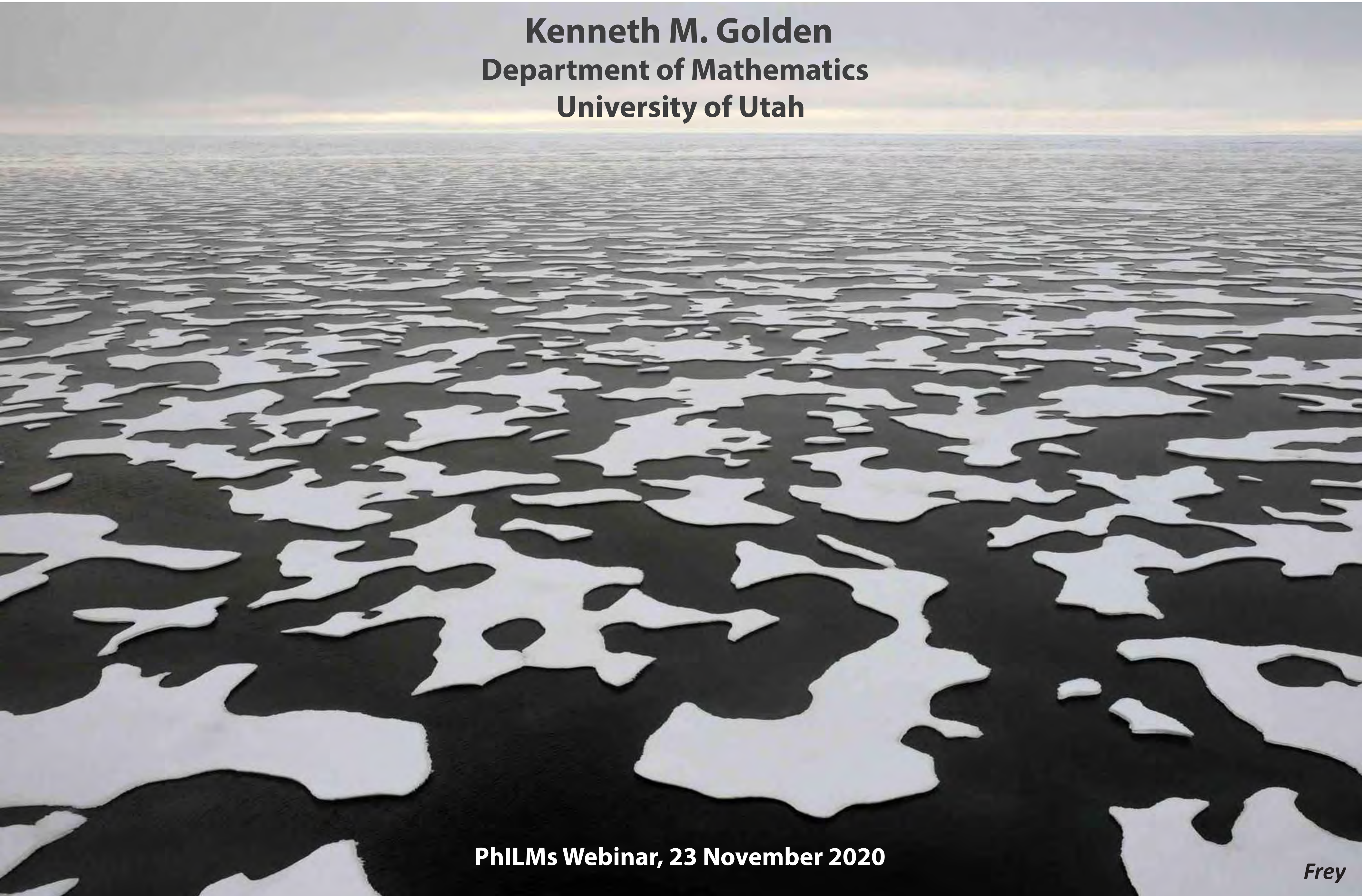

PhILMs Webinar, 23 November 2020

Frey

SEA ICE covers ~12% of Earth's ocean surface

- boundary between ocean and atmosphere
- mediates exchange of heat, gases, momentum
- global ocean circulation
- hosts rich ecosystem
- indicator of climate change

polar ice caps critical to global climate in reflecting incoming solar radiation

white snow and ice reflect

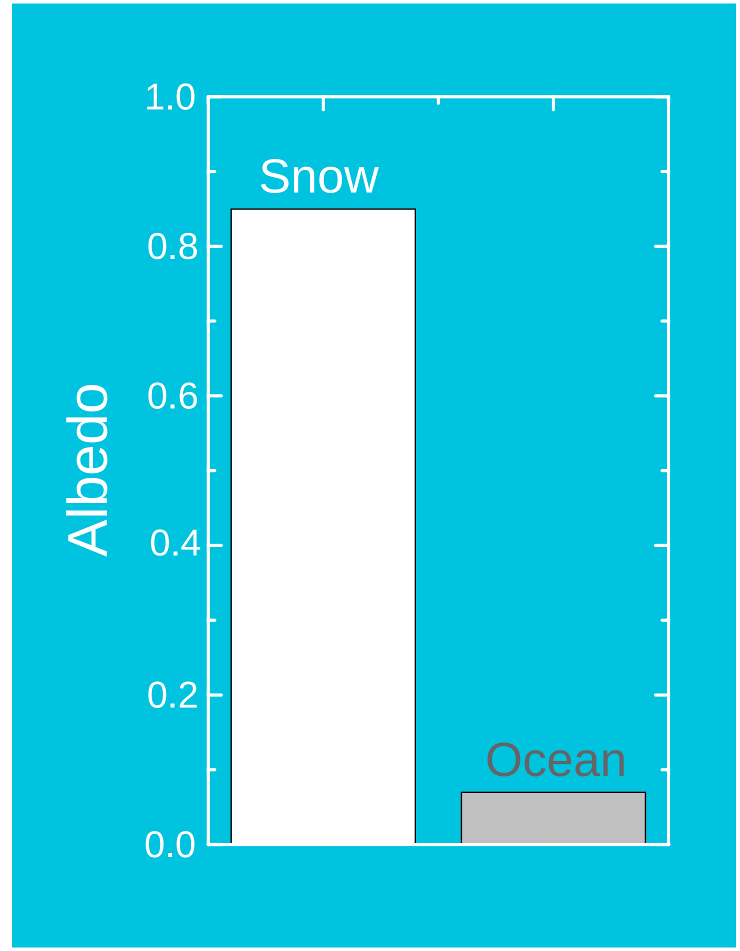

dark water and land absorb

$$\textbf{\textit{albedo}}\ \alpha = \frac{\text{reflected sunlight}}{\text{incident sunlight}}$$

the summer Arctic sea ice pack is melting

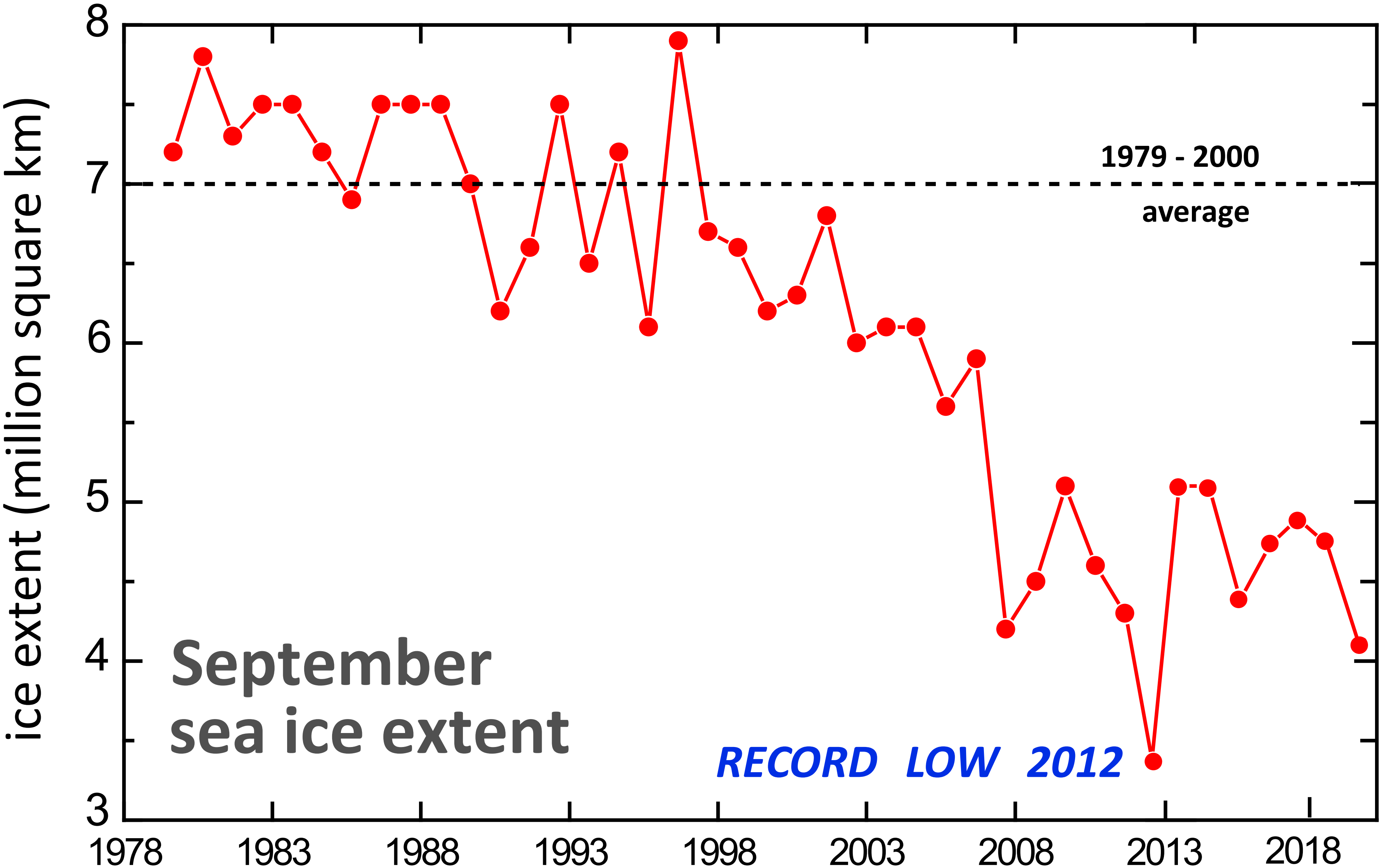

National Snow and Ice Data Center

Change in Arctic Sea Ice Extent

September 1980 -- 7.8 million km^2

September 2012 -- 3.4 million km^2

recent losses in comparison to the United States

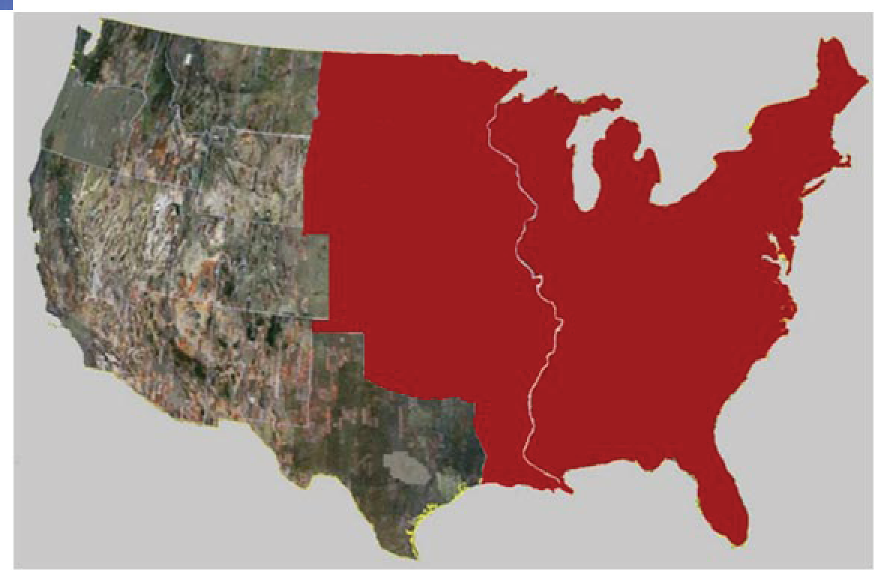

Perovich

Arctic sea ice decline: faster than predicted by climate models

Stroeve et al., GRL, 2007
Stroeve et al., GRL, 2012

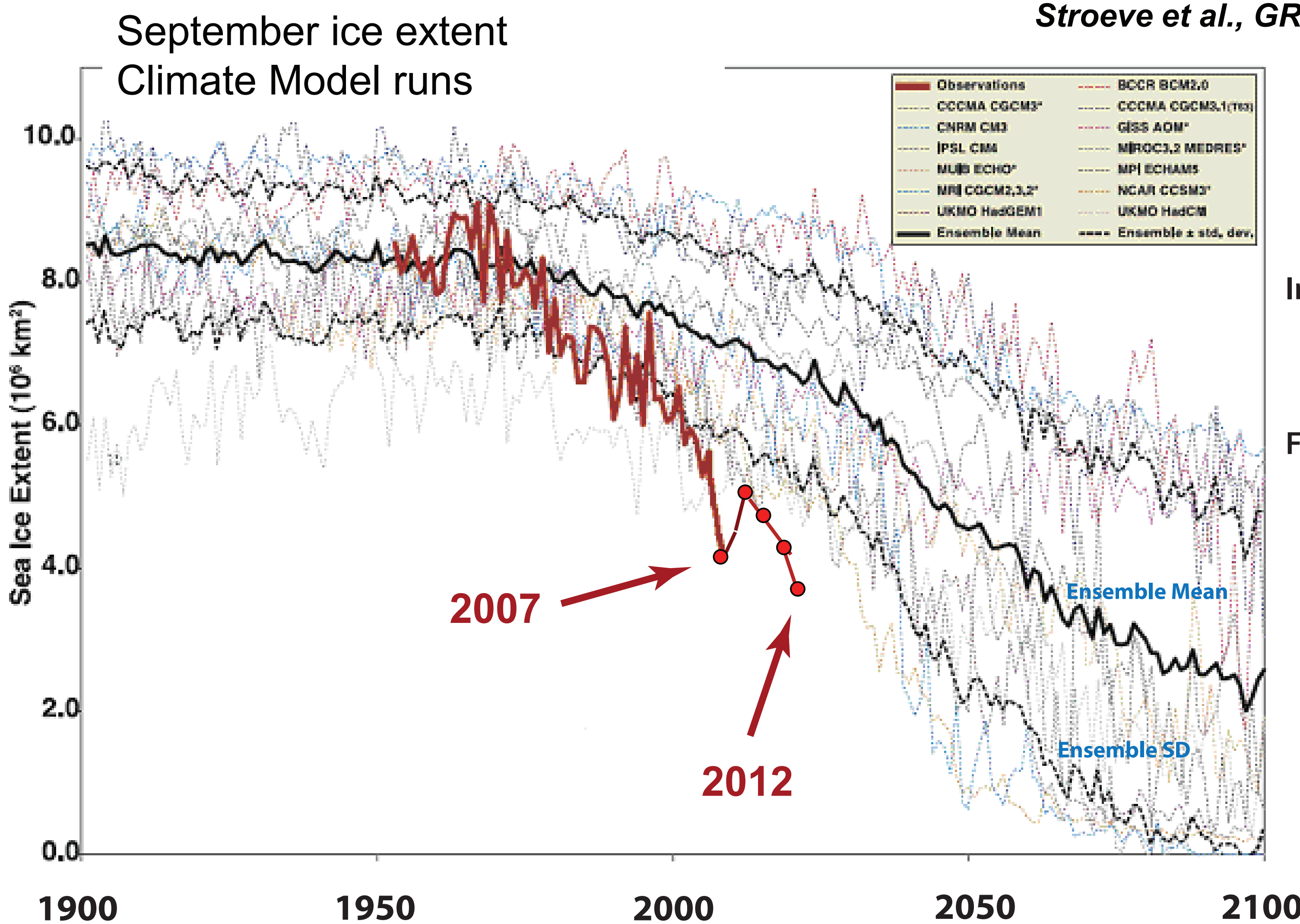

IPCC AR4 Models

Intergovernmental Panel on Climate Change (IPCC)

Fourth Assessment AR4, 2007

challenge

represent sea ice more realistically in climate models

account for key processes

such as melt pond evolution

How do patterns of dark and light evolve?

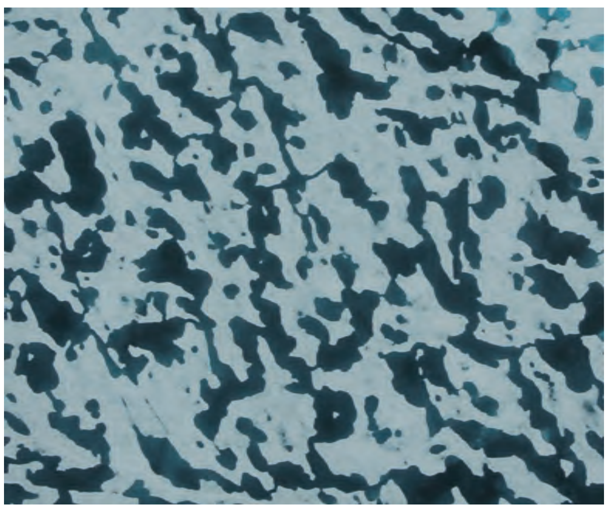

Impact of melt ponds on Arctic sea ice simulations from 1990 to 2007

Flocco, Schroeder, Feltham, Hunke, JGR Oceans 2012

For simulations with ponds September ice volume is nearly 40% lower.

... and other sub-grid scale structures and processes

linkage of scales

Sea Ice is a Multiscale Composite Material

sea ice microstructure

brine inclusions

Weeks & Assur 1969

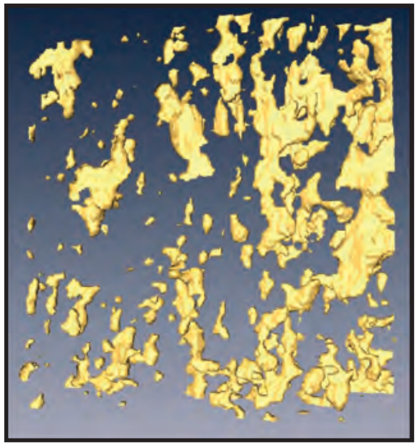

H. Eicken

Golden *et al. GRL* 2007

polycrystals

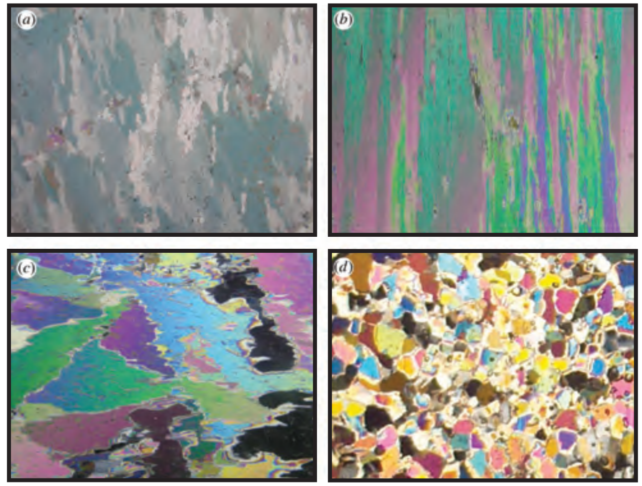

Gully *et al. Proc. Roy. Soc. A* 2015

brine channels

D. Cole

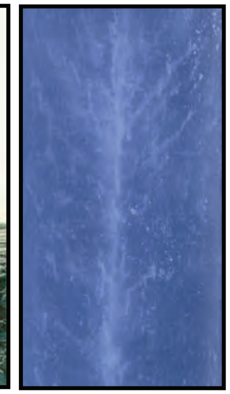

K. Golden

millimeters

centimeters

---

sea ice mesostructure

Arctic melt ponds

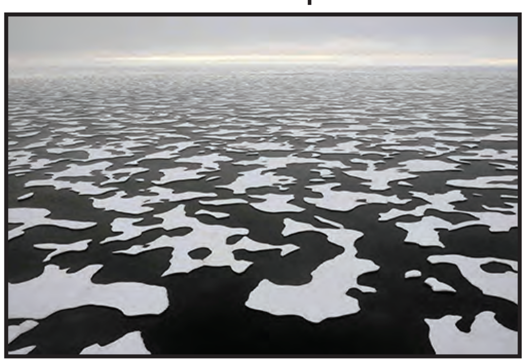

K. Frey

Antarctic pressure ridges

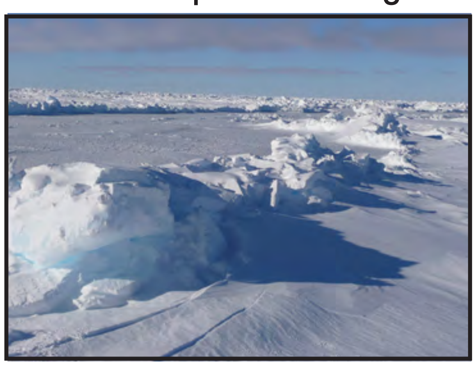

K. Golden

sea ice macrostructure

sea ice floes

J. Weller

sea ice pack

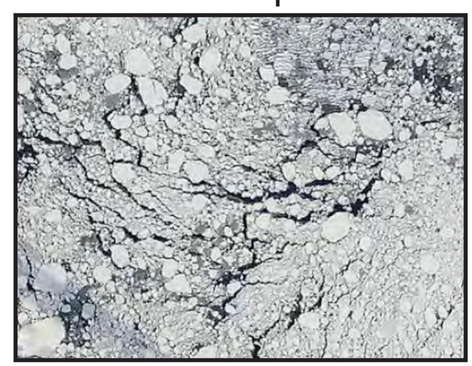

NASA

meters

kilometers

HOMOGENIZATION for Composite Materials

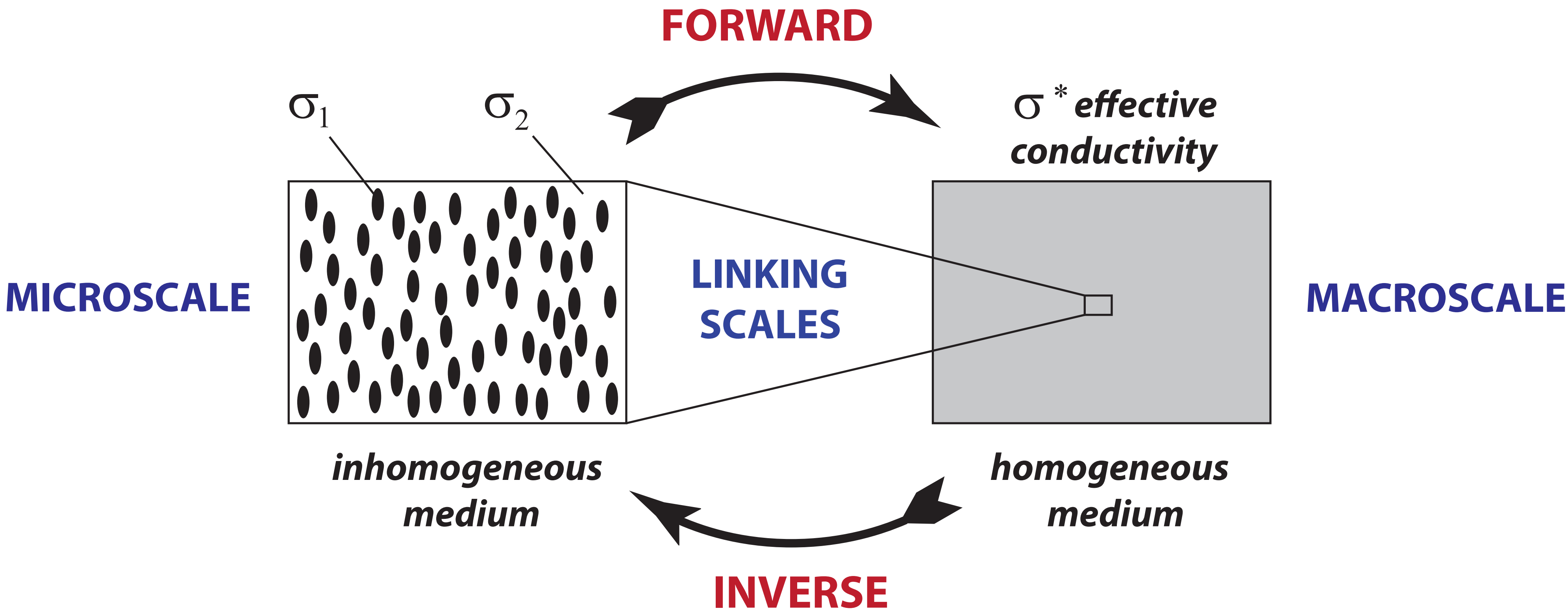

Maxwell 1873 : effective conductivity of a dilute suspension of spheres
Einstein 1906 : effective viscosity of a dilute suspension of rigid spheres in a fluid

*Wiener 1912 : arithmetic and harmonic mean **bounds** on effective conductivity*
*Hashin and Shtrikman 1962 : variational **bounds** on effective conductivity*

widespread use of composites in late 20th century due in large part to advances in mathematically predicting their effective properties

What is this talk about? homogenization for multiscale composites

the role of "microstructure" in determining sea ice effective properties

Using methods of **homogenization and statistical physics** to LINK SCALES in the sea ice system ... compute effective behavior on scales relevant to coarse-grained sea ice and climate models, process studies, ...

MICROSCALE: brine + polycrystalline structure; EM and fluid transport

MESOSCALE: advection diffusion, thermal transport, waves, melt ponds

MACROSCALE: ice transport, MIZ width and location, low order models

A tour of Stieltjes integrals in the study of sea ice and its role in climate.

Solving problems in physics of sea ice drives advances in theory of composite materials.

cross - pollination

bone, stealthy coatings
magnets, rat brains, RMT

How do scales interact in the sea ice system?

NASA

basin scale - grid scale albedo

Linking Scales

km scale melt ponds

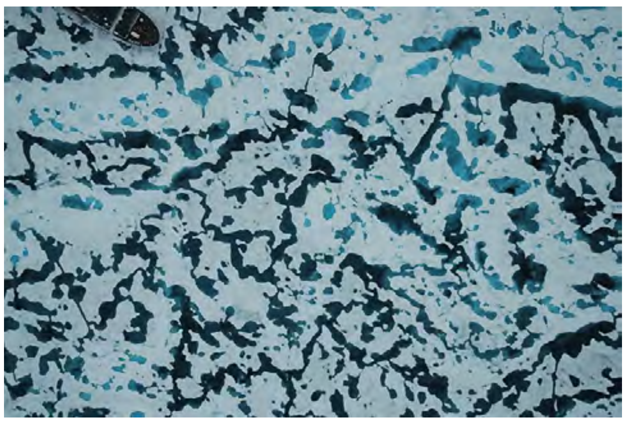

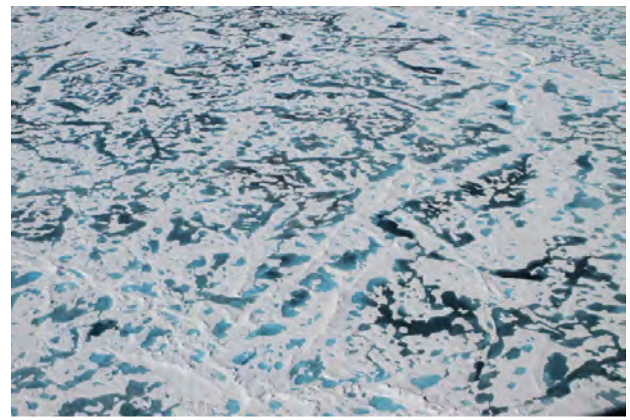

Perovich

km scale melt ponds

Linking Scales

mm scale brine inclusions

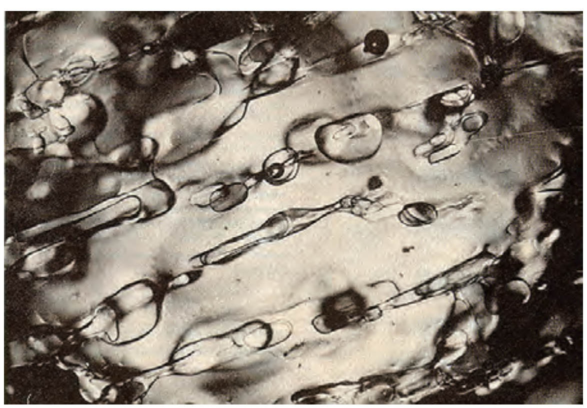

meter scale snow topography

sea ice microphysics

fluid transport

fluid flow through the porous microstructure of sea ice governs key processes in polar climate and ecosystems

evolution of Arctic melt ponds and sea ice albedo

nutrient flux for algal communities

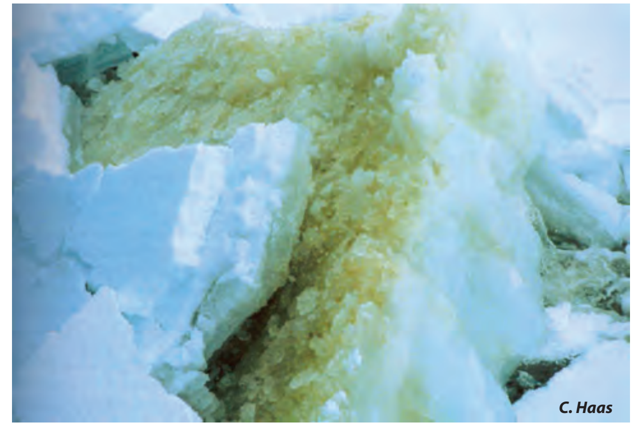

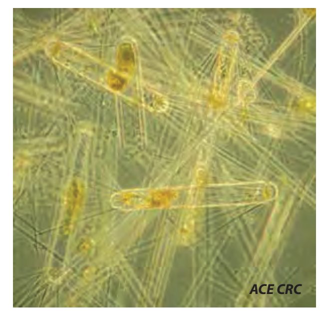

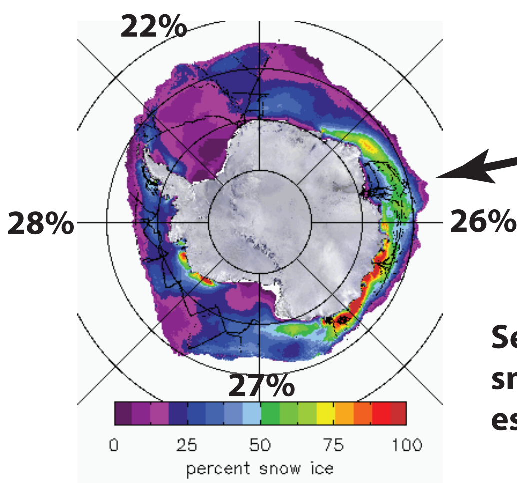

T. Maksym and T. Markus, 2008

September snow-ice estimates

Antarctic surface flooding and snow-ice formation

- evolution of salinity profiles

- ocean-ice-air exchanges of heat, CO_2

fluid permeability of a porous medium

how much water gets through the sample per unit time?

Darcy's Law

for slow viscous flow in a porous medium

averaged fluid velocity

pressure gradient

$$\mathbf{v} = -\frac{\mathbf{k}}{\eta} \nabla p$$

viscosity

$\mathbf{k}$ = fluid permeability tensor

HOMOGENIZATION

mathematics for analyzing effective behavior of heterogeneous systems

brine volume fraction and ***connectivity*** increase with temperature

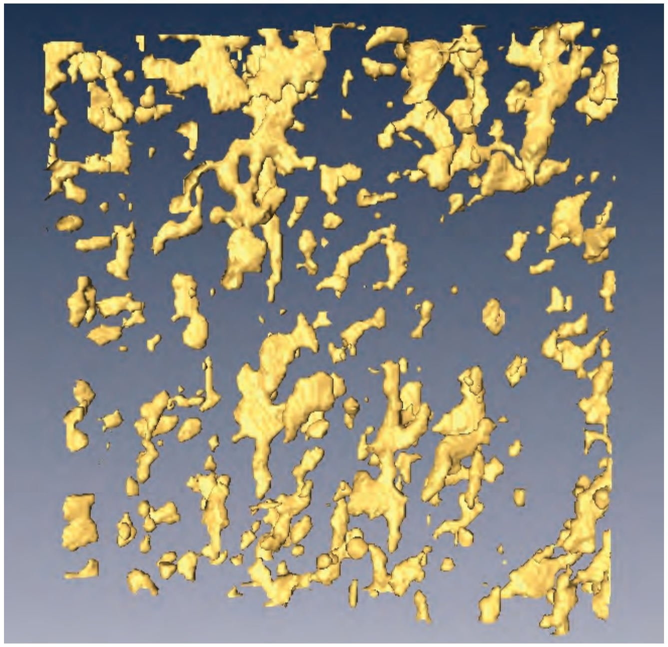

$T = -15\,^\circ\mathrm{C}$, $\phi = 0.033$

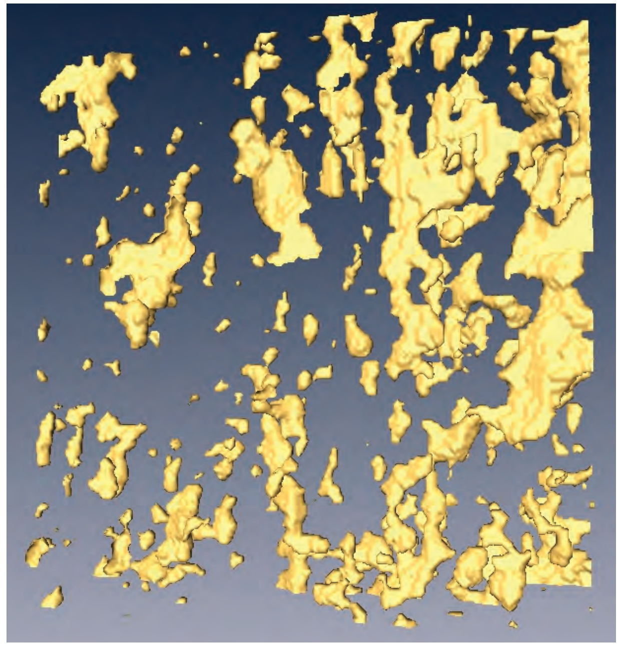

$T = -6\,^\circ\mathrm{C}$, $\phi = 0.075$

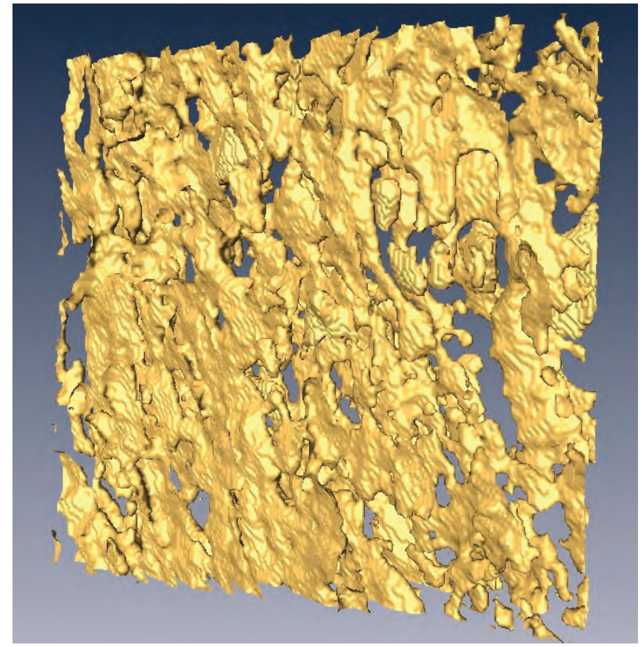

$T = -3\,^\circ\mathrm{C}$, $\phi = 0.143$

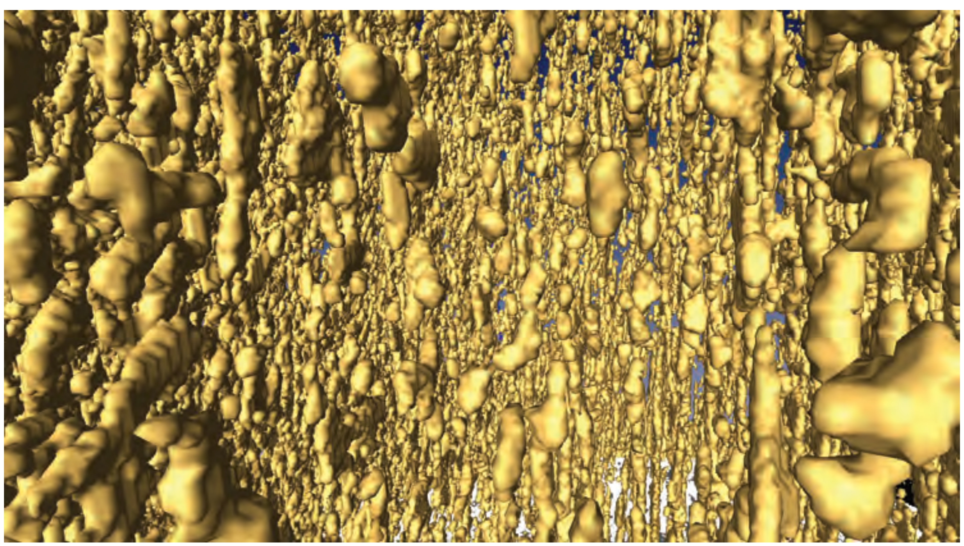

$T = -8\,^\circ\mathrm{C}$, $\phi = 0.057$

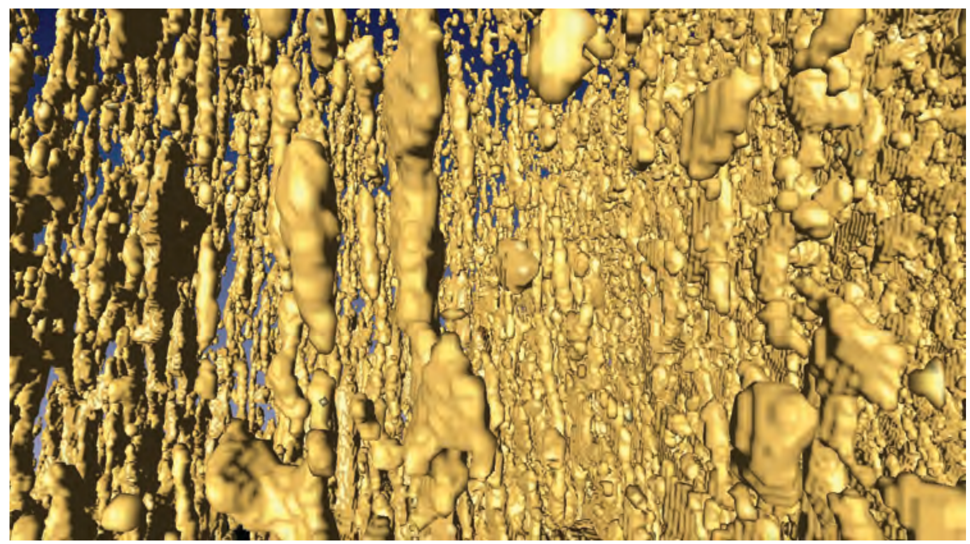

$T = -4\,^\circ\mathrm{C}$, $\phi = 0.113$

X-ray tomography for brine in sea ice

Golden *et al.*, *Geophysical Research Letters*, 2007

Critical behavior of fluid transport in sea ice

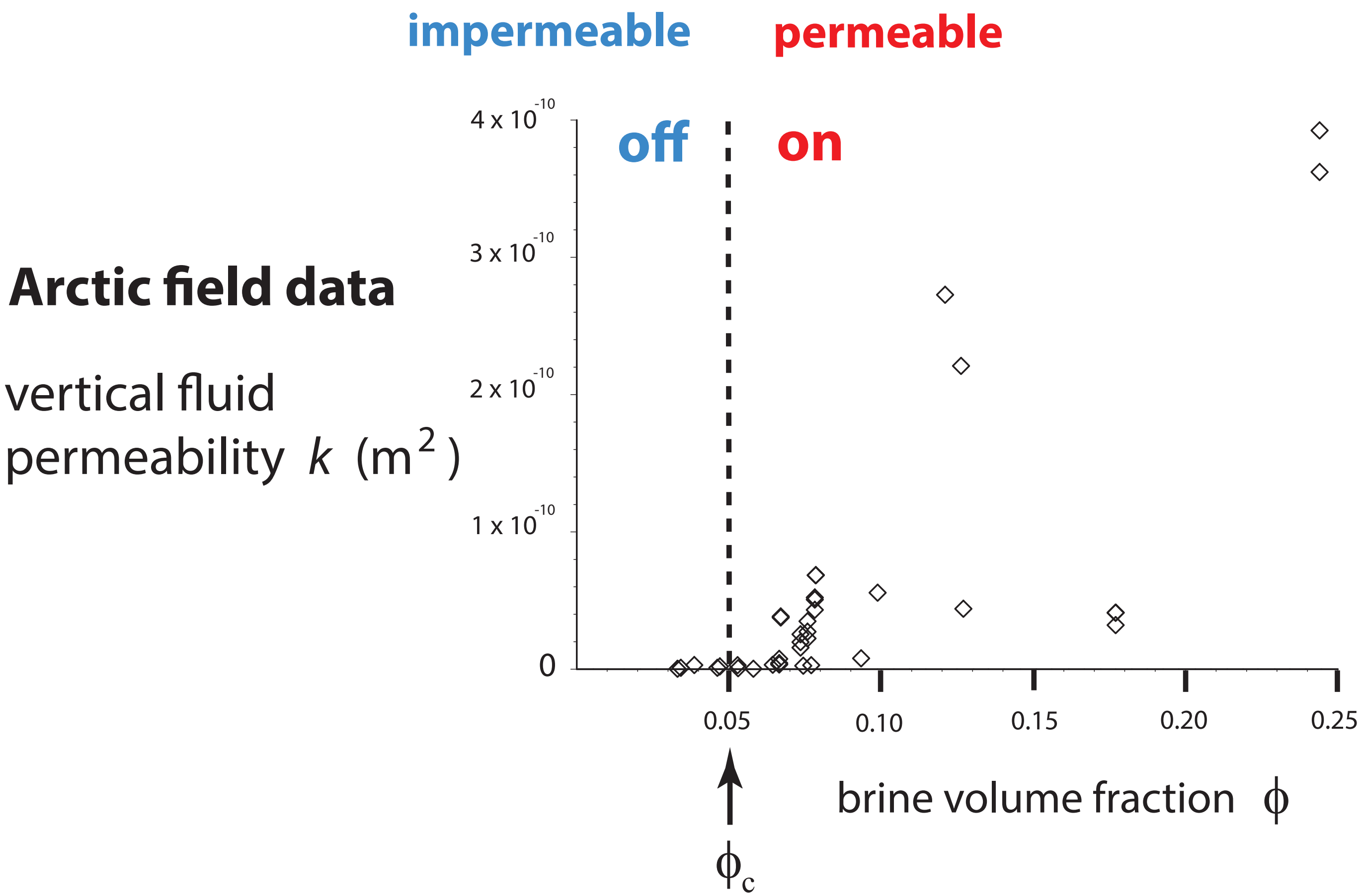

"on - off" switch for fluid flow

critical brine volume fraction $\phi_c \approx 5\% \longleftrightarrow T_c \approx -5^\circ$C, $S \approx 5$ ppt

RULE OF FIVES

Golden, Ackley, Lytle Science 1998
Golden, Eicken, Heaton, Miner, Pringle, Zhu GRL 2007
Pringle, Miner, Eicken, Golden J. Geophys. Res. 2009

percolation theory

probabilistic theory of connectedness

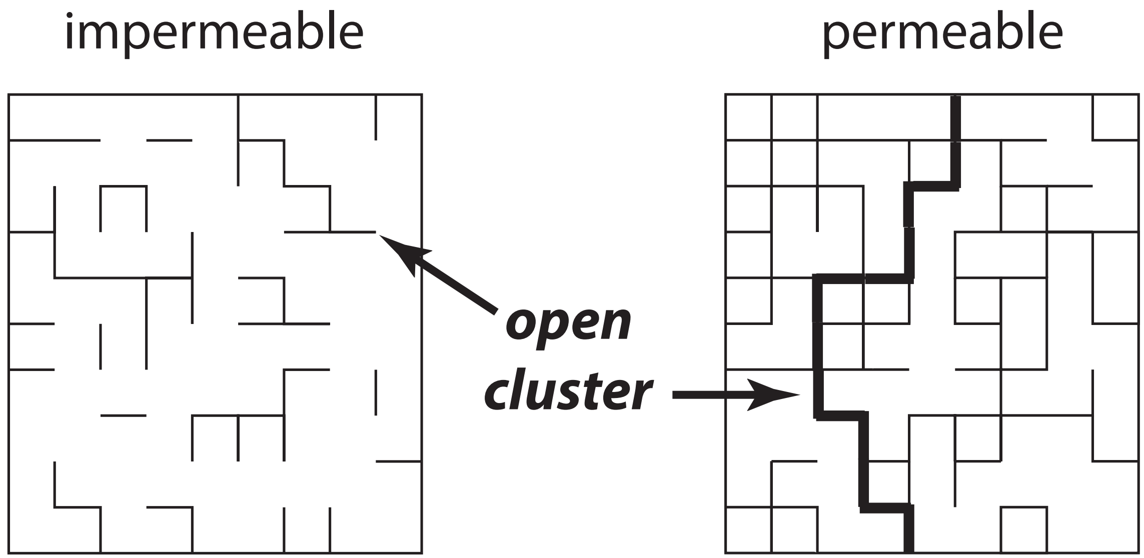

$p = 1/3$ $p = 2/3$

bond → *open* with probability p
closed with probability $1\text{-}p$

percolation threshold

$$p_c = 1/2 \quad \text{for} \quad d = 2$$

smallest *p* for which there is an infinite open cluster

Continuum percolation model for ***stealthy*** materials applied to sea ice microstructure explains **Rule of Fives** and Antarctic data on ice production and algal growth

$\phi_c \approx 5\ \%$ Golden, Ackley, Lytle, *Science*, 1998

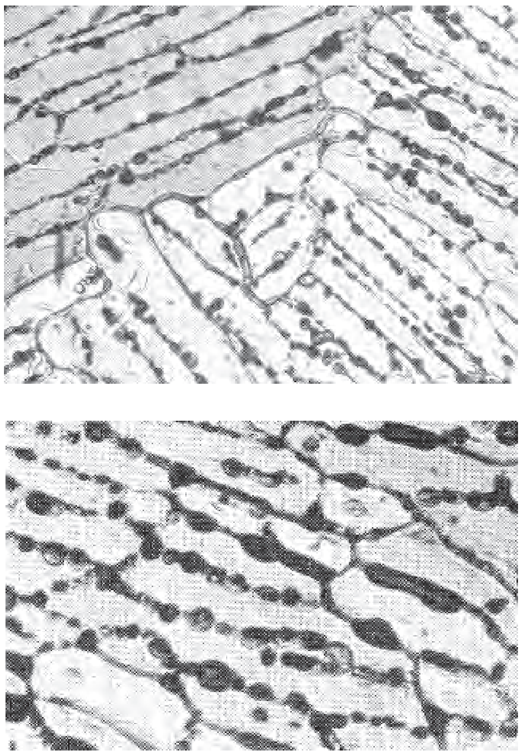

sea ice

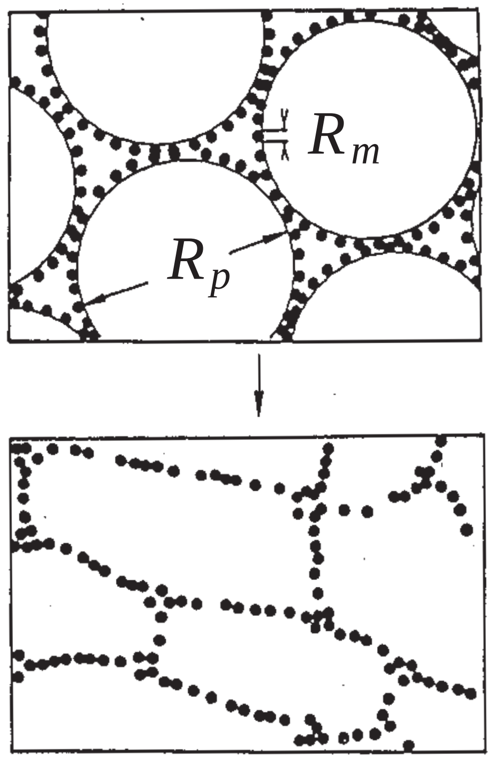

compressed powder

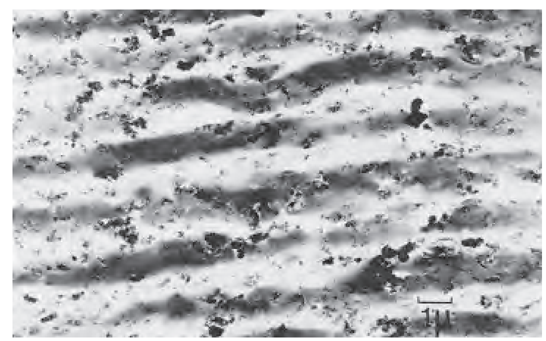

radar absorbing composite

sea ice is radar absorbing

Thermal evolution of permeability and microstructure in sea ice

Golden, Eicken, Heaton, Miner, Pringle, Zhu, Geophysical Research Letters 2007

micro-scale

controls

macro-scale

processes

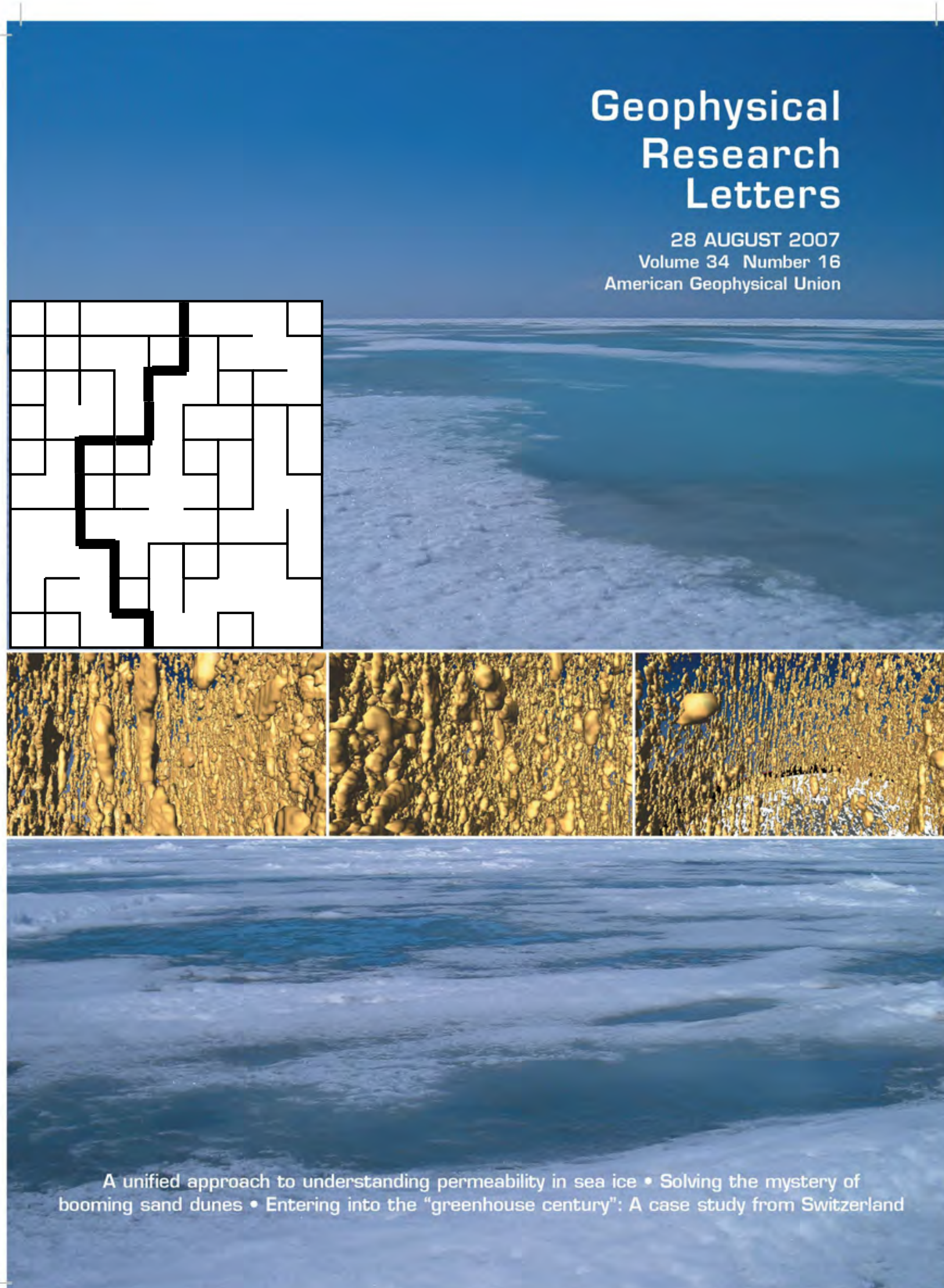

percolation theory

$$k(\phi) = k_0 (\phi - 0.05)^2$$

critical exponent t

$$k_0 = 3 \times 10^{-8} \text{ m}^2$$

hierarchical model
network model
rigorous bounds

agree closely with
field data

X-ray tomography for brine inclusions

unprecedented look at thermal evolution of brine phase and its connectivity

confirms rule of fives

Pringle, Miner, Eicken, Golden
J. Geophys. Res. 2009

Sea ice algae secrete extracellular polymeric substances (EPS) affecting evolution of brine microstructure.

How does EPS affect fluid transport?

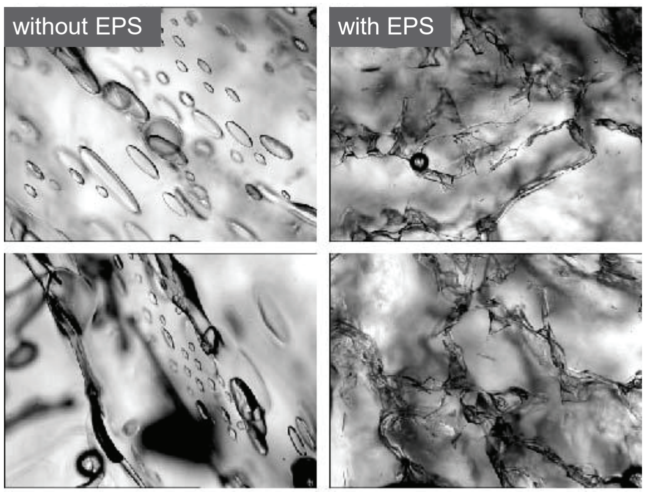

Krembs, Eicken, Deming, PNAS 2011

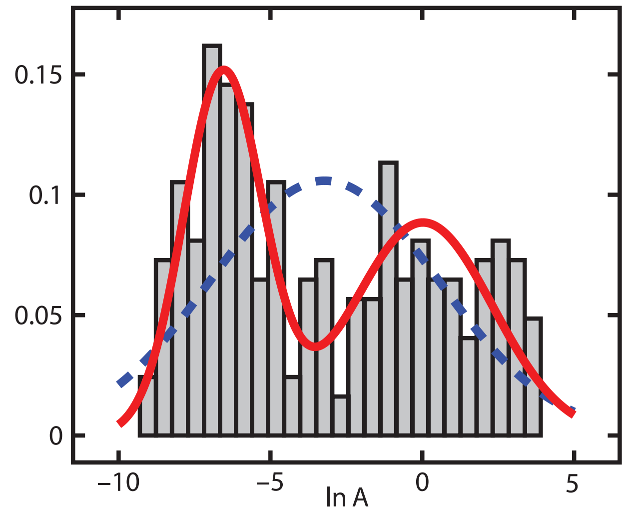

RANDOM PIPE MODEL

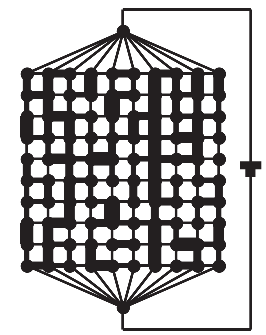

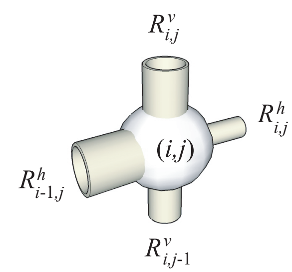

Zhu, Jabini, Golden, Eicken, Morris
Ann. Glac. 2006

- **Bimodal** lognormal distribution for brine inclusions
- Develop random pipe network model with bimodal distribution; Use numerical methods that can handle larger variances in sizes.
- Results predict observed drop in fluid permeability *k*.
- **Rigorous bound on *k* for bimodal distribution of pore sizes**

Steffen, Epshteyn, Zhu, Bowler, Deming, Golden
Multiscale Modeling and Simulation, 2018

How does the biology affect the physics?

photo by Jan Lieser

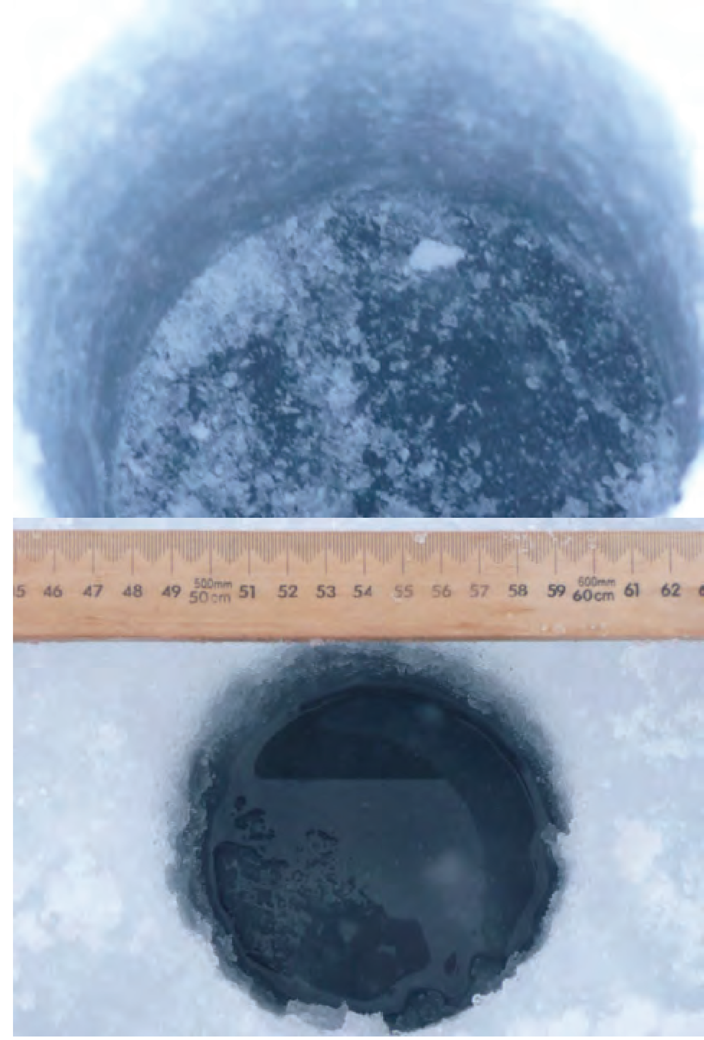

measuring fluid permeability of Antarctic sea ice

SIPEX 2007

The Melt Pond Conundrum:

How can ponds form on top of sea ice that is highly permeable?

C. Polashenski, K. M. Golden, D. K. Perovich, E. Skyllingstad, A. Arnsten, C. Stwertka, N. Wright

Percolation Blockage: A Process that Enables Melt Pond Formation on First Year Arctic Sea Ice

J. Geophys. Res. Oceans 2017

2014 Study of Under Ice Blooms in the Chuckchi Ecosystem (SUBICE) aboard USCGC Healy

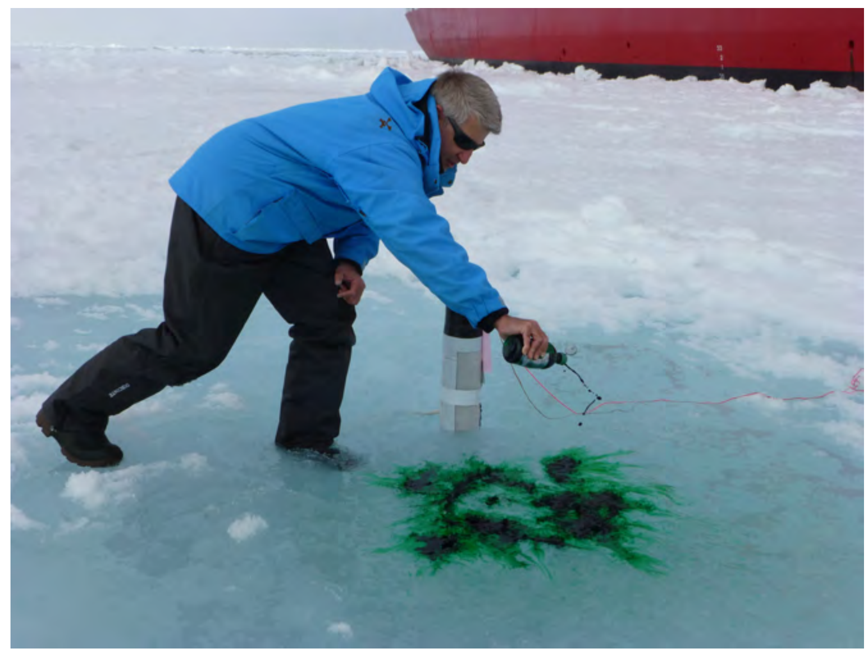

Remote sensing of sea ice

INVERSE PROBLEM

Recover sea ice properties from electromagnetic (EM) data

ε^*

effective complex permittivity
(dielectric constant, conductivity)

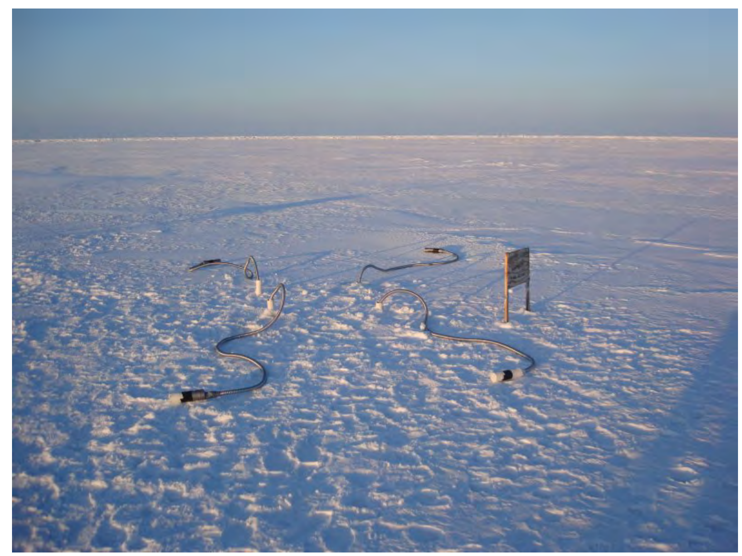

sea ice thickness
ice concentration

brine volume fraction
brine inclusion connectivity

Effective complex permittivity of a two phase composite in the quasistatic (long wavelength) limit

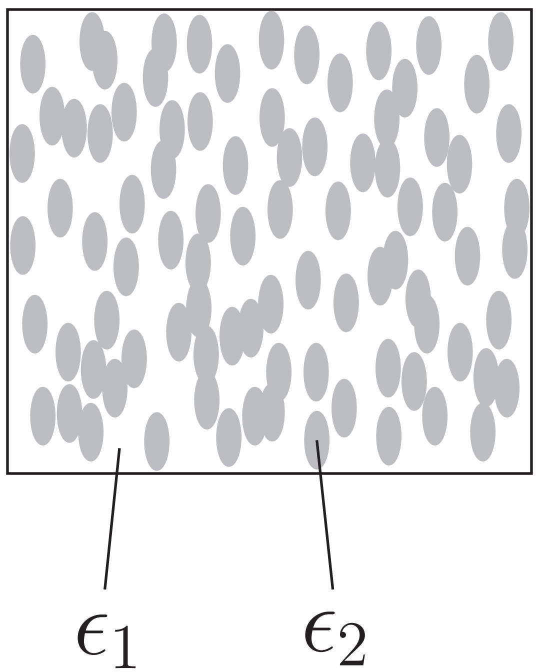

$$\epsilon^*$$

$$D = \epsilon E$$

$$\nabla \cdot D = 0$$

$$\nabla \times E = 0$$

$$\langle D \rangle = \epsilon^* \langle E \rangle$$

p_1 , p_2 = volume fractions of the components

$$\epsilon^* = \epsilon^* \left(\frac{\epsilon_1}{\epsilon_2} \, , \text{composite geometry} \right)$$

What are the effective propagation characteristics of an EM wave (radar, microwaves) in the medium?

Analytic Continuation Method for Homogenization

Bergman (1978), Milton (1979), Golden and Papanicolaou (1983), Theory of Composites, Milton (2002)

Stieltjes integral representation for homogenized parameter

separates geometry from parameters

geometry

$$F(s) = 1 - \frac{\epsilon^*}{\epsilon_2} = \int_0^1 \frac{d\mu(z)}{s - z} \qquad s = \frac{1}{1 - \epsilon_1/\epsilon_2}$$

material parameters

μ

- spectral measure of self adjoint operator $\Gamma\chi$
- mass $= p_1$
- higher moments depend on n-point correlations

$$\Gamma = \nabla(-\Delta)^{-1}\nabla\cdot$$

$\chi =$ characteristic function of the brine phase

$$E = s\,(s + \Gamma\chi)^{-1} e_k$$

$\Gamma\chi$: microscale $\longrightarrow$ macroscale

$\Gamma\chi$ *links scales*

Golden and Papanicolaou, Comm. Math. Phys. 1983

forward and inverse bounds on the complex permittivity of sea ice

forward bounds

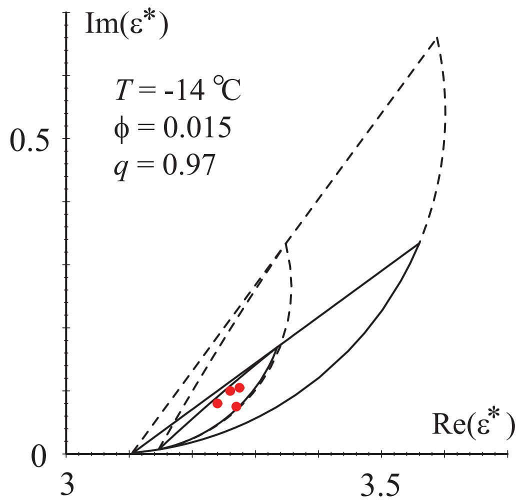

4.75 GHz data

matrix particle

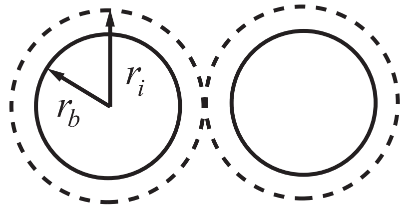

$$q = r_b \,/\, r_i$$

$$0 < q < 1$$

Golden 1995, 1997

inverse bounds

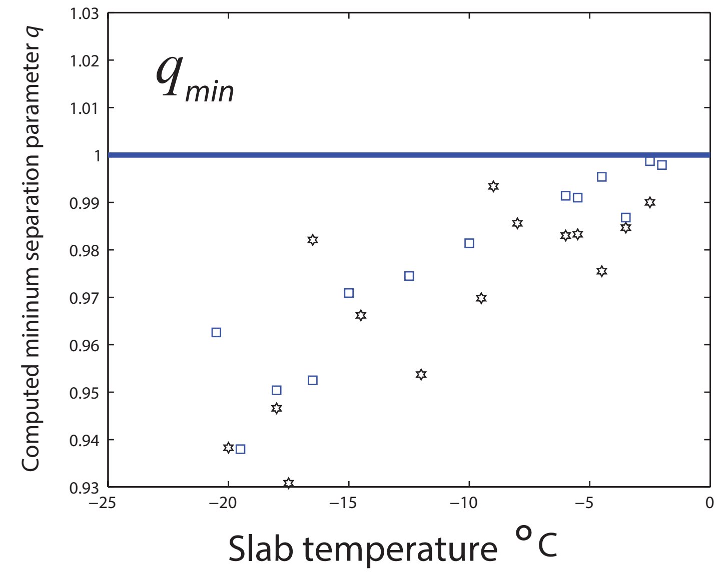

Inverse Homogenization

Cherkaev and Golden (1998), Day and Thorpe (1999), Cherkaev (2001), McPhedran, McKenzie, Milton (1982), *Theory of Composites*, Milton (2002)

ε^* $\longrightarrow$ ***composite geometry*** **(spectral measure μ)**

inverse bounds and recovery of brine porosity

Gully, Backstrom, Eicken, Golden
Physica B, 2007

inversion for brine inclusion separations in sea ice from measurements of effective complex permittivity ε^*

rigorous inverse bound on spectral gap

construct algebraic curves which bound admissible region in (p,q)-space

Orum, Cherkaev, Golden
Proc. Roy. Soc. A, 2012

SEA ICE **HUMAN BONE**

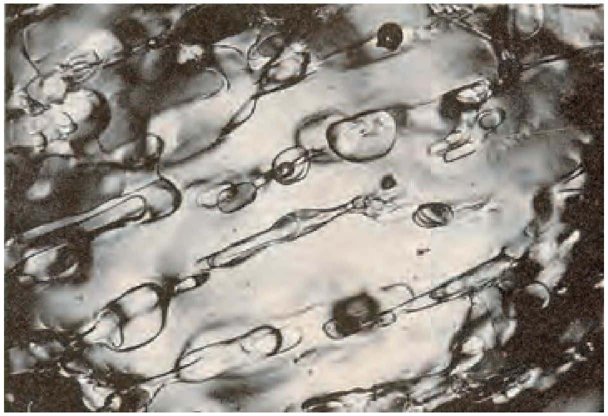

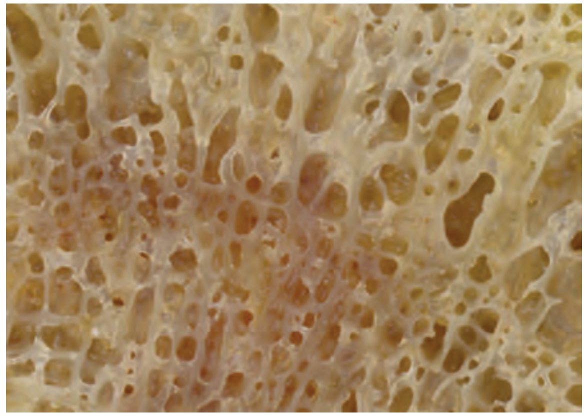

spectral characterization of porous microstructures in human bone

young healthy trabecular bone

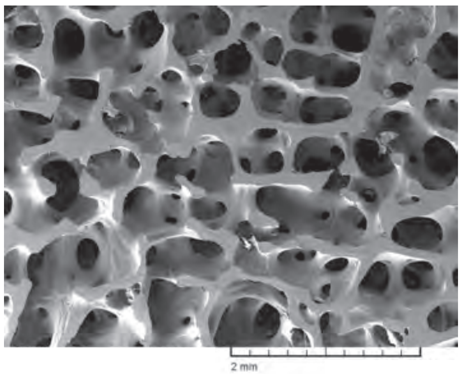

old osteoporotic trabecular bone

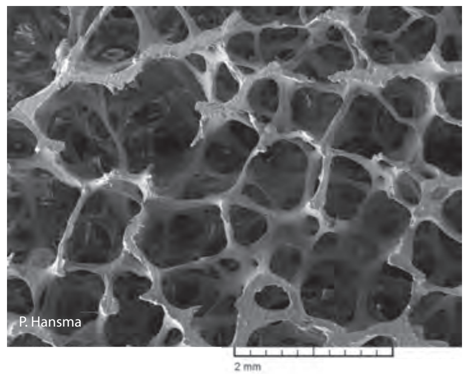

reconstruct spectral measures from complex permittivity data

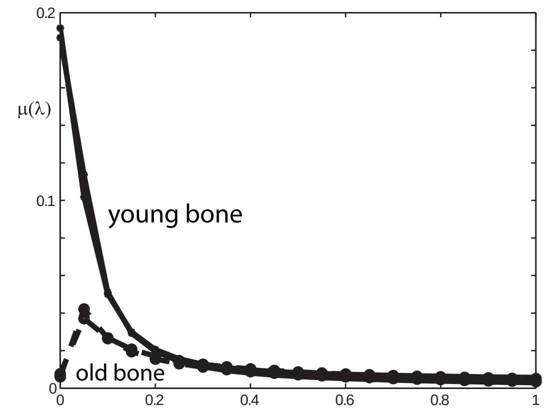

use regularized inversion scheme

apply spectral measure analysis of brine connectivity and spectral inversion to electromagnetic monitoring of osteoporosis

Golden, Murphy, Cherkaev, J. Biomechanics 2011

the math doesn't care if it's sea ice or bone!

direct calculation of spectral measures

Murphy, Hohenegger, Cherkaev, Golden, *Comm. Math. Sci.* 2015

- depends only on the composite geometry
- discretization of microstructural image gives binary network
- fundamental operator becomes a random matrix
- spectral measure computed from eigenvalues and eigenvectors

once we have the spectral measure μ it can be used in Stieltjes integrals for other transport coefficients:

electrical and thermal conductivity, complex permittivity, magnetic permeability, diffusion, fluid flow properties

earlier studies of spectral measures

Day and Thorpe 1996
Helsing, McPhedran, Milton 2011

Spectral statistics for 2D random resistor network

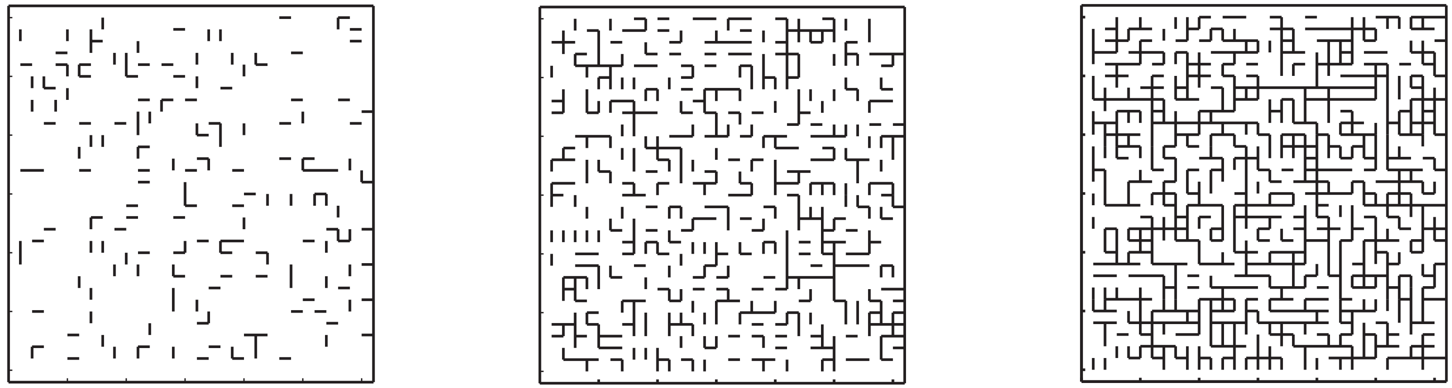

Spectral Measures

Murphy and Golden, *J. Math. Phys.*, 2012
Murphy et al. *Comm. Math. Sci.*, 2015

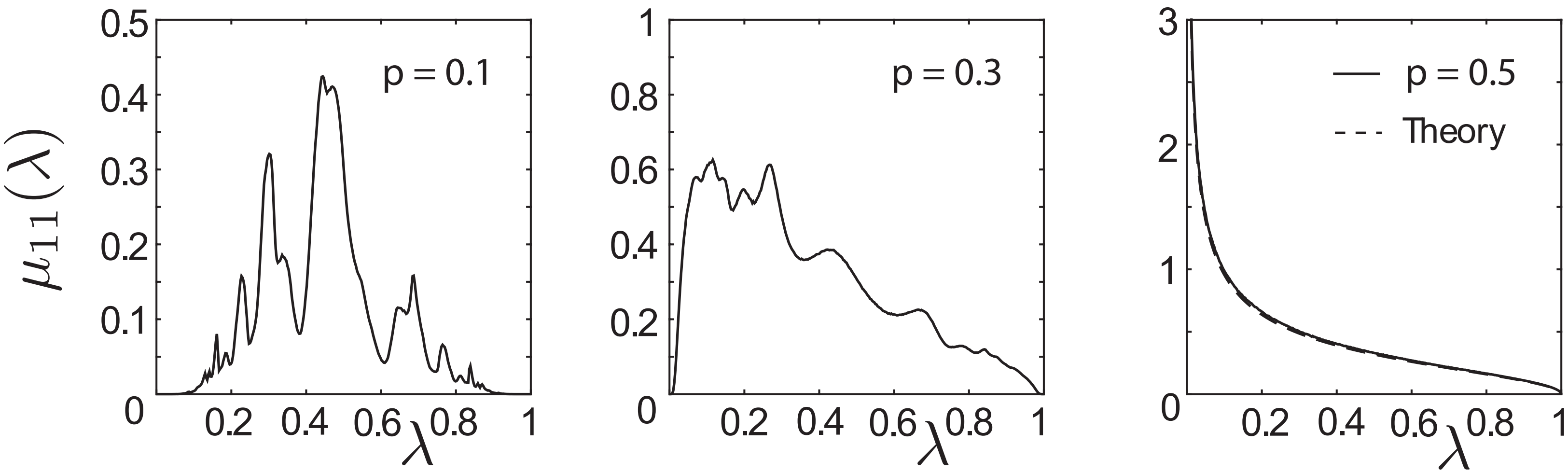

$p_c = 0.5$

Eigenvalue Spacing Distributions

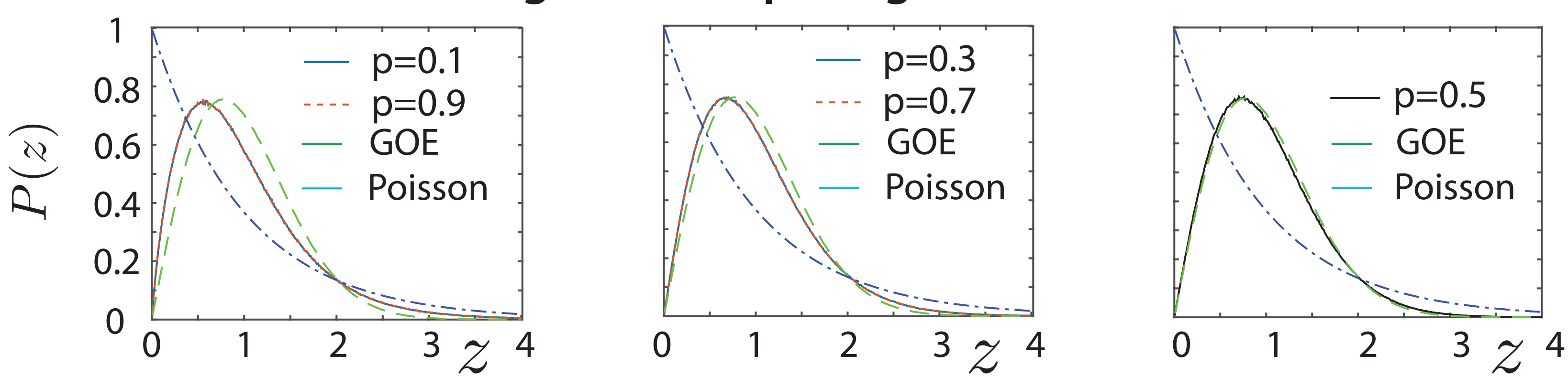

Murphy, Cherkaev, Golden, *PRL*, 2017

Eigenvalue Statistics of Random Matrix Theory

Wigner (1951) and Dyson (1953) first used random matrix theory (RMT) to describe quantized energy levels of heavy atomic nuclei.

$[\mathbf{N}]_{ij} \sim N(0,1),\qquad \mathbf{A} = (\mathbf{N}+\mathbf{N}^T)/2$ ***Gaussian orthogonal ensemble (GOE)***

$[\mathbf{N}]_{ij} \sim N(0,1)+iN(0,1),\qquad \mathbf{A} = (\mathbf{N}+\mathbf{N}^\dagger)/2$ ***Gaussian unitary ensemble (GUE)***

Short range and long range correlations of eigenvalues are measured by various eigenvalue statistics.

Spacing distributions of energy levels for heavy atomic nuclei

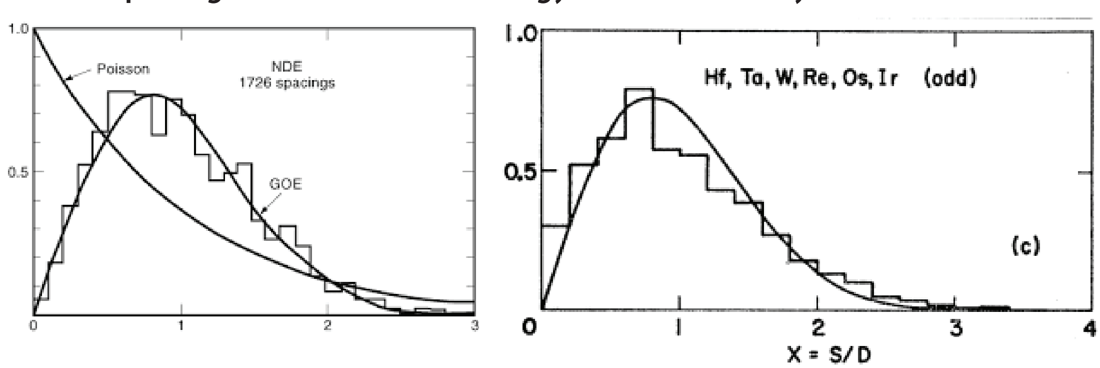

Spacing distributions of the first billion zeros of the Riemann zeta function

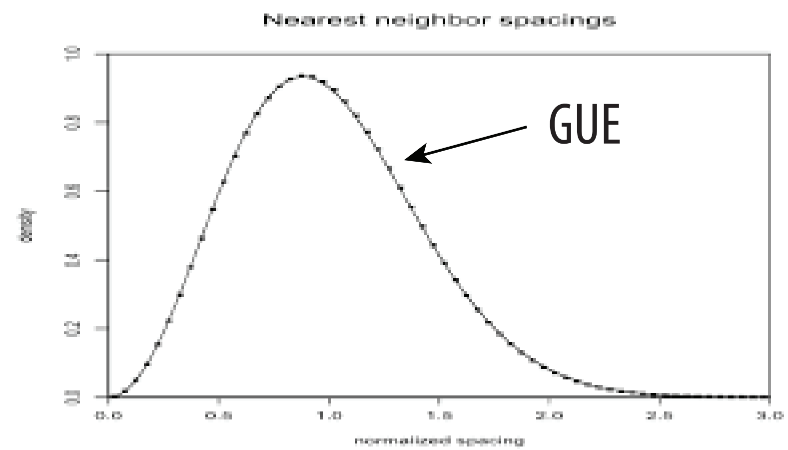

RMT used to characterize disorder-driven transitions in mesoscopic conductors, neural networks, random graph theory, etc.

Universal eigenvalue statistics arise in a broad range of "unrelated" problems!

Spectral computations for sea ice floe configurations

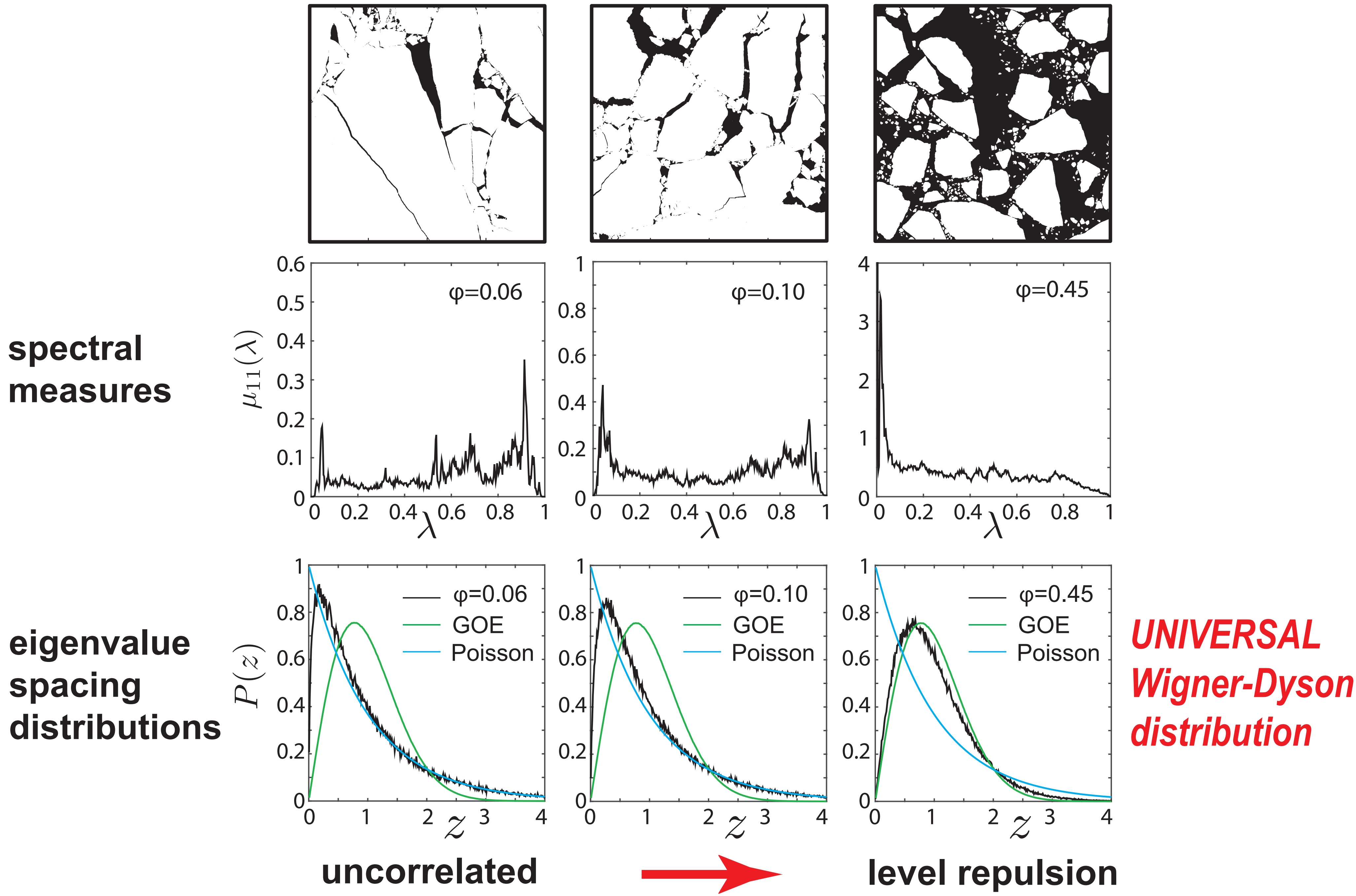

ANDERSON TRANSITION

Murphy, Cherkaev, Golden
Phys. Rev. Lett. 2017

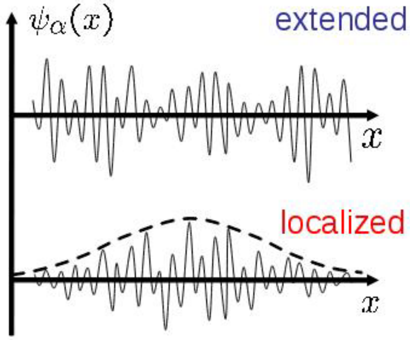

metal / insulator transition

localization

Anderson 1958
Mott 1949
Shklovshii et al 1993
Evangelou 1992

Anderson transition in wave physics:
quantum, optics, acoustics, water waves, ...

from analysis of spectral measures for brine, melt ponds, ice floes

we find percolation-driven

Anderson transition for classical transport in composites

mobility edges, localization transition, universal spectral statistics

Murphy, Cherkaev, Golden Phys. Rev. Lett. 2017

Order to disorder in quasiperiodic materials

Morison, Murphy, Cherkaev, Golden 2020

Parameterized Moiré Pattern Creates Tunable Microgeometry

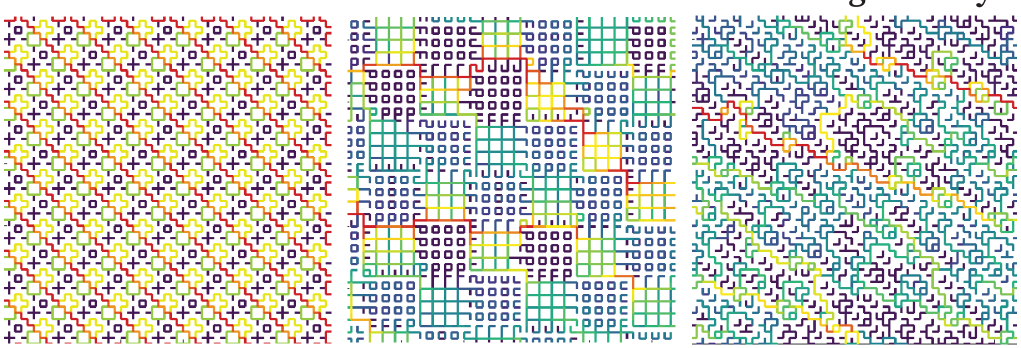

Anderson transition as QP is tuned

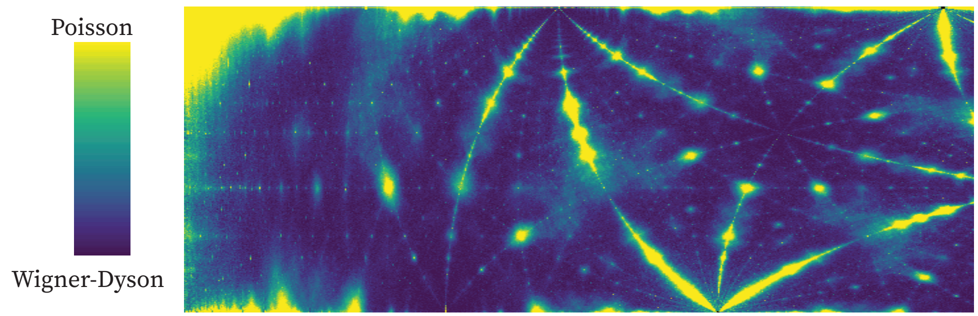

Homogenization for polycrystalline materials

Two-component composites

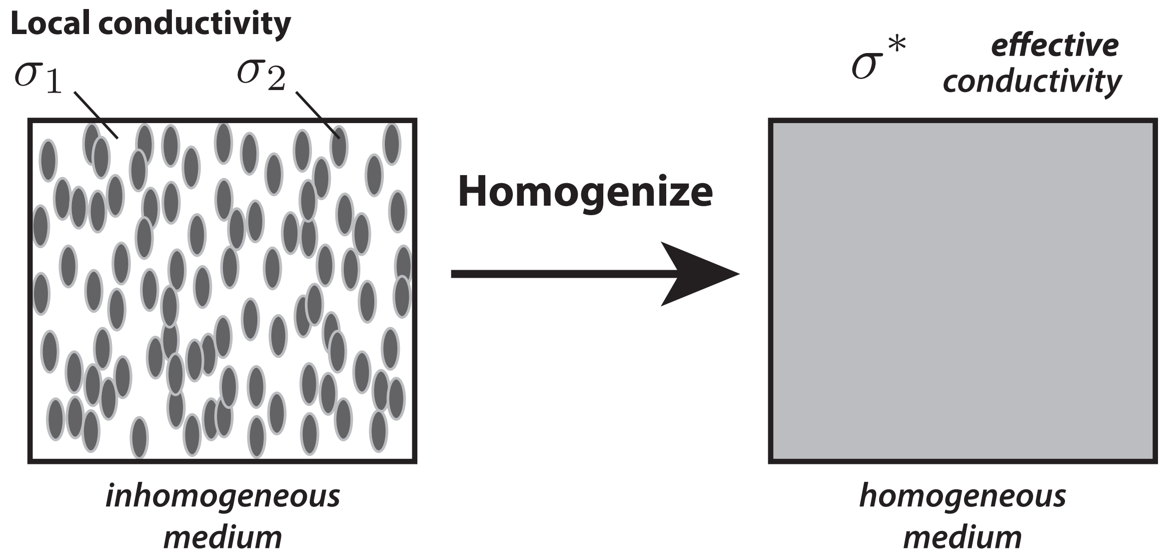

Find the homogeneous medium which behaves macroscopically the same as the inhomogeneous medium

Polycrystalline media

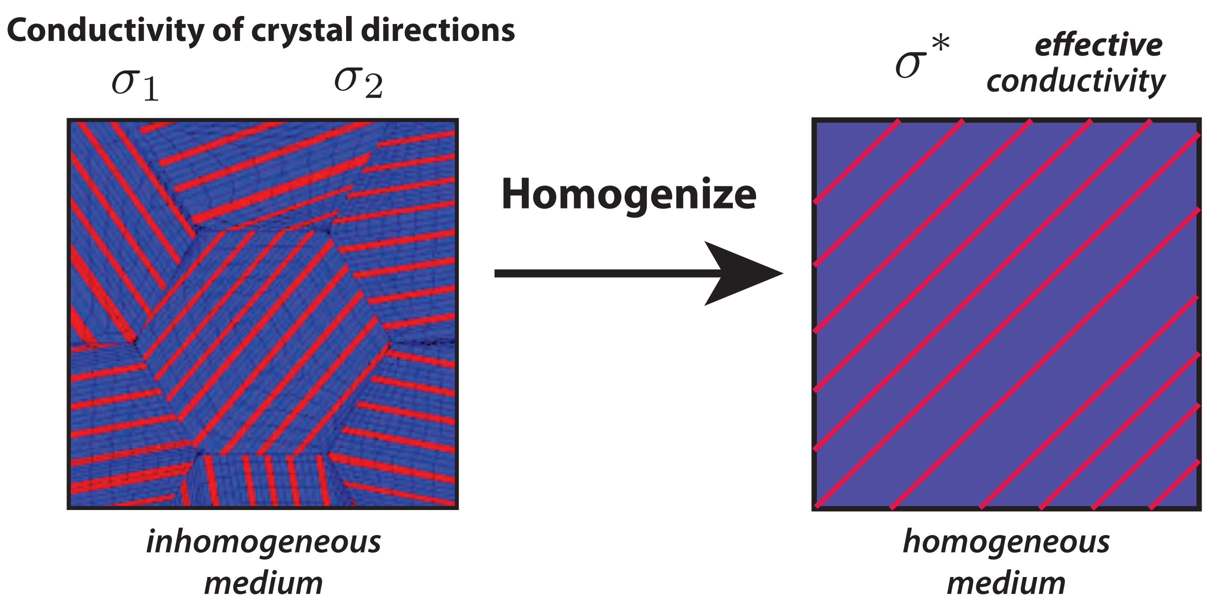

Bounds on the complex permittivity of polycrystalline materials by analytic continuation

Adam Gully, Joyce Lin,
Elena Cherkaev, Ken Golden

- **Stieltjes integral representation for effective complex permittivity**

  Milton (1981, 2002), Barabash and Stroud (1999), ...

- **Forward and inverse bounds**

  orientation statistics

- **Applied to sea ice using two-scale homogenization**

- **Inverse bounds give method for distinguishing ice types using remote sensing techniques**

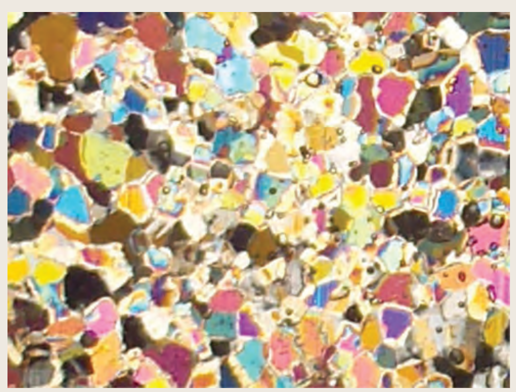

Proc. Roy. Soc. A 8 Feb 2015

Proc. R. Soc. A | Volume 471 | Issue 2174 | 8 February 2015

ISSN 1364-5021 | Volume 471 | Issue 2174 | 8 February 2015

PROCEEDINGS A

350 YEARS OF SCIENTIFIC PUBLISHING

An invited review commemorating 350 years of scientific publishing at the Royal Society

A method to distinguish between different types of sea ice using remote sensing techniques

A computer model to determine how a human should walk so as to expend the least energy

THE ROYAL SOCIETY PUBLISHING

21/01/15 1:47 PM

higher threshold for fluid flow in granular sea ice

microscale details impact "mesoscale" processes

nutrient fluxes for microbes
melt pond drainage
snow-ice formation

columnar | granular

5% | ***10%***

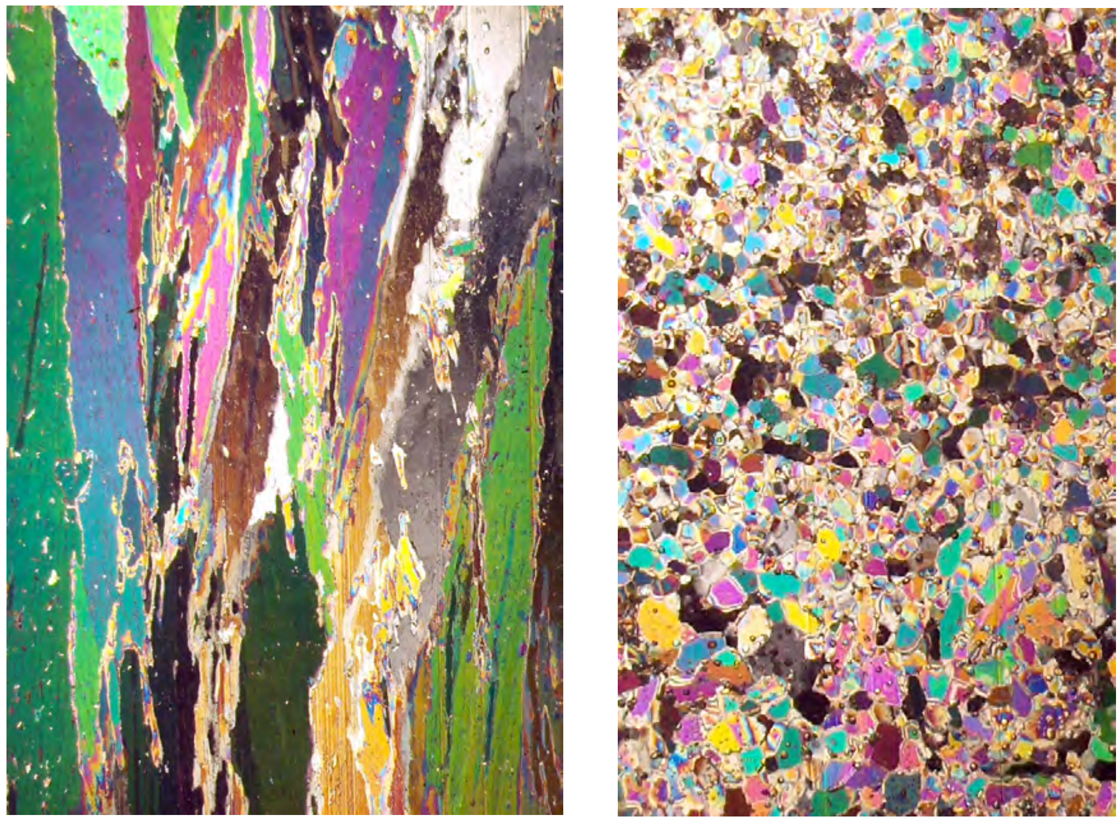

Golden, Sampson, Gully, Lubbers, Tison 2020

electromagnetically distinguishing ice types

Kitsel Lusted, Elena Cherkaev, Ken Golden

two scale homogenization for polycrystalline sea ice

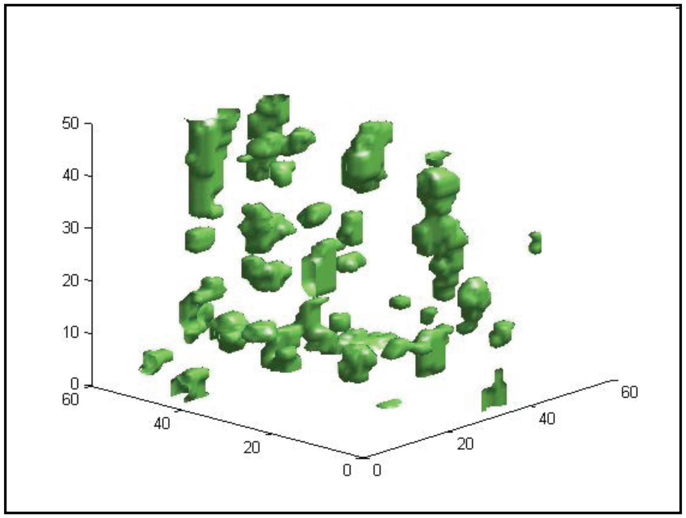

numerical homogenization
for single crystal

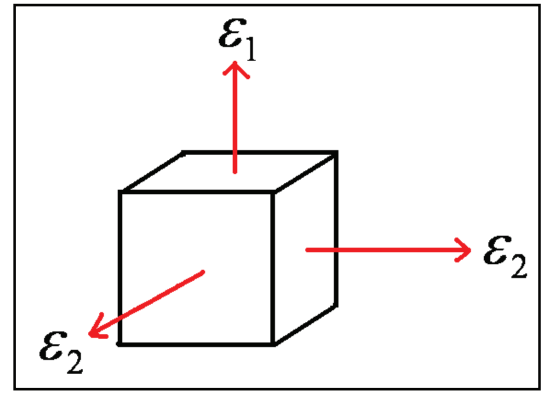

analytic continuation
for polycrystals

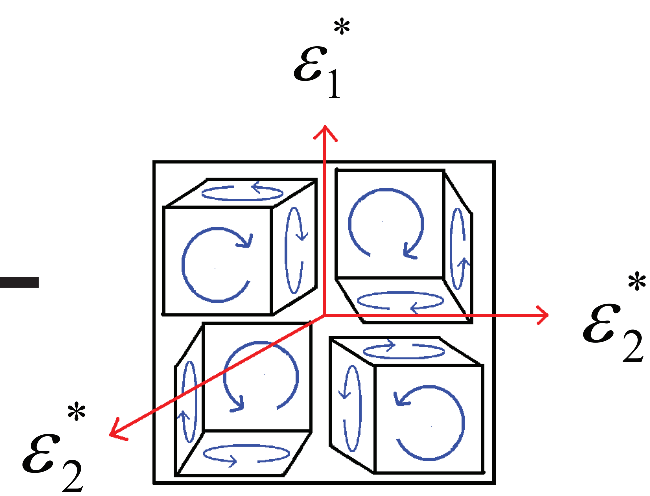

bounds

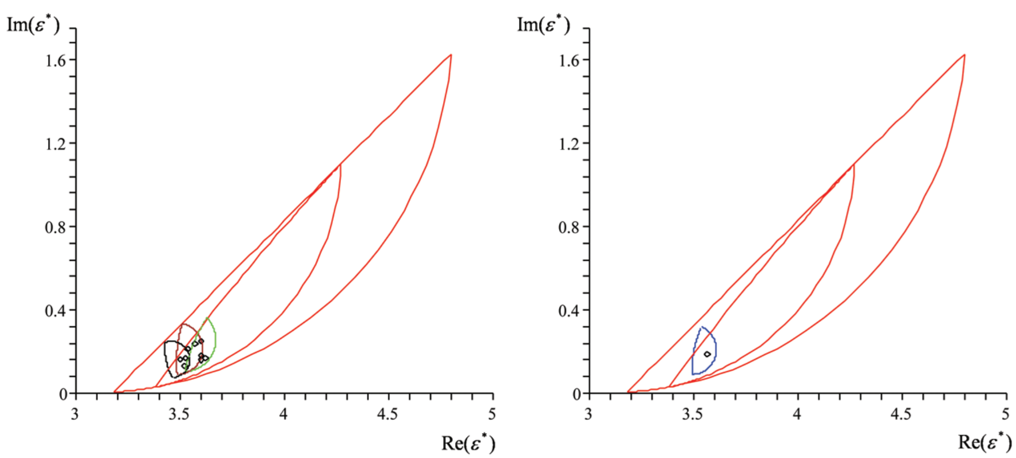

Gully, Lin, Cherkaev, Golden, Proc. Roy. Soc. A (and cover) 2015

Rigorous bounds on the complex permittivity tensor of sea ice with polycrystalline anisotropy within the horizontal plane

McKenzie McLean, Elena Cherkaev, Ken Golden 2020

motivated by **Weeks and Gow, *JGR* 1979: c-axis alignment in Arctic fast ice off Barrow**

Golden and Ackley, *JGR* 1981: radar propagation model in aligned sea ice

input: orientation statistics

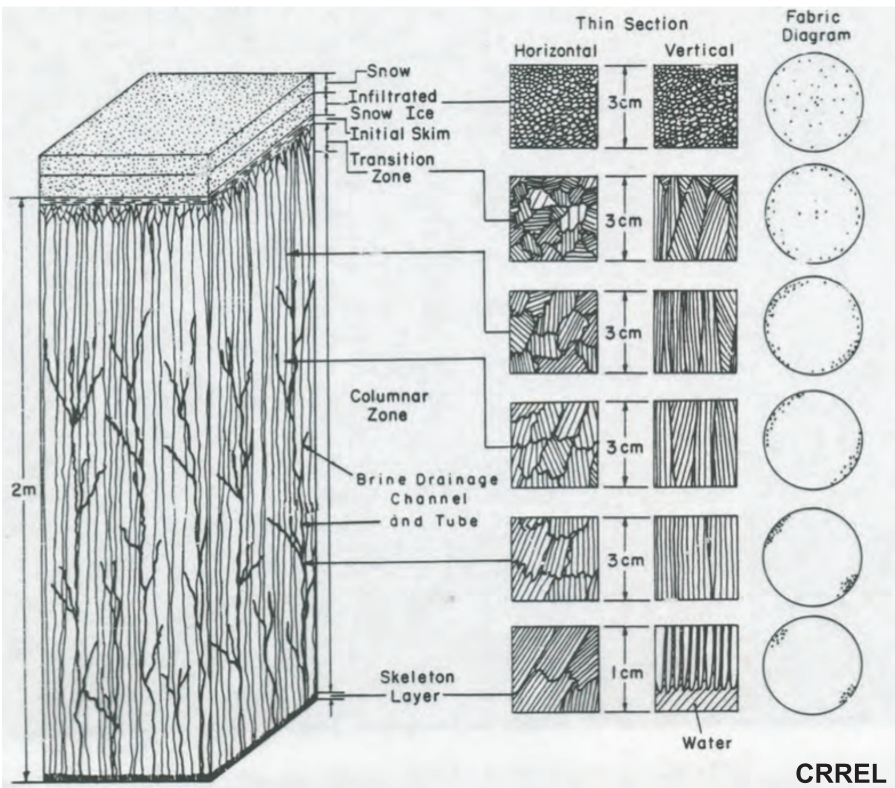

output: bounds

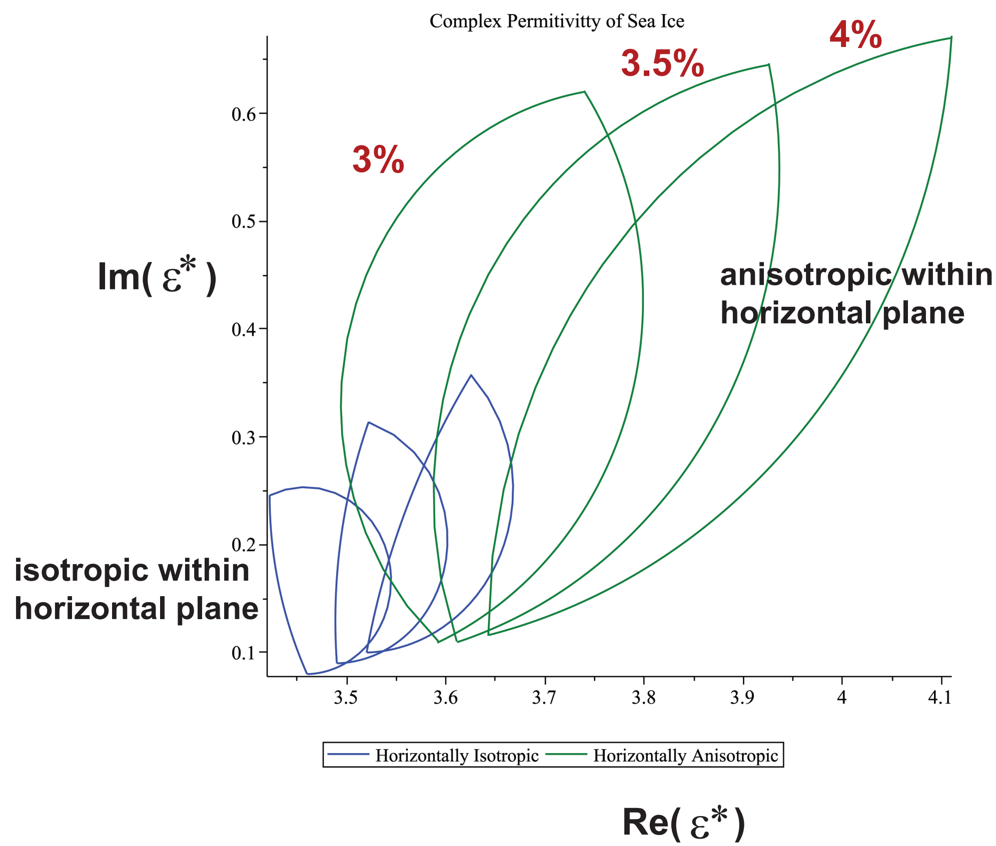

mesoscale

wave propagation in the marginal ice zone

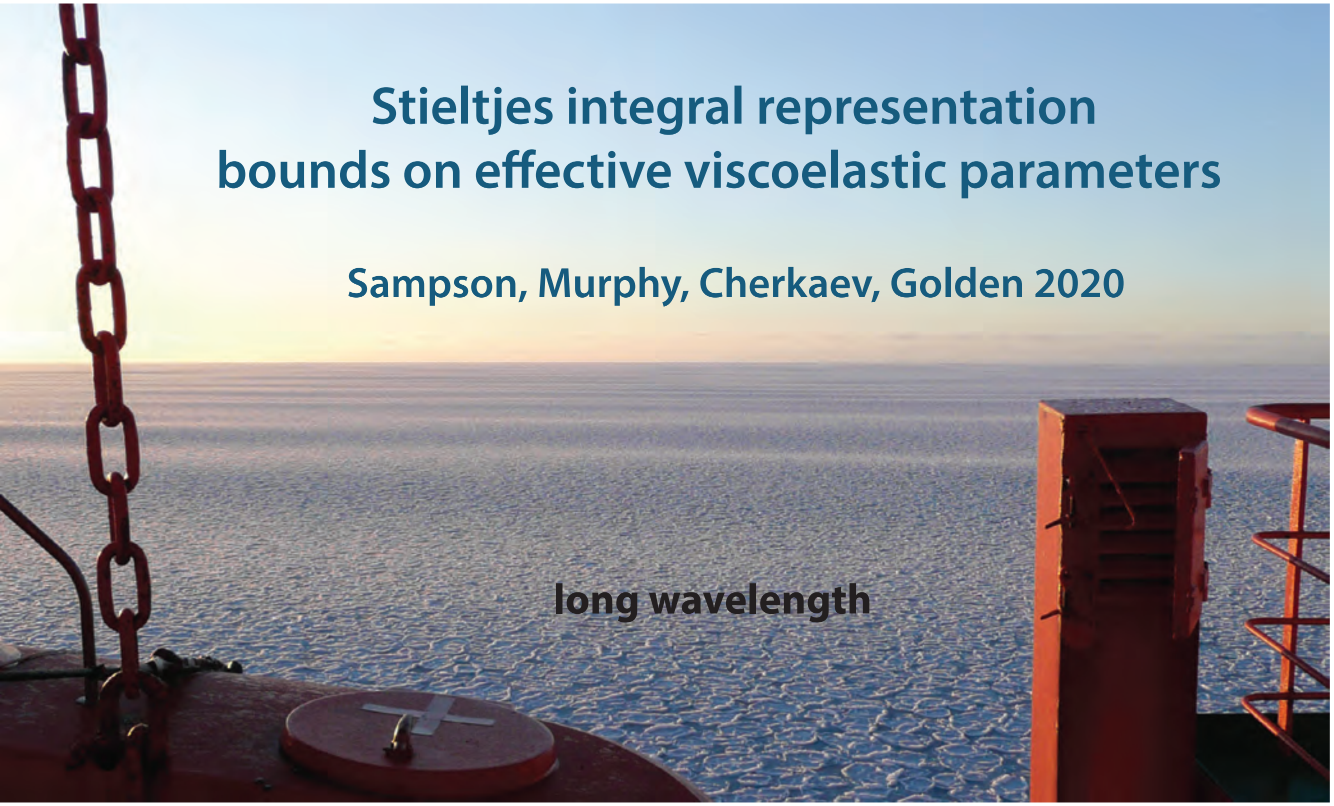

$$\langle \sigma_{ij} \rangle = C^*_{ijkl} \langle \epsilon_{kl} \rangle$$

ϵ_0 **avg strain**

$$C^*_{ijkl} = \nu^* \left(\delta_{ik}\delta_{jl} + \delta_{il}\delta_{jk} - \frac{2}{3}\delta_{ij}\delta_{kl} \right) = \nu^* \lambda_s$$

$$F(s) = 1 - \frac{\nu^*}{\nu_2} \qquad s = \frac{1}{1 - \frac{\nu_1}{\nu_2}}$$

$$F(s) = ||\epsilon_0||^{-2} \int_\Sigma \frac{d\mu(\lambda)}{s - \lambda}$$

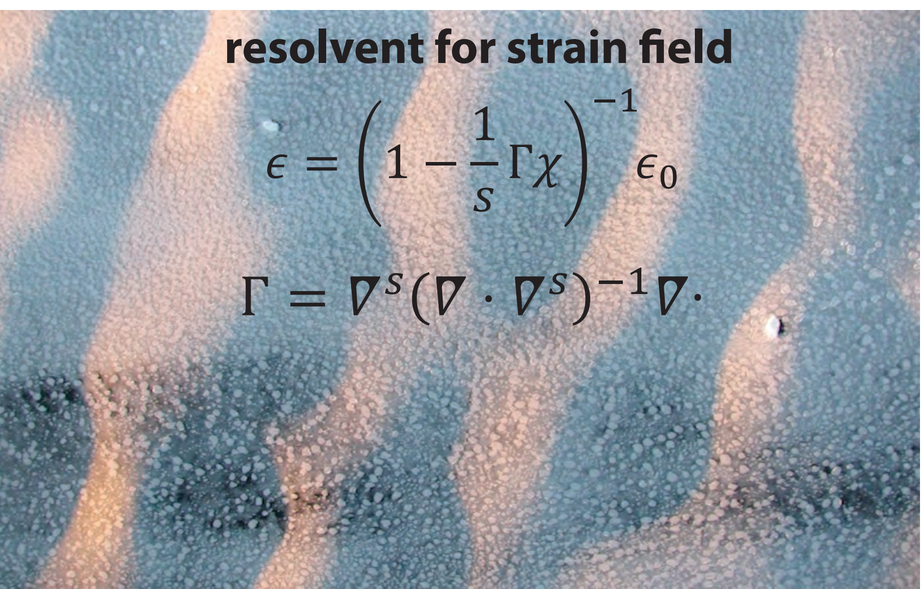

local

$$\sigma_{ij} = C_{ijkl} \epsilon_{kl}$$

quasistatic

$$\nabla \cdot \sigma = 0$$

bounds on the effective complex viscoelasticity

complex elementary bounds (fixed area fraction of floes)

$\nu_1 = 10^7 + i\,4875$ **pancake ice**

$\nu_2 = 5 + i\,0.0975$ **slush / frazil**

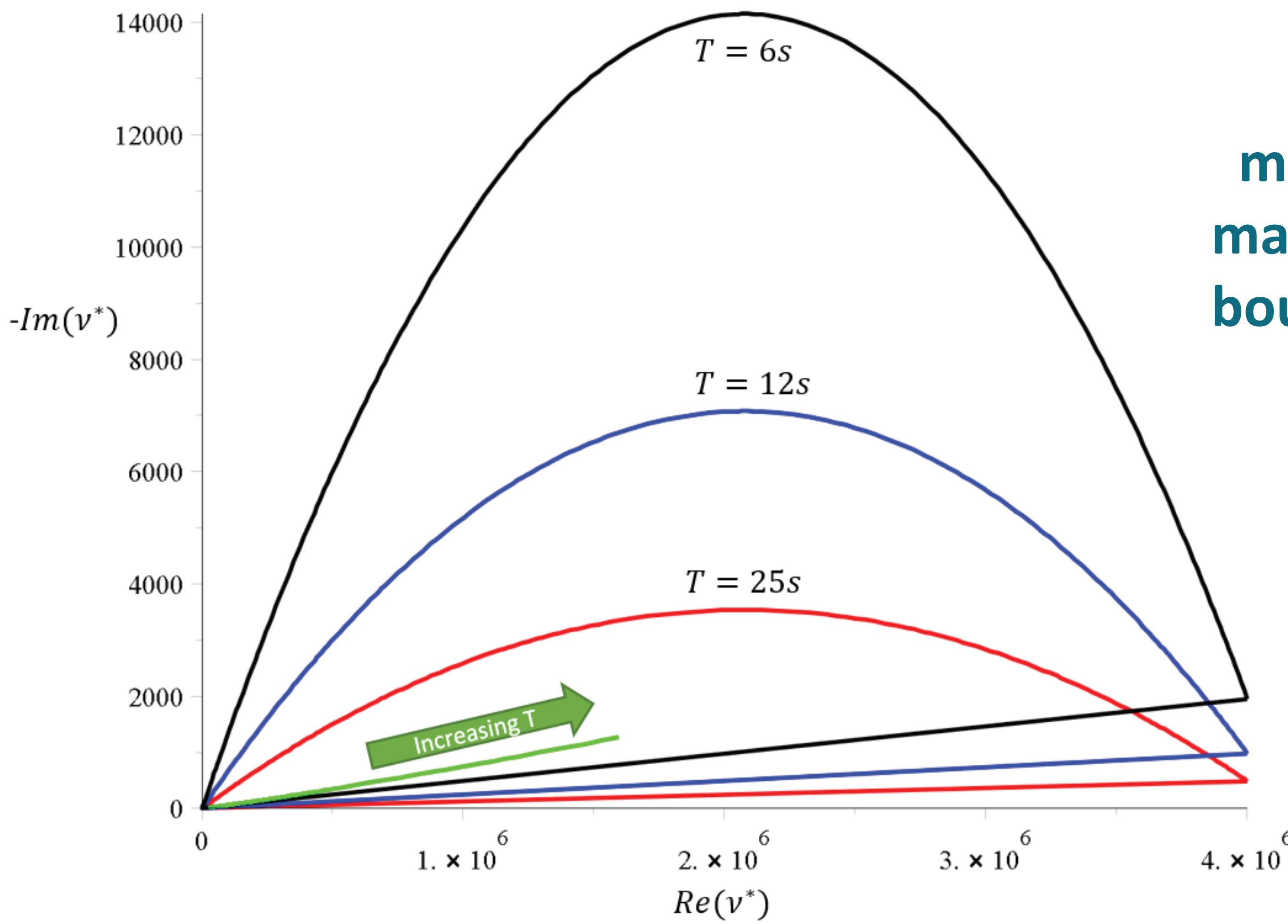

+ much tighter matrix particle bounds + data

Sampson, Murphy, Cherkaev, Golden 2020

advection enhanced diffusion

effective diffusivity

nutrient and salt transport in sea ice
heat transport in sea ice with convection
sea ice floes in winds and ocean currents
tracers, buoys diffusing in ocean eddies
diffusion of pollutants in atmosphere

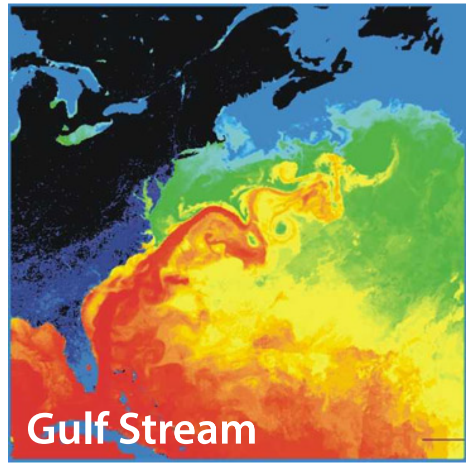

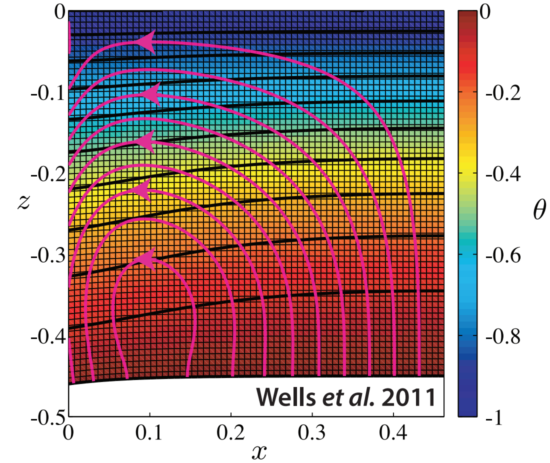

advection diffusion equation with a velocity field $\vec{u}$

$$\frac{\partial T}{\partial t} + \vec{u} \cdot \vec{\nabla} T = \kappa_0 \Delta T$$

$$\vec{\nabla} \cdot \vec{u} = 0$$

homogenize

$$\frac{\partial \overline{T}}{\partial t} = \kappa^* \Delta \overline{T}$$

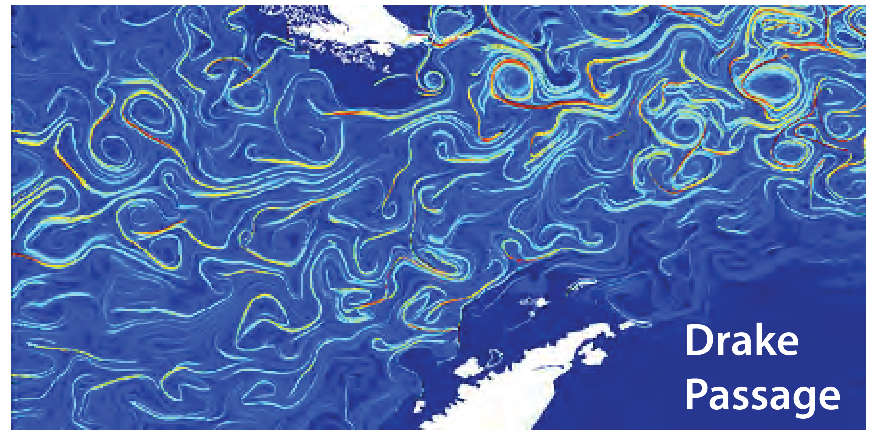

κ^* ***effective diffusivity***

Stieltjes integral for κ^* with spectral measure

Avellaneda and Majda, PRL 89, CMP 91

Murphy, Cherkaev, Xin, Zhu, Golden, *Ann. Math. Sci. Appl.* 2017
Murphy, Cherkaev, Zhu, Xin, Golden, *J. Math. Phys.* 2020

tracers flowing through inverted sea ice blocks

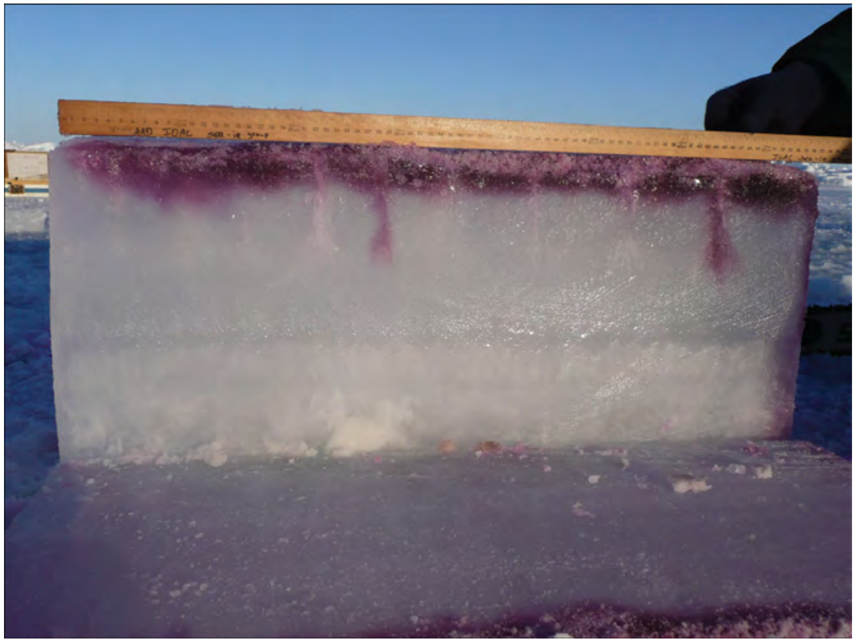

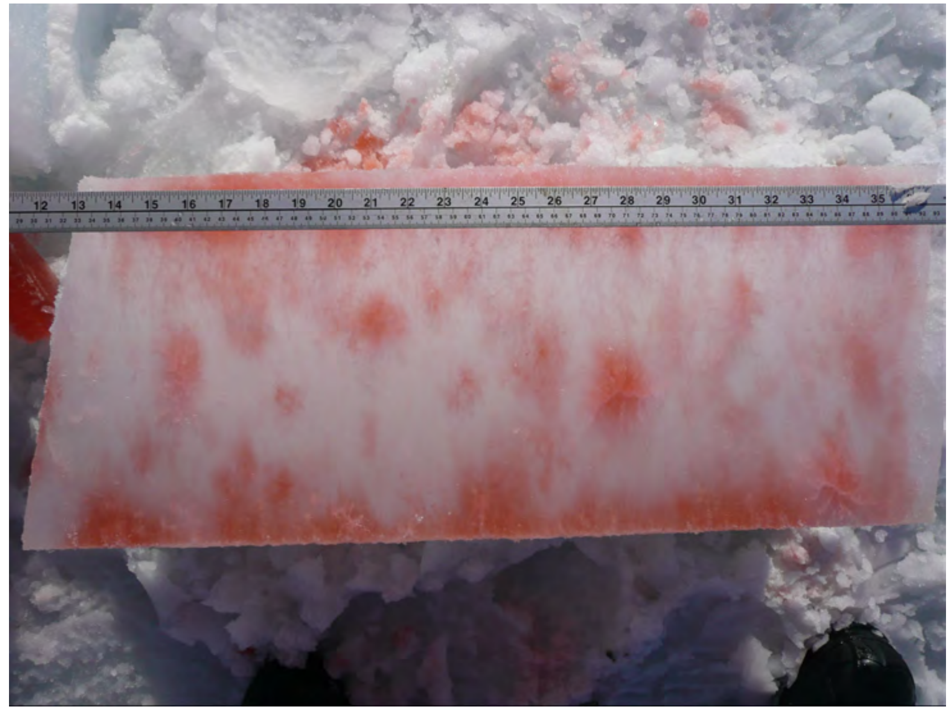

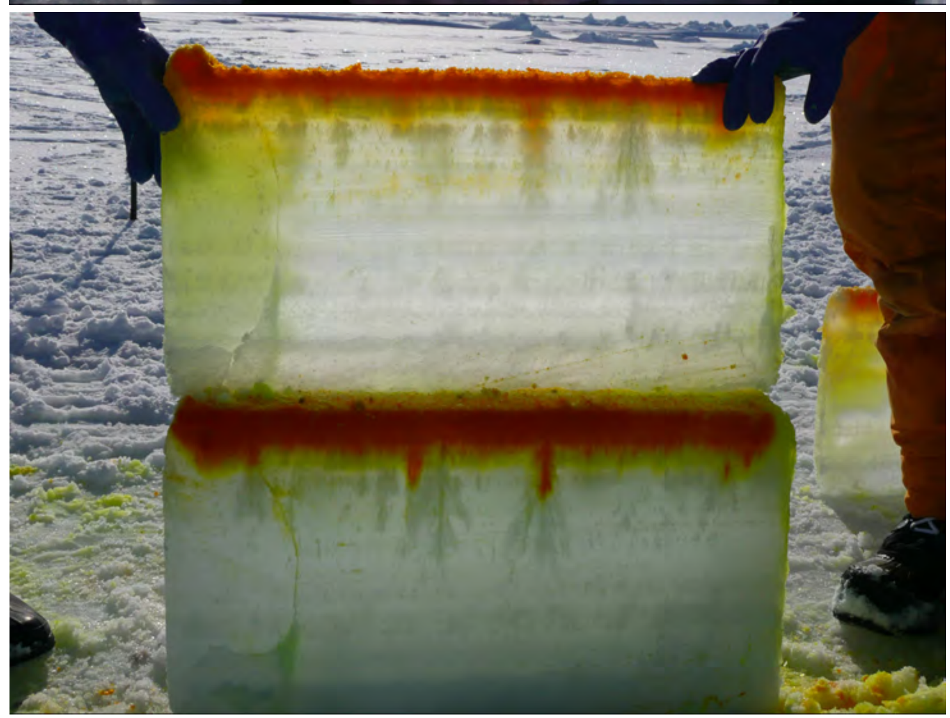

Stieltjes Integral Representation for Advection Diffusion

Murphy, Cherkaev, Zhu, Xin, Golden, *J. Math. Phys.* 2020

$$\kappa^* = \kappa \left(1 + \int_{-\infty}^{\infty} \frac{d\mu(\tau)}{\kappa^2 + \tau^2} \right), \quad F(\kappa) = \int_{-\infty}^{\infty} \frac{d\mu(\tau)}{\kappa^2 + \tau^2}$$

- μ is a positive definite measure corresponding to the spectral resolution of the self-adjoint operator $i\Gamma H\Gamma$
- $H =$ stream matrix , $\kappa =$ local diffusivity
- $\Gamma := -\nabla(-\Delta)^{-1}\nabla\cdot$, Δ is the Laplace operator
- $i\Gamma H\Gamma$ is bounded for time independent flows
- $F(\kappa)$ is analytic off the spectral interval in the κ-plane

rigorous framework for numerical computations of
spectral measures and effective diffusivity for model flows

new integral representations, theory of moment calculations

separation of material properties and flow field

Rigorous bounds on convection enhanced thermal conductivity of sea ice

Kraitzman, Hardenbrook, Murphy, Zhu, Cherkaev, Strong, Golden 2020

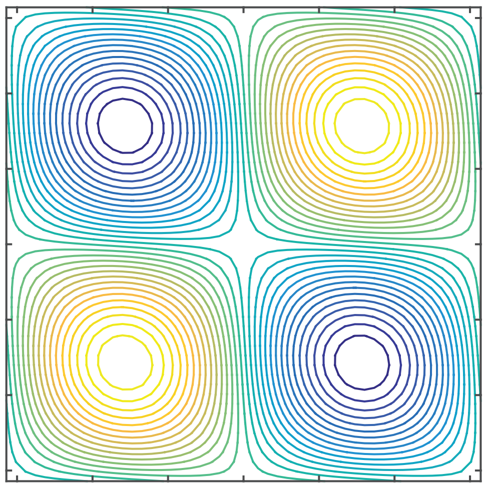

cat's eye flow model for brine convection cells

similar bounds
for shear flows

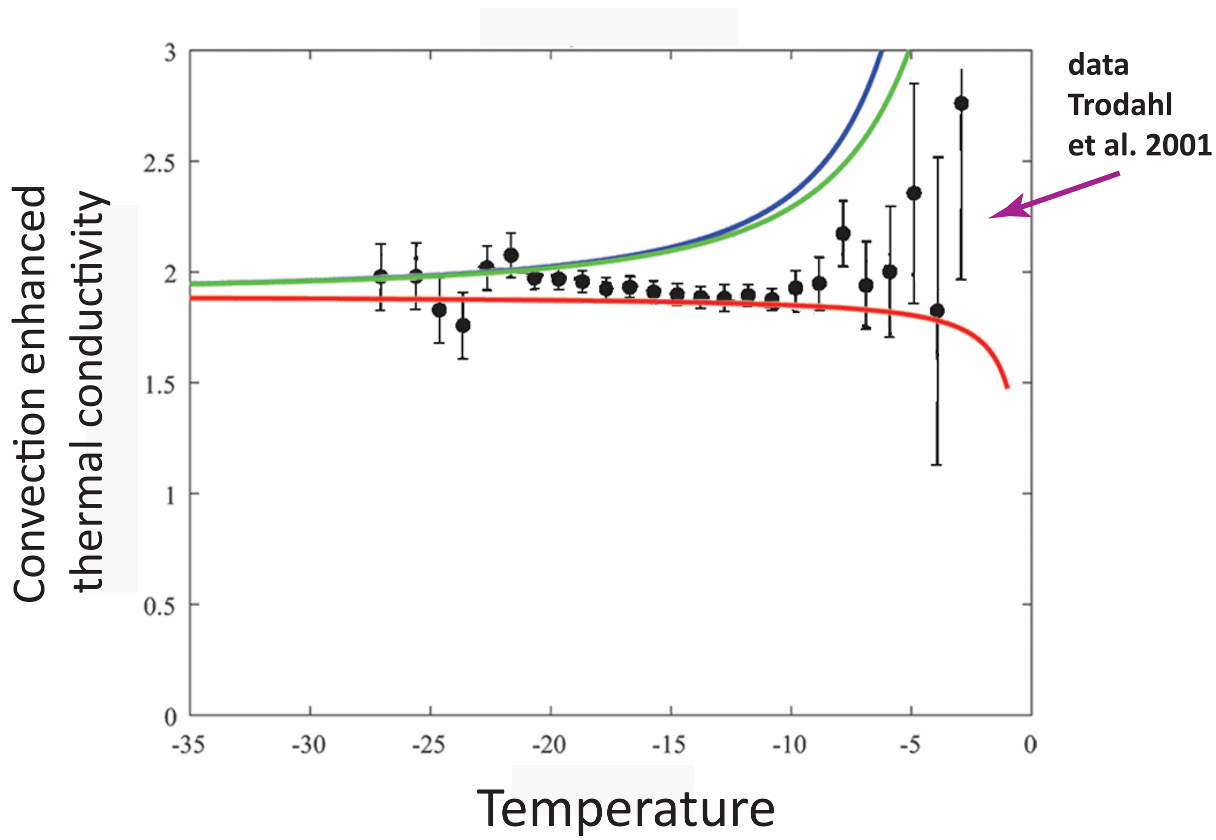

rigorous Padé bounds from Stieltjes integral +
analytical calculations of moments of measure

rigorous bounds assuming information on flow field INSIDE inclusions

Kraitzman, Cherkaev, Golden
SIAM J. Appl. Math. **(in revision), 2020**

melt pond formation and albedo evolution:

- major drivers in polar climate
- key challenge for global climate models

numerical models of melt pond evolution, including topography, drainage (permeability), etc.

Lüthje, Feltham, Taylor, Worster 2006

Flocco, Feltham 2007

Skyllingstad, Paulson, Perovich 2009

Flocco, Feltham, Hunke 2012

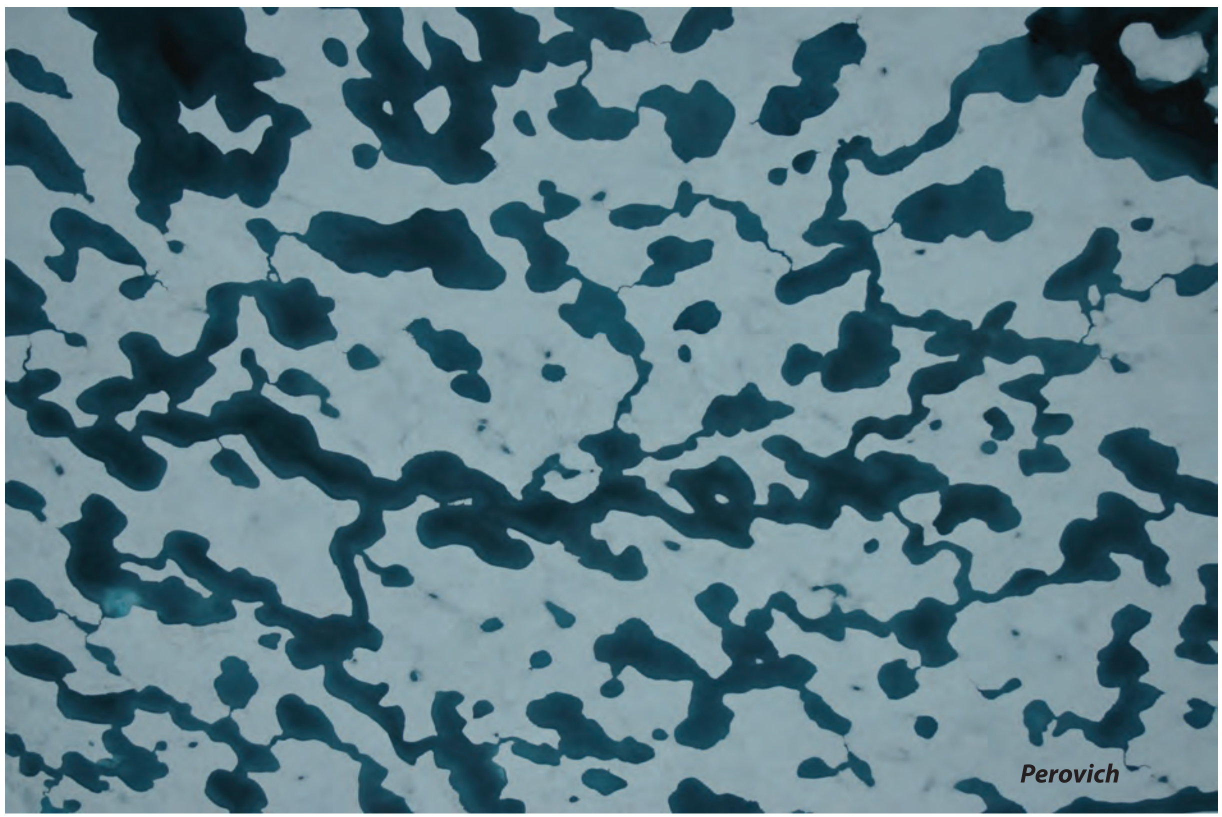

Are there universal features of the evolution similar to phase transitions in statistical physics?

fractal curves in the plane

they wiggle so much that their dimension is >1

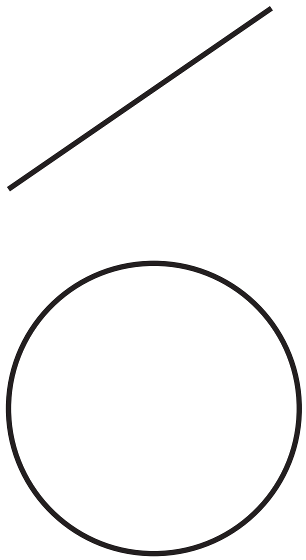

simple curves

$D = 1$

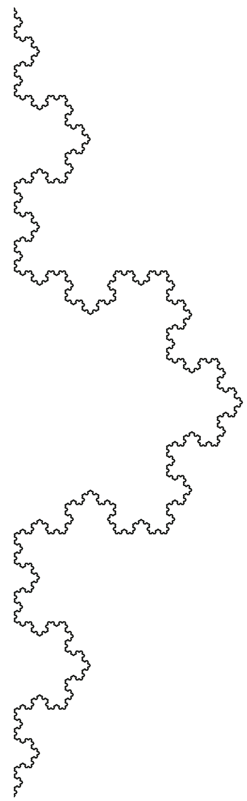

Koch snowflake

$D = 1.26$

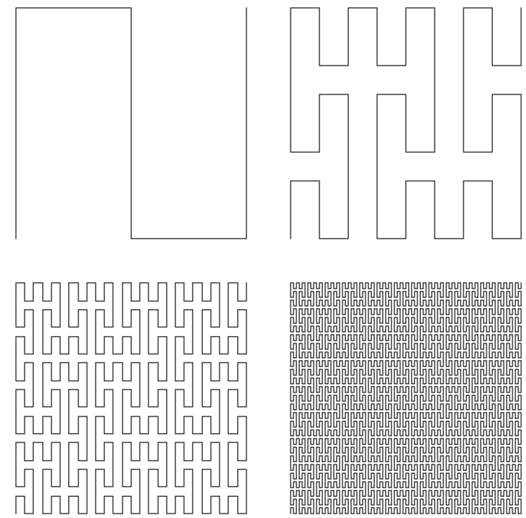

space filling curves

$D = 2$

Transition in the fractal geometry of Arctic melt ponds

Christel Hohenegger, Bacim Alali, Kyle Steffen, Don Perovich, Ken Golden

The Cryosphere, 2012

complexity grows with length scale

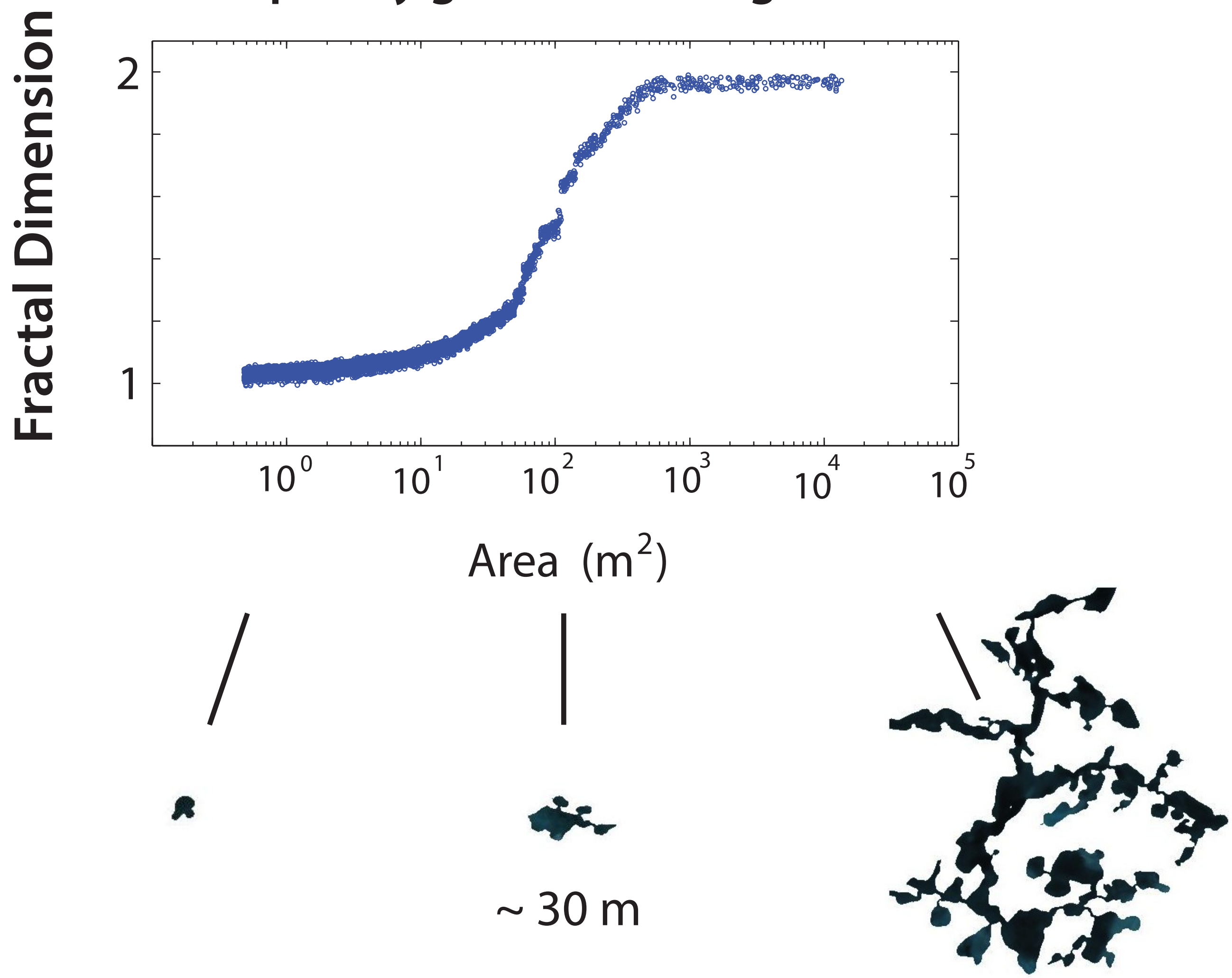

simple pond ***transitional pond*** ***complex pond***

Continuum percolation model for melt pond evolution

level sets of random surfaces

Brady Bowen, Court Strong, Ken Golden, J. Fractal Geometry 2018

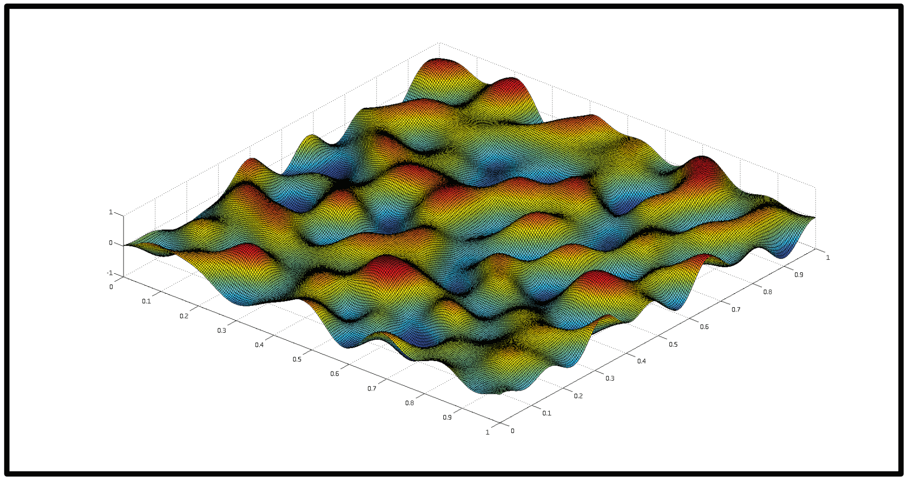

random Fourier series representation of surface topography

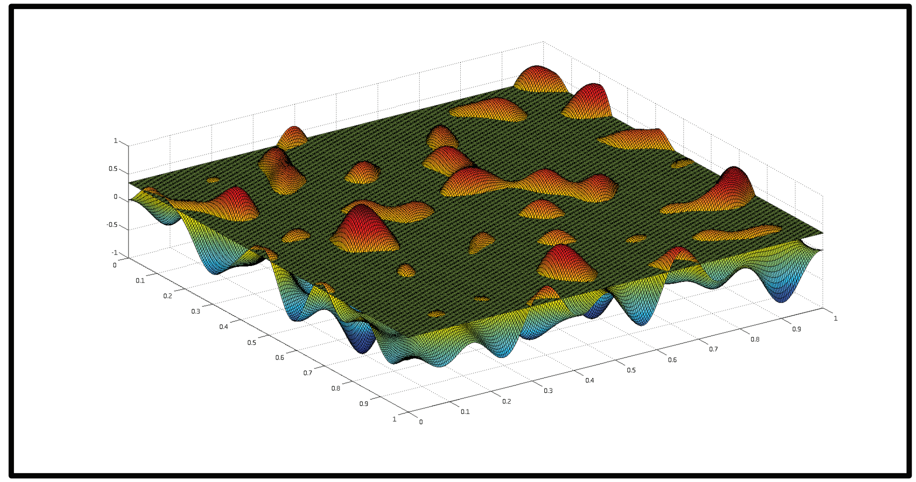

intersections of a plane with the surface define melt ponds

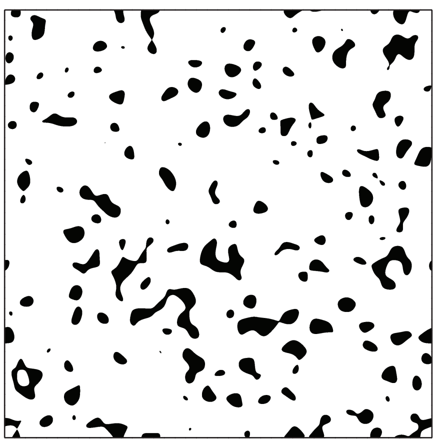

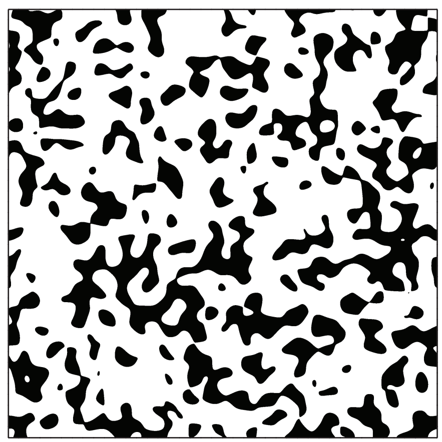

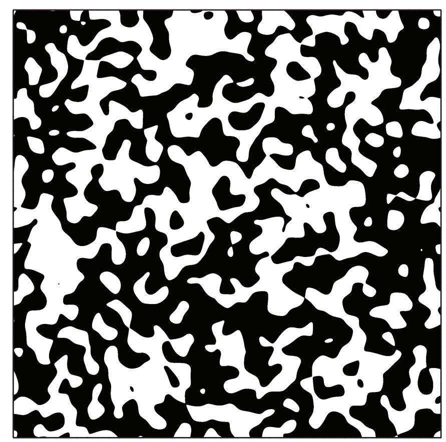

electronic transport in disordered media

diffusion in turbulent plasmas

Isichenko, Rev. Mod. Phys., 1992

fractal dimension curves depend on statistical parameters defining random surface

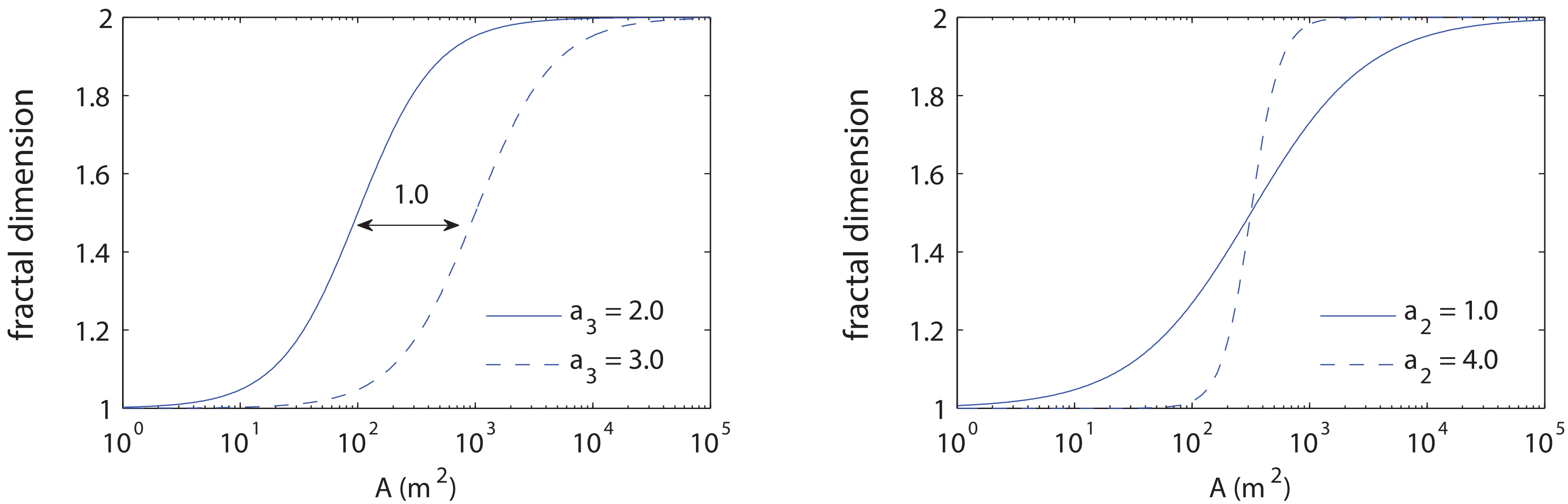

Saddle Points: The Key to Melt Pond Evolution

Ryleigh Moore, Jacob Jones, Dane Gollero, Court Strong, Ken Golden 2020

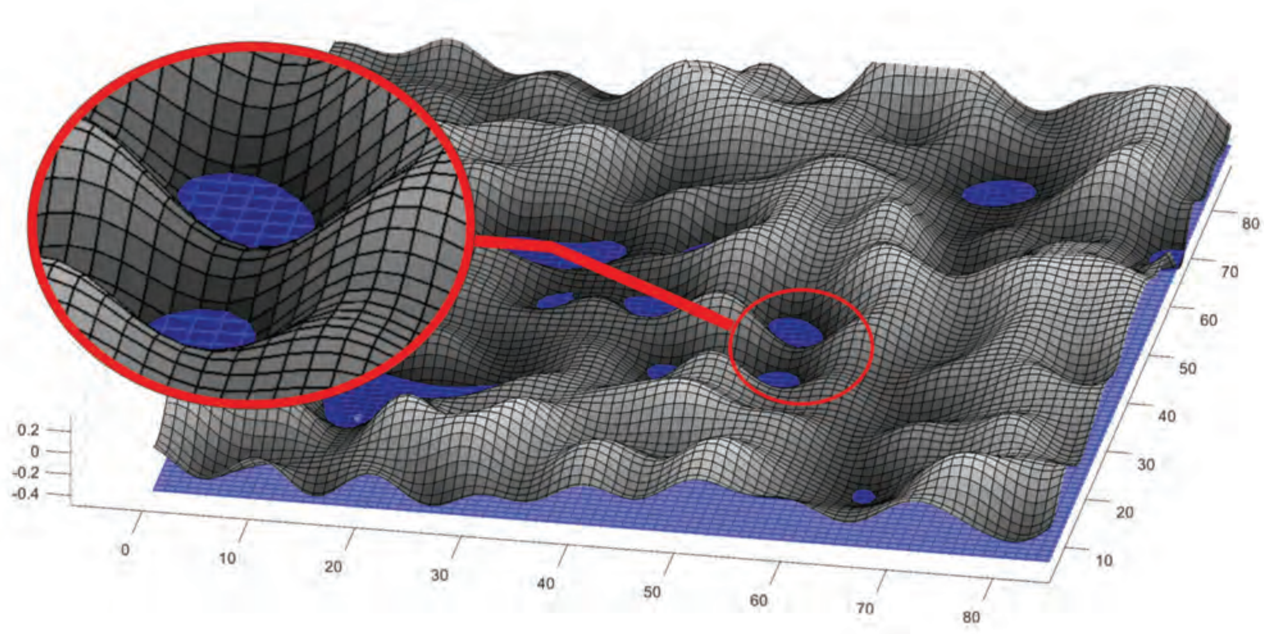

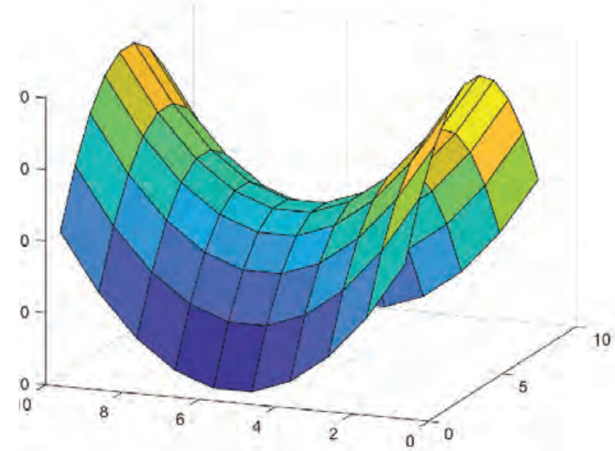

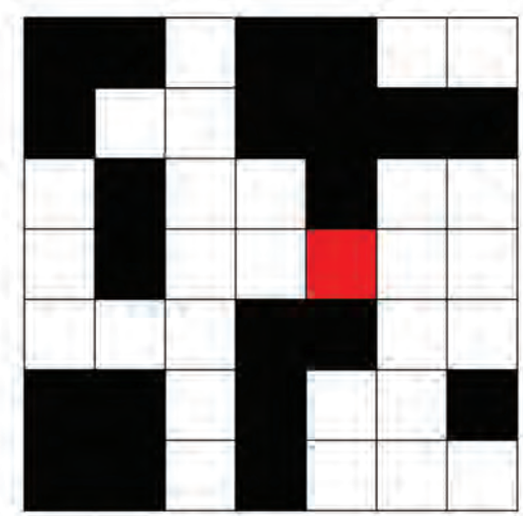

- Ponds connect through saddle points (Morse Theory).
- Red bond bond in percolation theory ~ saddle point.

Evolution of Isoperimetric Quotient with Melt Pond Growth (from real snow topography data)

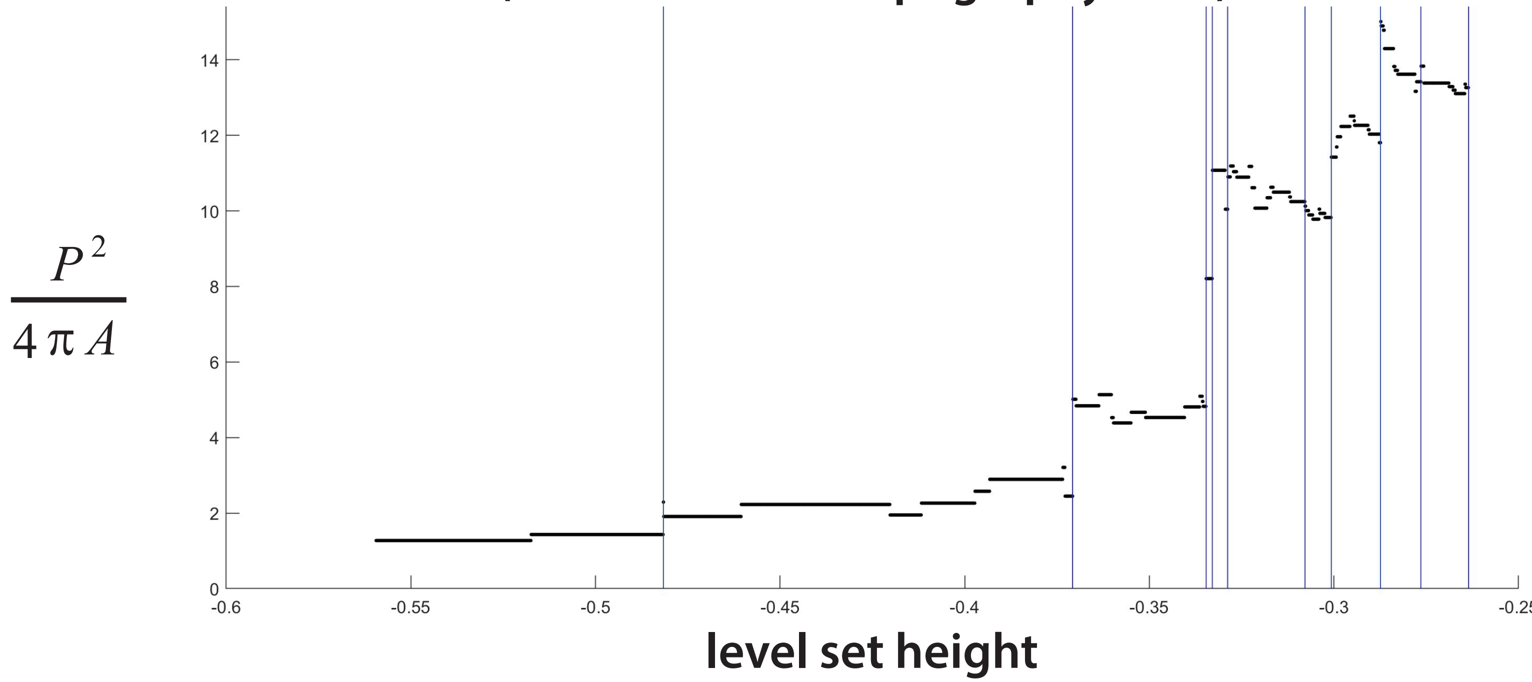

pond coalescence and thickening

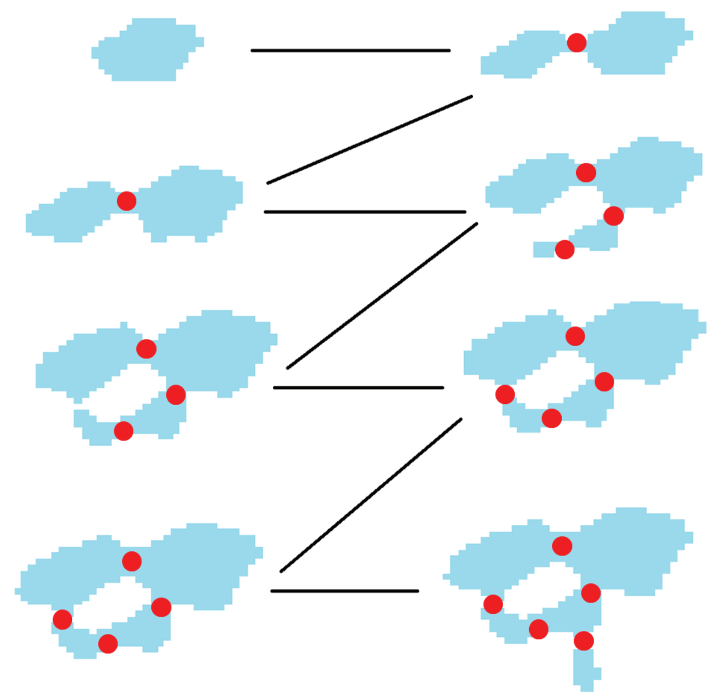

In the graph, we follow a single pond's growth. The vertical lines denote when the pond goes through a saddle point.

We see that large jumps in fractal dimension occur through saddle points.

Ryleigh Moore, University of Utah

Multidisciplinary drifting Observatory
for the Study of Arctic Climate (**MOSAiC**)

MOSAiC School
aboard the icebreaker ***RV Akademik Federov***

September 20 - October 28, 2019

20 grad students from around the world
(3 from U.S., 1 mathematician)

Ising Model for a Ferromagnet

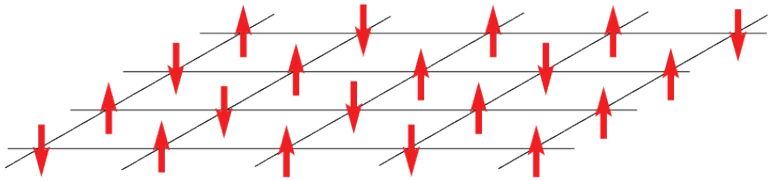

applied magnetic field H

$$s_i = \begin{cases} +1 & \text{spin up} \\ -1 & \text{spin down} \end{cases}$$

blue

white

$$\mathcal{H} = -H \sum_i s_i - J \sum_{<i,j>} s_i s_j$$

nearest neighbor Ising Hamiltonian

ferromagnetic interaction $J \geq 0$

islands of like spins

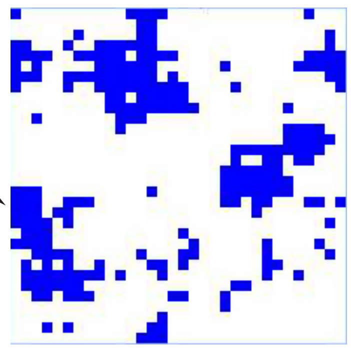

magnetization

homogenized parameter like effective conductivity

$$M(T,H) = \lim_{N\to\infty} \frac{1}{N} \left\langle \sum_j s_j \right\rangle$$

energy is lowered when nearby spins align with each other, forming magnetic domains

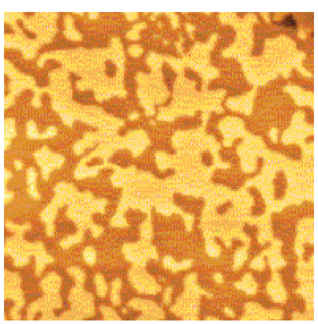

magnetic domains in cobalt

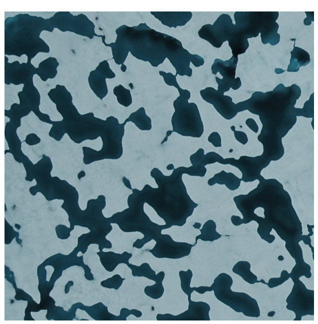

melt ponds (Perovich)

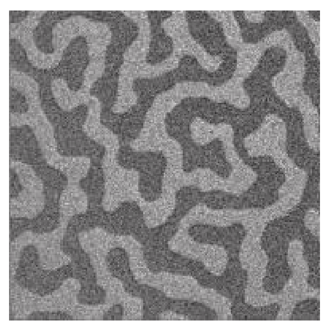

magnetic domains in cobalt-iron-boron

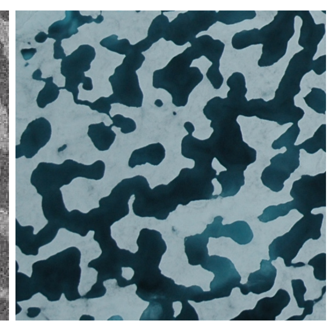

melt ponds (Perovich)

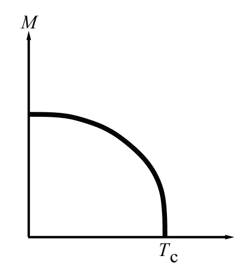

Curie point critical temperature

Ising model for ferromagnets $\longrightarrow$ Ising model for melt ponds

Ma, Sudakov, Strong, Golden, *New J. Phys.*, 2019

$$\mathcal{H} = -\sum_{i}^{N} H_i\, s_i - J \sum_{<i,j>}^{N} s_i s_j \qquad s_i = \begin{cases} \uparrow & +1 \quad \text{water} \quad \text{(spin up)} \\ \downarrow & -1 \quad \text{ice} \quad \text{(spin down)} \end{cases}$$

random magnetic field represents snow topography

magnetization M **pond coverage** $\frac{(M+1)}{2}$

~ albedo

only nearest neighbor patches interact

Starting with random initial configurations, as Hamiltonian energy is minimized by Glauber spin flip dynamics, system "flows" toward metastable equilibria.

Order from Disorder

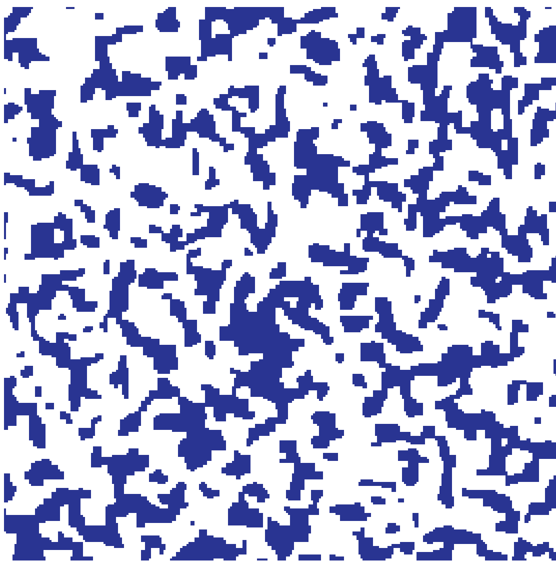

Ising model

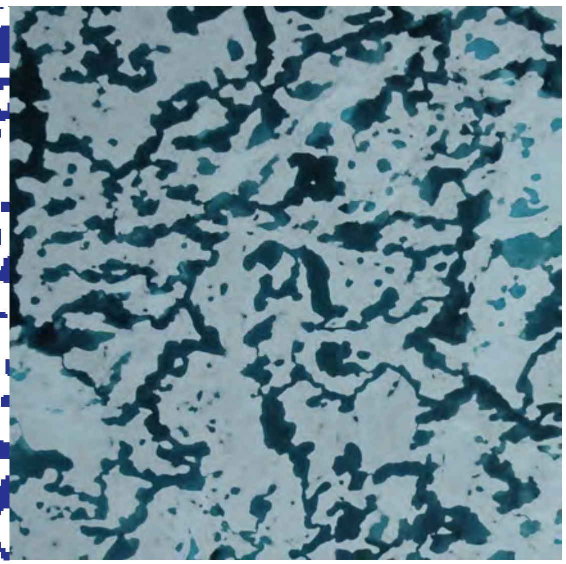

melt pond photo (Perovich)

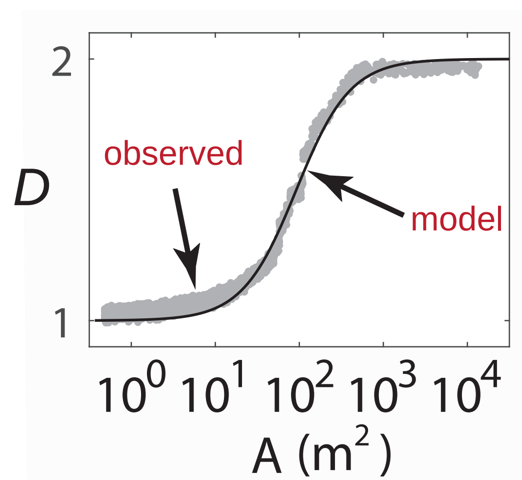

pond size distribution exponent

observed -1.5

(Perovich, *et al.* 2002)

model -1.58

ONLY MEASURED INPUT = LENGTH SCALE (GRID SIZE) from snow topography data

2011 massive under-ice algal bloom

Arrigo et al., *Science* 2012

melt ponds act as *WINDOWS* allowing light through sea ice

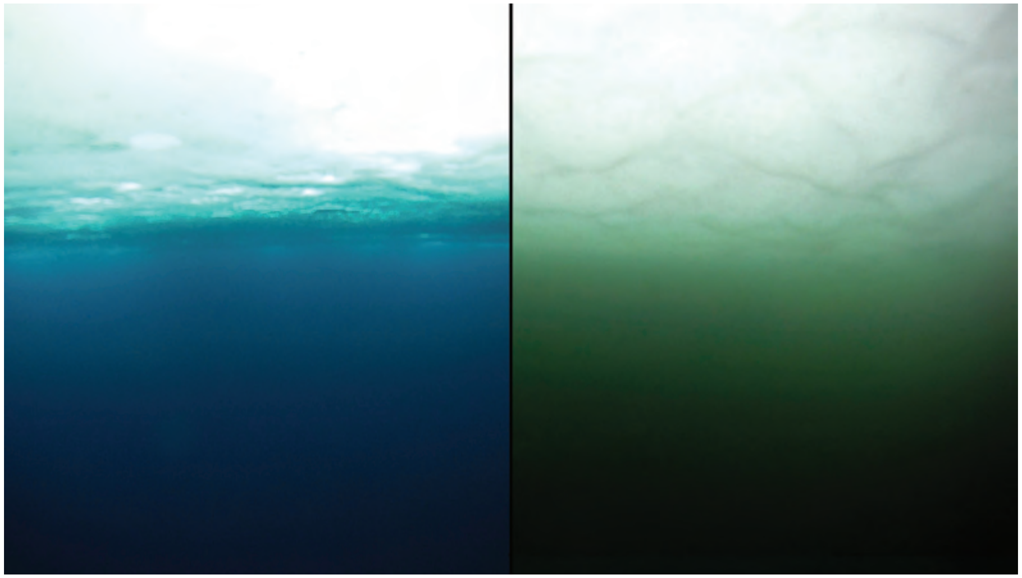

no bloom bloom

Have we crossed into a new ecological regime?

The frequency and extent of sub-ice phytoplankton blooms in the Arctic Ocean

Horvat, Rees Jones, Iams, Schroeder, Flocco, Feltham, *Science Advances*, 2017

(2015 AMS MRC, Snowbird)

The effect of melt pond geometry on the distribution of solar energy under first-year sea ice

Horvat, Flocco, Rees Jones, Roach, Golden, *Geophys. Res. Lett.* 2020

- Model for 3D light field under ponded sea ice.

- Distribution of solar energy at depth influenced by ***shape and connectivity*** of melt ponds, as well as area fraction.

- Aggregate properties of the sub-ice light field, such as a significant enhancement of available solar energy under the ice, are controlled by parameter closely related to pond fractal geometry.

- Model and analysis explain how melt pond geometry ***homogenizes*** under-ice light field, affecting habitability.

Pond geometry affects ecology and partitioning of solar energy in the upper Arctic Ocean.

macroscale

Anomalous diffusion in sea ice dynamics

Ice floe diffusion in winds and currents

Jennifer Lukovich, Jennifer Hutchings, David Barber, *Ann. Glac.* 2015

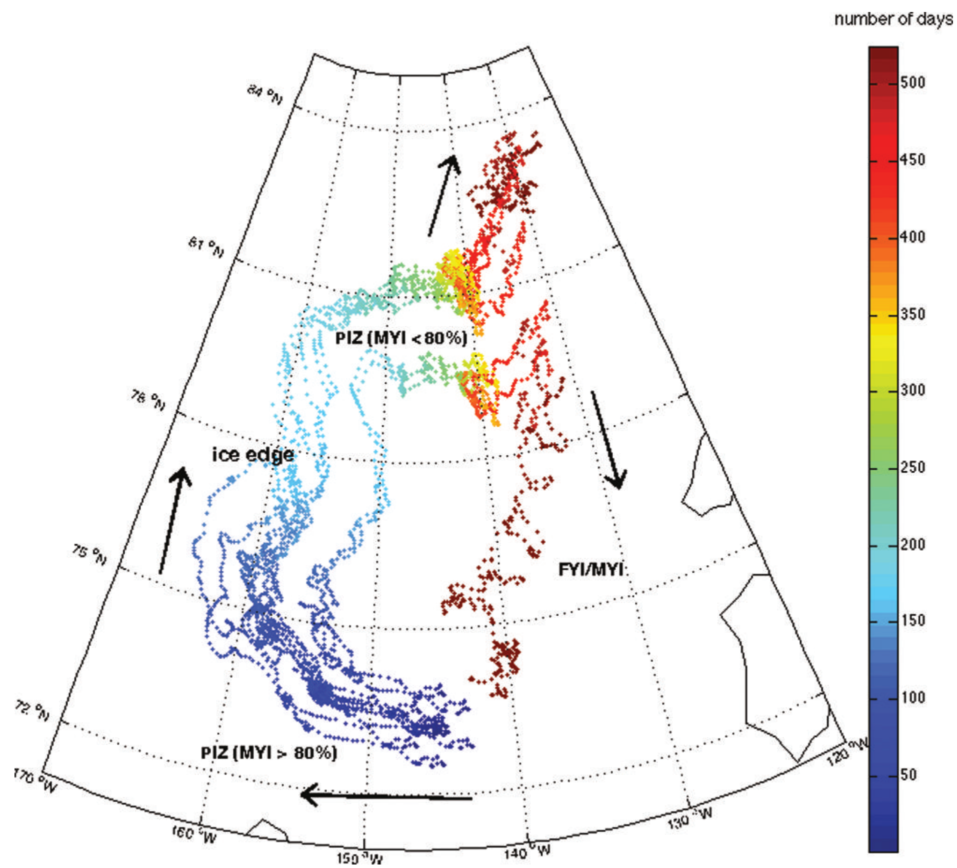

- On short time scales floes observed (buoy data) to exhibit Brownian-like behavior, but they are also being advected by winds and currents.
- Effective behavior is purely diffusive, sub-diffusive or super-diffusive depending on ice pack and advective conditions - Hurst exponent.

Floe Scale Model of Anomalous Diffusion in Sea Ice Dynamics

Huy Dinh, Elena Cherkaev, Court Strong, Ken Golden 2020

$$\left\langle \left|\mathbf{x}(t) - \mathbf{x}(0) - \langle \mathbf{x}(t) - \mathbf{x}(0) \rangle \right|^2 \right\rangle \sim t^{\alpha}$$

$\alpha =$ Hurst exponent, a measure of anomalous diffusion.

Measured from bouy position data. Detects ice pack crowding and advective forcing.

J.V. Lukovich, J.K. Hutchings, D.G. Barber ***Annals of Glaciology*** **2015**

diffusive $\alpha = 1$ Sparse packing, uncorrelated advective field.

sub-diffusive $\alpha < 1$ Dense packing, crowding dominates advection.

super-diffusive $\alpha = 5/4$ Sparse packing, shear dominates advection.

$\alpha = 5/3$ Sparse packing, vorticity dominates advection.

Goal: Develop numerical model to analyze regimes of transport in terms of ice pack crowding and advective conditions.

Model Results

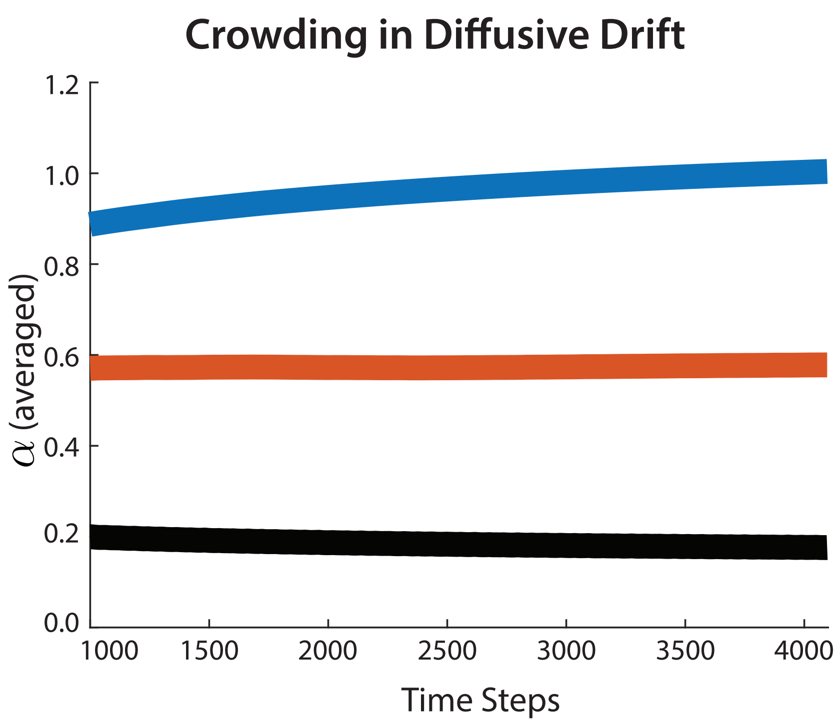

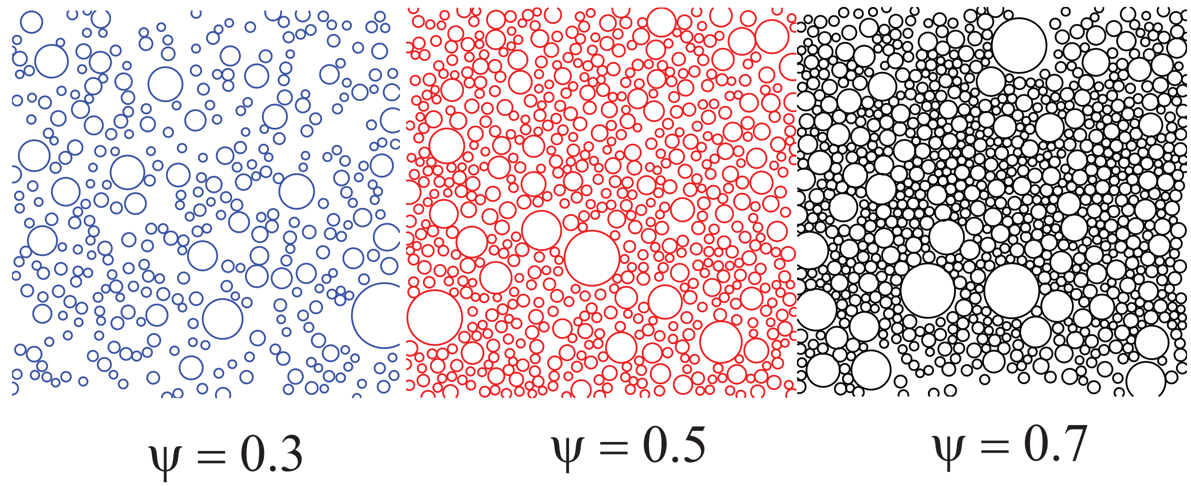

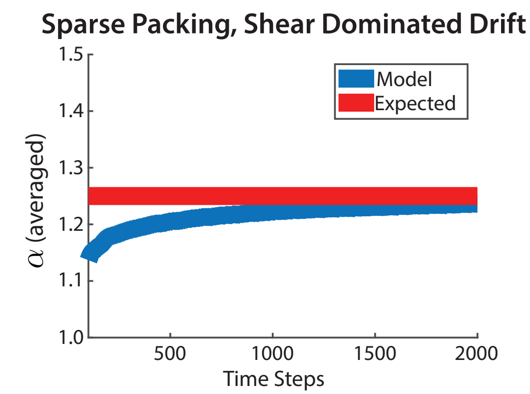

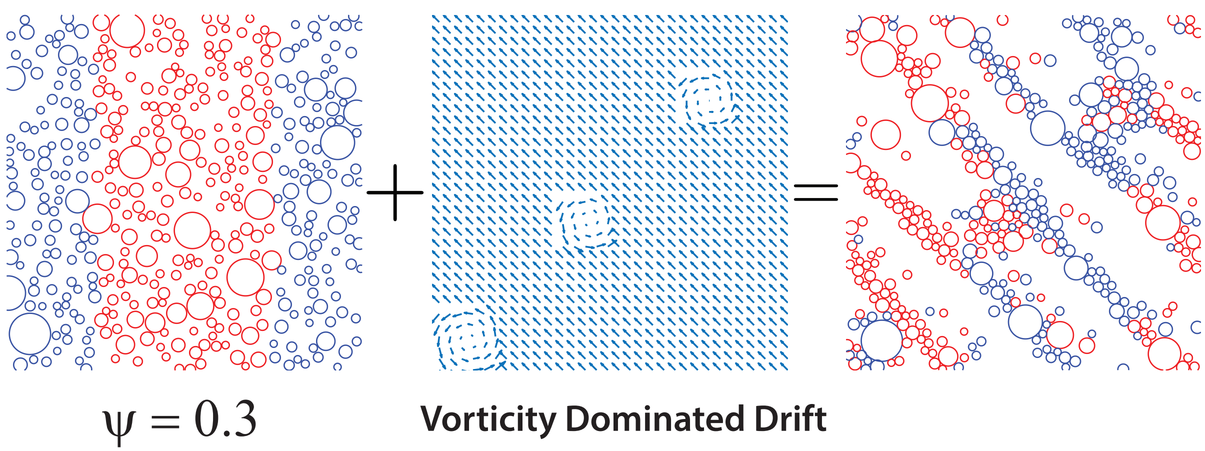

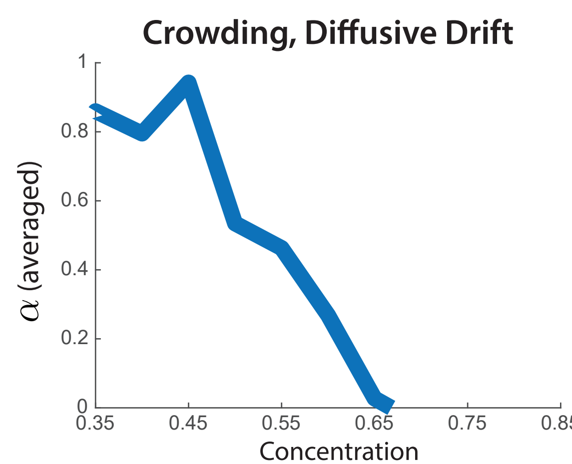

Marginal Ice Zone

MIZ

- biologically active region
- intense ocean-sea ice-atmosphere interactions
- region of significant wave-ice interactions

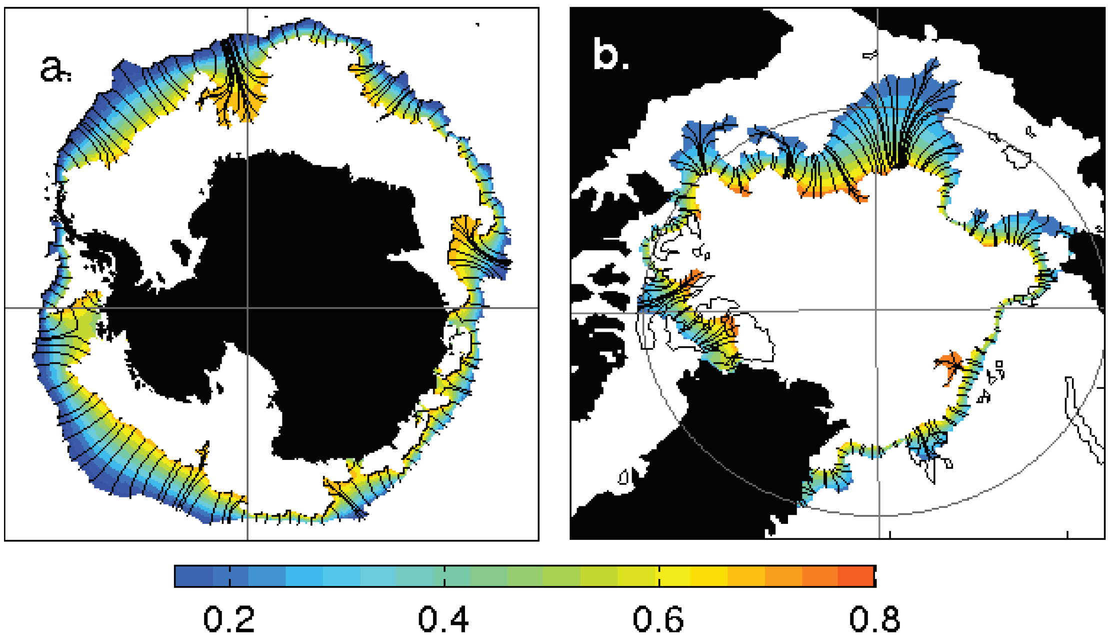

transitional region between dense interior pack ($c > 80\%$) sparse outer fringes ($c < 15\%$)

MIZ WIDTH

fundamental length scale of ecological and climate dynamics

Strong, *Climate Dynamics* 2012

Strong and Rigor, *GRL* 2013

How to objectively measure the "width" of this complex, non-convex region?

Objective method for measuring MIZ width motivated by medical imaging and diagnostics

Strong, *Climate Dynamics* 2012
Strong and Rigor, *GRL* 2013

39% widening
1979 - 2012

streamlines of a solution to Laplace's equation

"average" lengths of streamlines

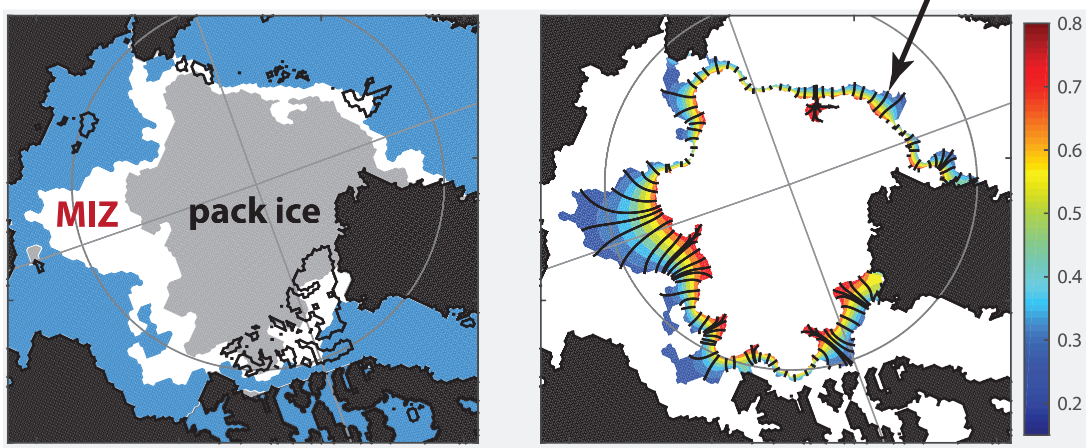

Arctic Marginal Ice Zone

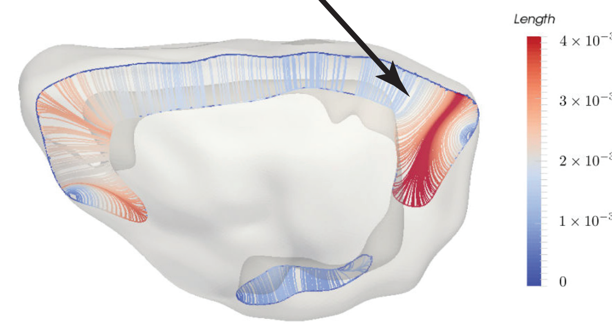

crossection of the cerebral cortex of a rodent brain

analysis of different MIZ WIDTH definitions

Strong, Foster, Cherkaev, Eisenman, Golden
J. Atmos. Oceanic Tech. 2017

Strong and Golden
Society for Industrial and Applied Mathematics News, April 2017

MIZ fractal dimension

Jerry Zhang, Court Strong, Ken Golden

The shape of the MIZ becomes more complex during the melt season, increasing its fractal dimension.

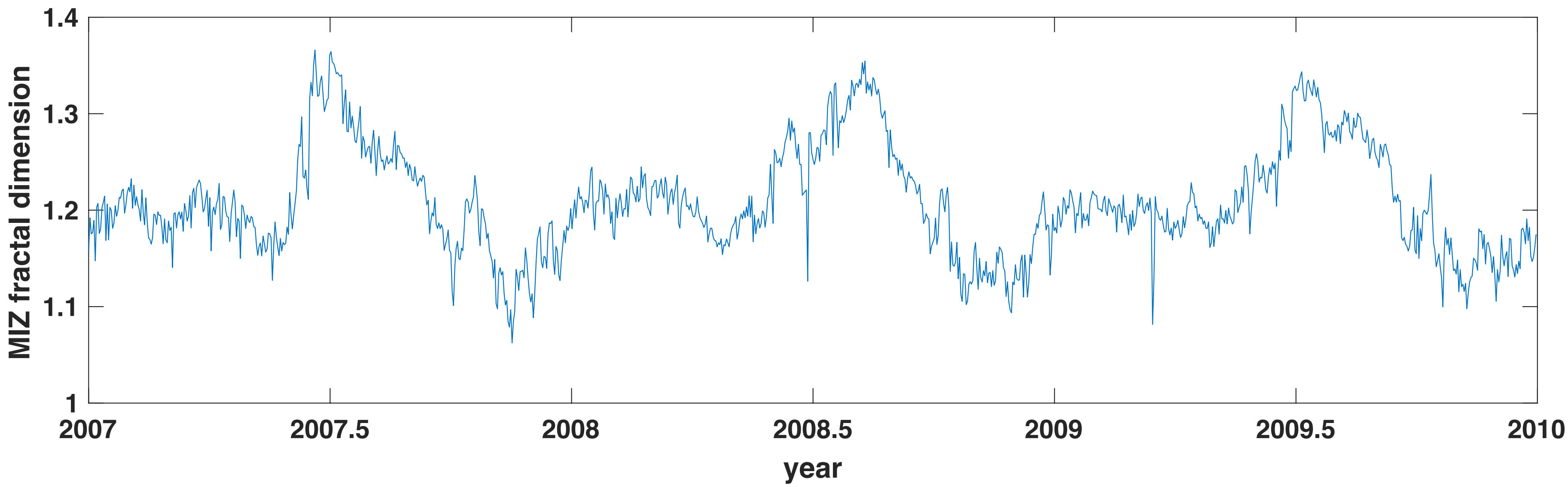

- MIZ fractal dimension undergoes a pronounced seasonal cycle, maximizing around July
- We have preliminary evidence of decadal trends in MIZ fractal dimension

MIZ fractal dimension

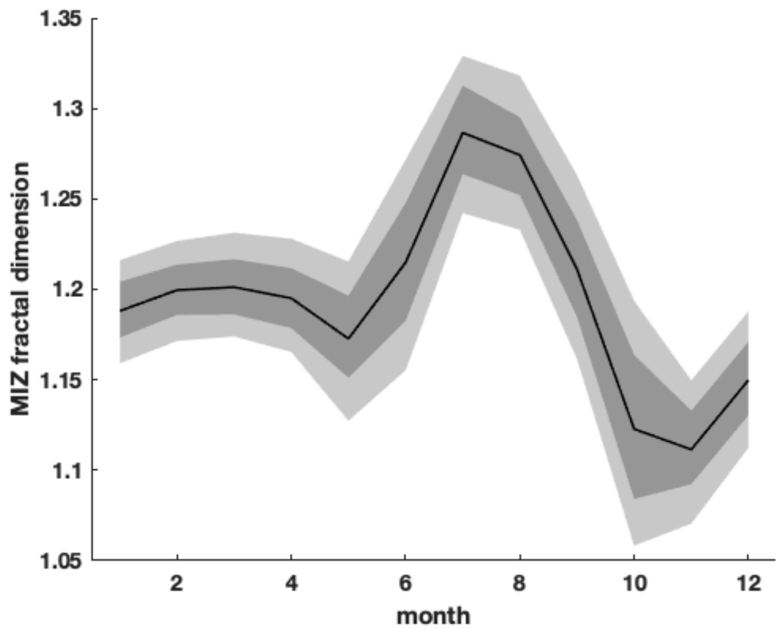

For daily Arctic values 1979-2019

Bold curve: mean

Shading: 10^{th}-90^{th} and 25^{th}-75^{th} percentiles

- MIZ fractal dimension undergoes a pronounced seasonal cycle, maximizing around July
- We have preliminary evidence of decadal trends in MIZ fractal dimension

Filling the polar data gap with partial differential equations

hole in satellite coverage of sea ice concentration field

previously assumed ice covered

Gap radius: 611 km
06 January 1985

Gap radius: 311 km
30 August 2007

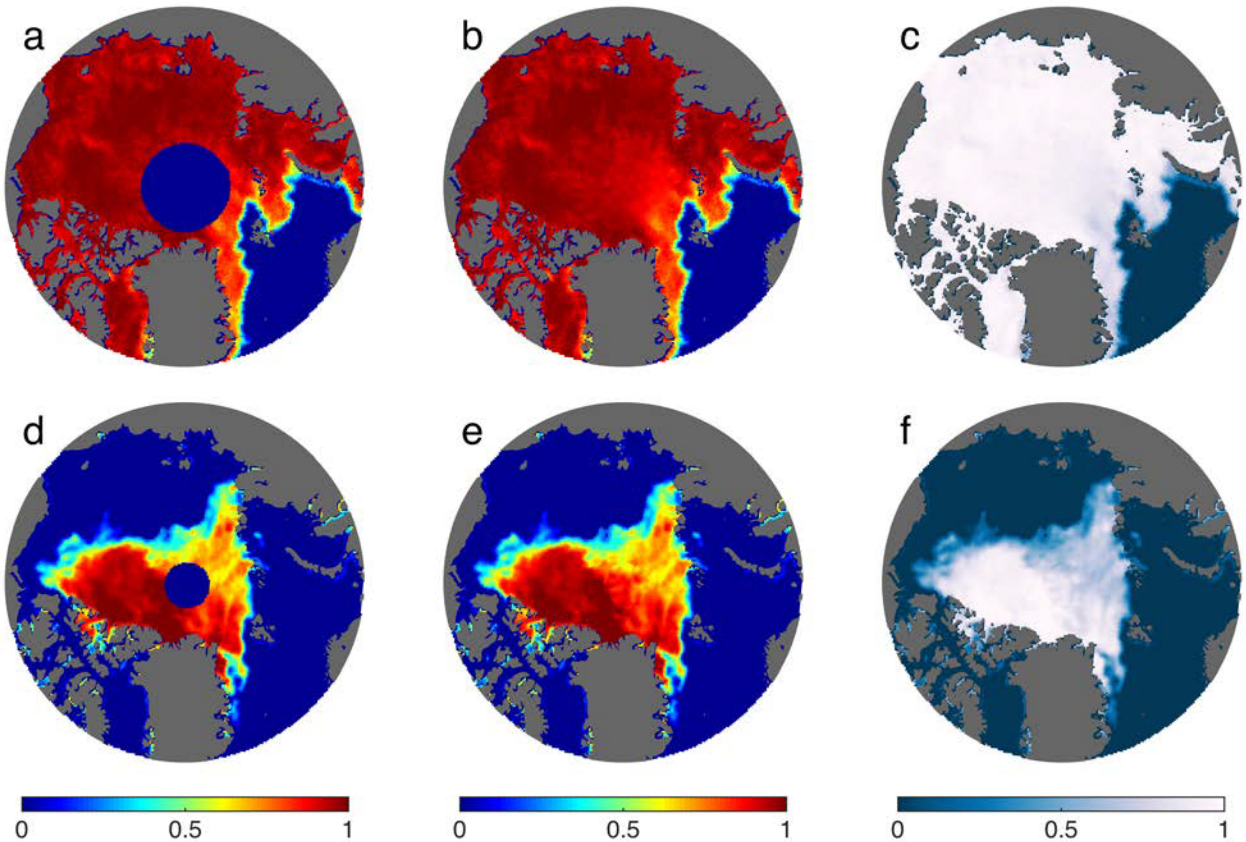

$$\Delta\psi=0$$

fill with harmonic function satisfying satellite BC's plus stochastic term

Strong and Golden, *Remote Sensing* 2016
Strong and Golden, *SIAM News* 2017

NOAA/NSIDC Sea Ice Concentration CDR product update will use our PDE method.

University of Utah Sea Ice Modeling Group (2017-2020)

Senior Personnel: Ken Golden, Distinguished Professor of Mathematics
Elena Cherkaev, Professor of Mathematics
Court Strong, Associate Professor of Atmospheric Sciences
Ben Murphy, Ph.D.

Postdoctoral Researcher: Noa Kraitzman (now at Australian National University)

Graduate Students: Kyle Steffen (now at UT Austin with Clint Dawson)
Christian Sampson (now at UNC Chapel Hill with Chris Jones)
Huy Dinh (starting sea ice MURI Postdoc at NYU/Courant)
Rebecca Hardenbrook
David Morison (Physics Department)
Ryleigh Moore
Delaney Mosier, Daniel Hallman

Undergraduate Students: Kenzie McLean, Jacqueline Cinella Rich, Dane Gollero,
Samir Suthar, Anna Hyde, Kitsel Lusted, Ruby Bowers
Kimball Johnston, Jerry Zhang

High School Students: Jeremiah Chapman, Titus Quah, Dylan Webb

---

Sea Ice Ecology Group Postdoc Jody Reimer, Grad Student Julie Sherman,
Undergrads Anna Hyde, Kayla Stewart + incoming

Conclusions

1. Sea ice is a fascinating multiscale composite with structure similar to many other natural and man-made materials.

2. Mathematical methods developed for sea ice advance the theory of composites and inverse problems in general.

2. Homogenization and statistical physics help ***link scales in sea ice and composites***; provide rigorous methods for finding effective behavior; advance sea ice representations in climate models.

3. Fluid flow through sea ice mediates melt pond evolution and many processes important to climate change and polar ecosystems.

5. Field experiments are essential to developing relevant mathematics.

6. Our research will help to improve projections of climate change, the fate of Earth's sea ice packs, and the ecosystems they support.

Buchanan Bay, Antarctica   Mertz Glacier Polynya Experiment   July 1999

ISSN 0002-9920 (print)
ISSN 1088-9477 (online)

Notices

of the American Mathematical Society

November 2020 **Volume 67, Number 10**

AMERICAN MATHEMATICAL SOCIETY

Advancing research. Creating connections.

The cover is based on “Modeling Sea Ice,” page 1535.

Modeling Sea Ice

Kenneth M. Golden, Luke G. Bennetts, Elena Cherkaev, Ian Eisenman, Daniel Feltham, Christopher Horvat, Elizabeth Hunke, Christopher Jones, Donald K. Perovich, Pedro Ponte-Castañeda, Courtenay Strong, Deborah Sulsky, and Andrew J. Wells

Kenneth M. Golden is a Distinguished Professor of Mathematics at the University of Utah. His email address is `golden@math.utah.edu`.

Luke G. Bennetts is an associate professor of applied mathematics at the University of Adelaide. His email address is `luke.bennetts@adelaide.edu.au`.

Elena Cherkaev is a professor of mathematics at the University of Utah. Her email address is `elena@math.utah.edu`.

Ian Eisenman is an associate professor of climate, atmospheric science, and physical oceanography at the Scripps Institution of Oceanography at the University of California San Diego. His email address is `eisenman@ucsd.edu`.

Daniel Feltham is a professor of climate physics at the University of Reading. His email address is `d.l.feltham@reading.ac.uk`.

Christopher Horvat is a NOAA Climate and Global Change Postdoctoral Fellow at the Institute at Brown for Environment and Society at Brown University. His email address is `christopher_horvat@brown.edu`.

Elizabeth Hunke is a deputy group leader, T-3 fluid dynamics and solid mechanics group at the Los Alamos National Laboratory. Her email address is `eclare@lanl.gov`.

Christopher Jones is a Bill Guthridge Distinguished Professor of Mathematics at the University of North Carolina, Chapel Hill. His email address is `ckrtj@unc.edu`.

Donald K. Perovich is a professor of engineering at the Thayer School of Engineering at Dartmouth College. His email address is `donald.k.perovich@dartmouth.edu`.

Pedro Ponte-Castañeda is a Raymond S. Markowitz Faculty Fellow and professor of mechanical engineering and applied mechanics and of mathematics at the University of Pennsylvania. His email address is `ponte@seas.upenn.edu`.

Courtenay Strong is an associate professor of atmospheric sciences at the University of Utah. His email address is `court.strong@utah.edu`.

Deborah Sulsky is a professor of mathematics and statistics and of mechanical engineering at the University of New Mexico. Her email address is `sulsky@math.unm.edu`.

Andrew J. Wells is an associate professor of physical climate science at the University of Oxford. His email address is `Andrew.Wells@physics.ox.ac.uk`.

Communicated by Notices *Associate Editor Reza Malek-Madani.*

For permission to reprint this article, please contact: `reprint-permission@ams.org`.

Newsjournal of the Society for Industrial and Applied Mathematics
sinews.siam.org

SIAM NEWS

Volume 53/ Issue 9
November 2020

Special Issue on the Mathematics of Planet Earth

*Read about the application of mathematics and computational science to issues concerning invasive populations, Arctic sea ice, insect flight, and more in this Planet Earth **special issue**!*

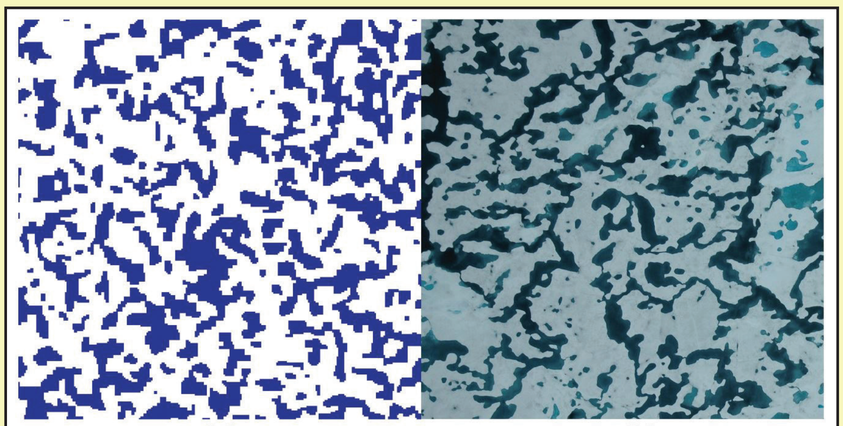

Figure 3. *Comparison of real Arctic melt ponds with metastable equilibria in our melt pond Ising model.* **3a.** *Ising model simulation.* **3b.** *Real melt pond photo. Figure 3a courtesy of Yiping Ma, 3b courtesy of Donald Perovich.*

Vast labyrinthine ponds on the surface of melting Arctic sea ice are key players in the polar climate system and upper ocean ecology. Researchers have adapted the Ising model, which was originally developed to understand magnetic materials, to study the geometry of meltwater's distribution over the sea ice surface. In an article on page 5, Kenneth Golden, Yiping Ma, Courtenay Strong, and Ivan Sudakov explore model predictions.

Controlling Invasive Populations in Rivers

By Yu Jin and Suzanne Lenhart

Flow regimes can change significantly over time and space and strongly impact all levels of river biodiversity, from the individual to the ecosystem. Invasive species in rivers—such as bighead and silver carp, as well as quagga and zebra mussels—continue to cause damage. Management of these species may include targeted adjustment of flow rates in rivers, based on recent research that examines the effects of river morphology and water flow on rivers' ecological statuses. While many previous methodologies rely on habitat suitability models or oversimplification of the hydrodynamics, few studies have focused on the integration of ecological dynamics into water flow assessments.

Earlier work yielded a hybrid modeling approach that directly links river hydrology with stream population models [3]. The hybrid model's hydrodynamic component is based on the water depth in a gradually varying river structure. The model derives the steady advective flow from this structure and relates it to flow features like water discharge, depth, velocity, cross-sectional area, bottom roughness, bottom slope, and gravitational acceleration. This approach facilitates both theoretical understanding and the generation of quantitative predictions, thus providing a way for scientists to analyze the effects of river fluctuations on population processes.

When a population spreads longitudinally in a one-dimensional (1D) river with spatial heterogeneities in habitat and temporal fluctuations in discharge, the resulting hydrodynamic population model is

$$N_t = -A_t(x,t)\frac{N}{A(x,t)} + \frac{1}{A(x,t)}\Big(D(x,t)A(x,t)N_x\Big)_x - \frac{Q(t)}{A(x,t)}N_x + rN\left(1-\frac{N}{K}\right)$$

$$\begin{aligned} N(0,t) &= 0 && \text{on } (0,T), x=0, \\ N_x(L,t) &= 0 && \text{on } (0,T), x=L, \\ N(x,0) &= N_0(x) && \text{on } (0,L), t=0 \end{aligned} \qquad (1)$$

See **Invasive Populations** *on page 4*

Modeling Resource Demands and Constraints for COVID-19 Intervention Strategies

By Erin C.S. Acquesta, Walt Beyeler, Pat Finley, Katherine Klise, Monear Makvandi, and Emma Stanislawski

As the world desperately attempts to control the spread of COVID-19, the need for a model that accounts for realistic trade-offs between time, resources, and corresponding epidemiological implications is apparent. Some early mathematical models of the outbreak compared trade-offs for non-pharmaceutical interventions [3], while others derived the necessary level of test coverage for case-based interventions [4] and demonstrated the value of prioritized testing for close contacts [7].

Isolated analyses provide valuable insights, but real-world intervention strategies are interconnected. Contact tracing is the lynchpin of infection control [6] and forms the basis of prioritized testing. Therefore, quantifying the effectiveness of contact tracing is crucial to understanding the real-life implications of disease control strategies.

Contact Tracing Demands

Contact tracers are skilled, culturally competent interviewers who apply their knowledge of disease and risk factors when notifying people who have come into contact with COVID-19-infected individuals. They also continue to monitor the situation after case investigations [1].

Case investigation consists of four steps:

1. Identify and notify cases
2. Interview cases
3. Locate and notify contacts
4. Monitor contacts.

Most health departments are implementing case investigation, contact identification, and quarantine to disrupt COVID-19 transmission. The timeliness of contact tracing is constrained by the length of the infectious period, the turn-around time for testing and result reporting, and the ability to successfully reach and interview patients and their contacts. The European Centre for Disease Prevention and Control approximates that contact tracers spend one to two hours conducting an interview [2]. Estimates regarding the timelines of other steps are limited to subject matter expert elicitation and can vary based on cases' access to phone service or willingness to participate in interviews.

Bounded Exponential

The fundamental structure of our model follows traditional susceptible-exposed-infected-recovered (SEIR) compartmental modeling [5]. We add an asymptomatic population A, a hospitalized population H, and disease-related deaths D, as well as corresponding quarantine states. We define the states $\{S_i, E_i, A_i, I_i, H, R, D\}_{i=0,1}$ for our compartments, such that $i=0$ and $i=1$ correspond to unquarantined and quarantined respectively. Rather than focus on the dynamics that are associated with the state transition diagram in Figure 1, we introduce a formulation for the real-time demands on contact tracers' time as a function of infection prevalence, while also respecting constraints on resources.

When the work that is required to investigate new cases and monitor existing contacts exceeds available resources, a backlog develops. To simulate this backlog, we introduce a new compartment C for tracking the dynamic states of cases:

$$\frac{dC}{dt} = [flow_{in}] - [flow_{out}].$$

Flow into the backlog compartment, represented by $[flow_{in}]$, reflects case identification that is associated with the following transitions in the model:

– The rate of random testing: $q_{rA}(t)A_0(t) \rightarrow A_1(t)$ and $q_{rI}(t)I_0(t) \rightarrow I_1(t)$

– Testing triggered by contact tracing: $q_{tA}(t)A_0(t) \rightarrow A_1(t)$, $q_{tI}(t)I_0(t) \rightarrow I_1(t)$, and $q_{tE}(t)E_1(t) \rightarrow \{A_1(t), I_1(t)\}$

– The population that was missed by the non-pharmaceutical interventions that require hospitalization: $\tau_{IH}(t)I_0(t) \rightarrow H(t)$.

Here, $q_{r*}(t)$ defines the time-dependent rate of random testing, $q_{t*}(t)$ signifies the time-dependent rate of testing that is triggered by contact tracing, and τ_{IH} is the inverse of the expected amount of time for which an infected individual is symptomatic before hospitalization. These terms collectively provide the simulated number of newly-identified positive COVID-19 cases. However, we also need the average number of contacts per case. We thus define function $\mathcal{K}(\kappa, T_S, \phi_\kappa)$ that depends on the average number of contacts a day (κ), the average number of days for which an individual is infectious before going into isolation (T_S), and the likelihood that the individual

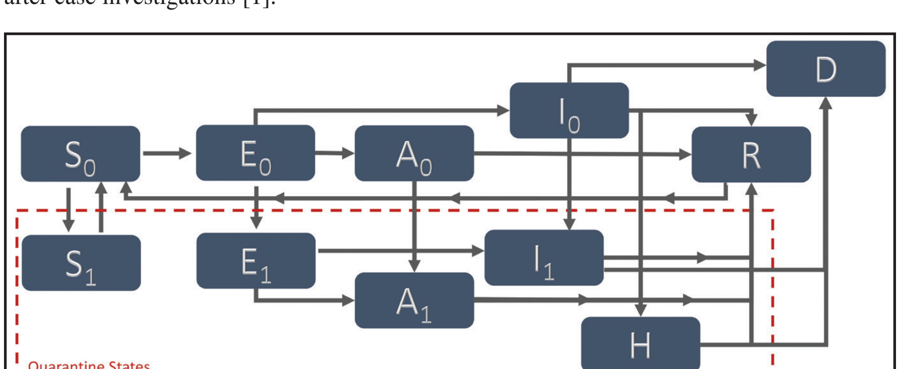

Figure 1. *Disease state diagram for the compartmental infectious disease model. Figure courtesy of the authors.*

See **COVID-19 Intervention** *on page 3*

Nonprofit Org
U.S. Postage
PAID
Permit No 360
Bellmawr, NJ

SIAM
SOCIETY for INDUSTRIAL and APPLIED MATHEMATICS
3600 Market Street, 6th Floor
Philadelphia, PA 19104-2688 USA

Two Layer Models and Effective Rheological Parameters

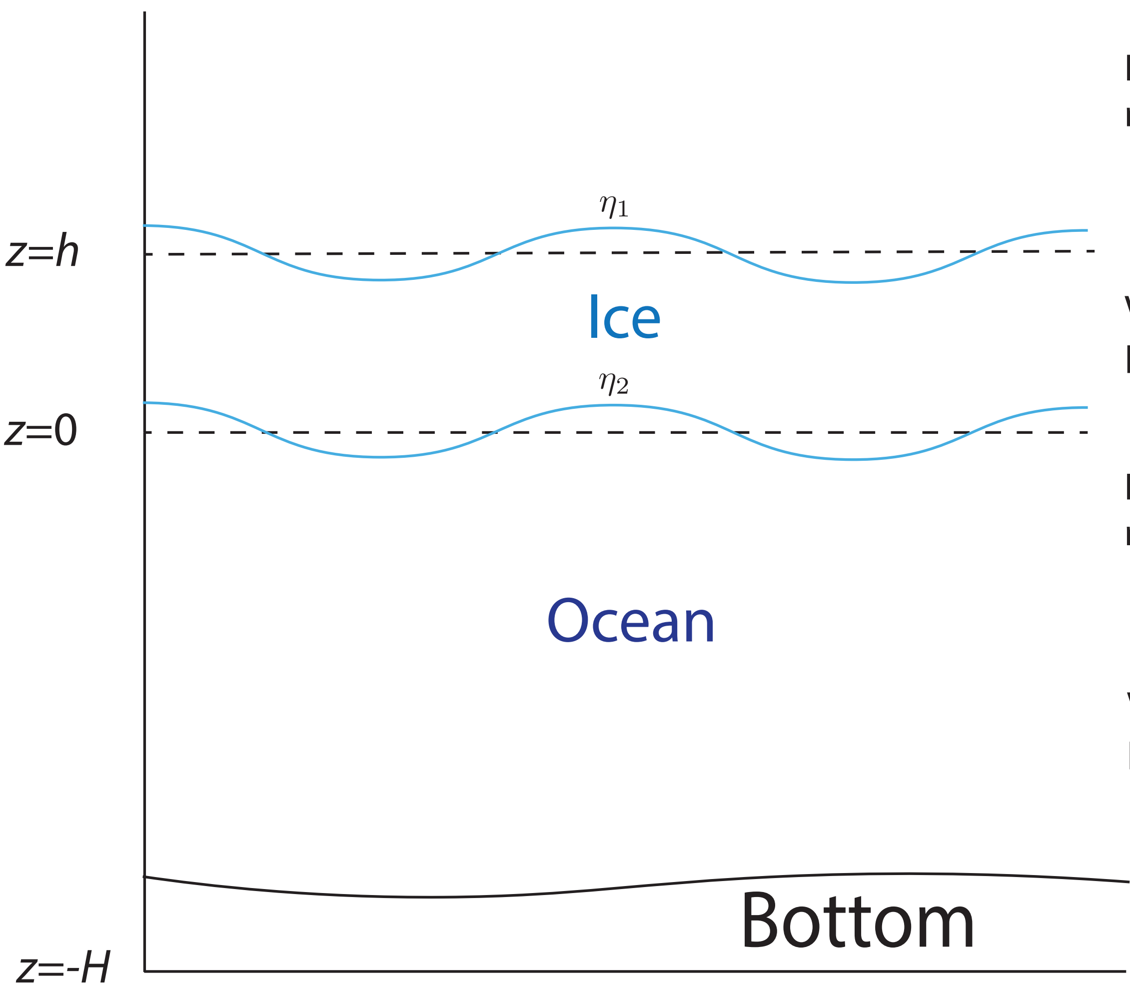

G shear modulus P pressure ω angular frequency U velocity field

ν viscosity λ Poission ratio ρ density g gravity

Viscous fluid layer (Keller 1998)

E˜ ective Viscosity $\boxed{\nu}$

Equations of motion:

$$\frac{\partial U}{\partial t} = -\frac{1}{\rho}\nabla P + \nu \nabla^2 U + g$$

Viscoelastic fluid layer (Wang-Shen 2010)

E˜ ective Complex Viscosity $\boxed{\nu_e = \nu + iG/\rho\omega}$

Equations of motion

$$\frac{\partial U}{\partial t} = -\frac{1}{\rho}\nabla P + \nu_e \nabla^2 U + g$$

Viscoelastic thin beam (Mosig *et al.* 2015)

E˜ ective Complex Shear Modulus $\boxed{G_v = G - i\omega\rho\nu}$

Stieltjes integral representation for effective complex viscoelastic parameter; bounds

Sampson, Murphy, Cherkaev, Golden 2019

Homogenization for two phase viscoelastic composite

$\nu_1 = 10^7 + i\,4875$ **pancake ice**

$\nu_2 = 5 + i\,0.0975$ **slush / frazil**

microscale $\sigma = C_{ijkl}\epsilon_{kl} = C : \epsilon$

$$C = 2(\chi_1\nu_1 + \chi_2\nu_2)\Lambda_s$$

macroscale $\langle\sigma\rangle = C^* : \langle\epsilon\rangle$

$$\langle\epsilon\rangle = \epsilon^0$$

quasistatic assumption $\nabla \cdot \sigma = 0$

Strain Field

$$\epsilon = \frac{1}{2}[\nabla u + (\nabla u)^T] = \nabla^s u \quad \nabla \cdot u = 0$$

Resolvent

$$\epsilon = \left(1 - \frac{1}{s}\Gamma\chi_1\right)^{-1}\epsilon^0 \;\Rightarrow\; \boxed{\frac{\nu^*}{\nu_2} = \left(1 - \|\epsilon^0\|^{-2} F(s)\right)}$$

$$F(s) = \int_0^1 \frac{d\mu(\lambda)}{s - \lambda} \qquad s = \frac{1}{1 - \frac{\nu_1}{\nu_2}}$$

$$\Gamma = \nabla^s(\nabla \cdot \nabla^s)^{-1}\nabla\,\cdot$$

Model Approximations

Floes $\approx$ Discs

Forces on Disc $= \quad F_{drag} + F_{collision}$

A. Herman ***Physical Review E*** **2011**

Floe-Floe Interactions: Linear Elastic Collisions

$F_{collision}$ follows Hooke's Law.

Advective Forcing: Passive, Linear Drag Law

v is the advective velocity field.

F_{drag} is proportional to relative velocity.

Ice Pack Characteristics

ϕ = sea ice concentration (floe area fraction)

Power Law Size Distribution: $N(D) \sim D^{-k}$

T. Toyota, S. Takatsuji, M. Nakayama Geophysical Review Letters 2006

k = floe diameter exponent

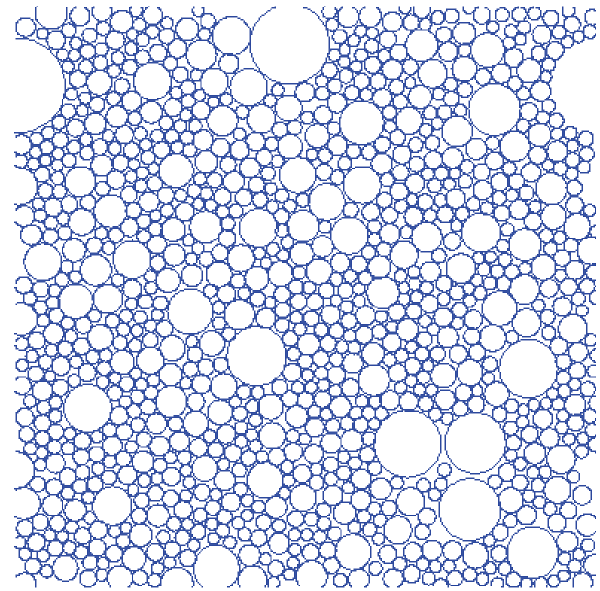

$k = 2.9$, $\phi = 0.8$

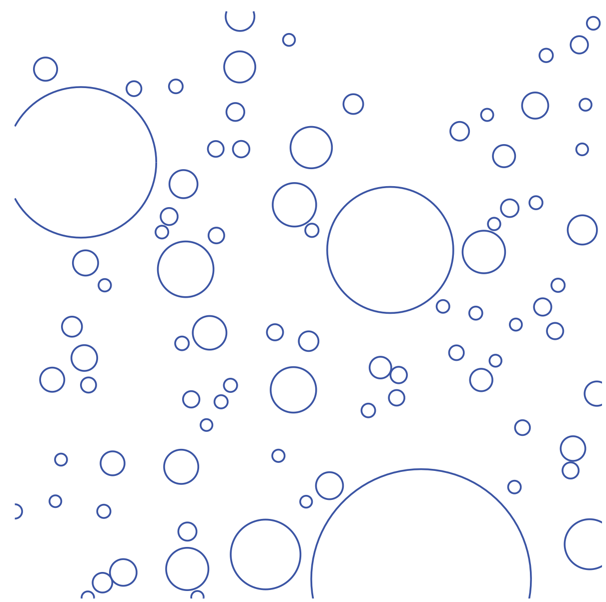

$k = 1.7$, $\phi = 0.1$

Model Results

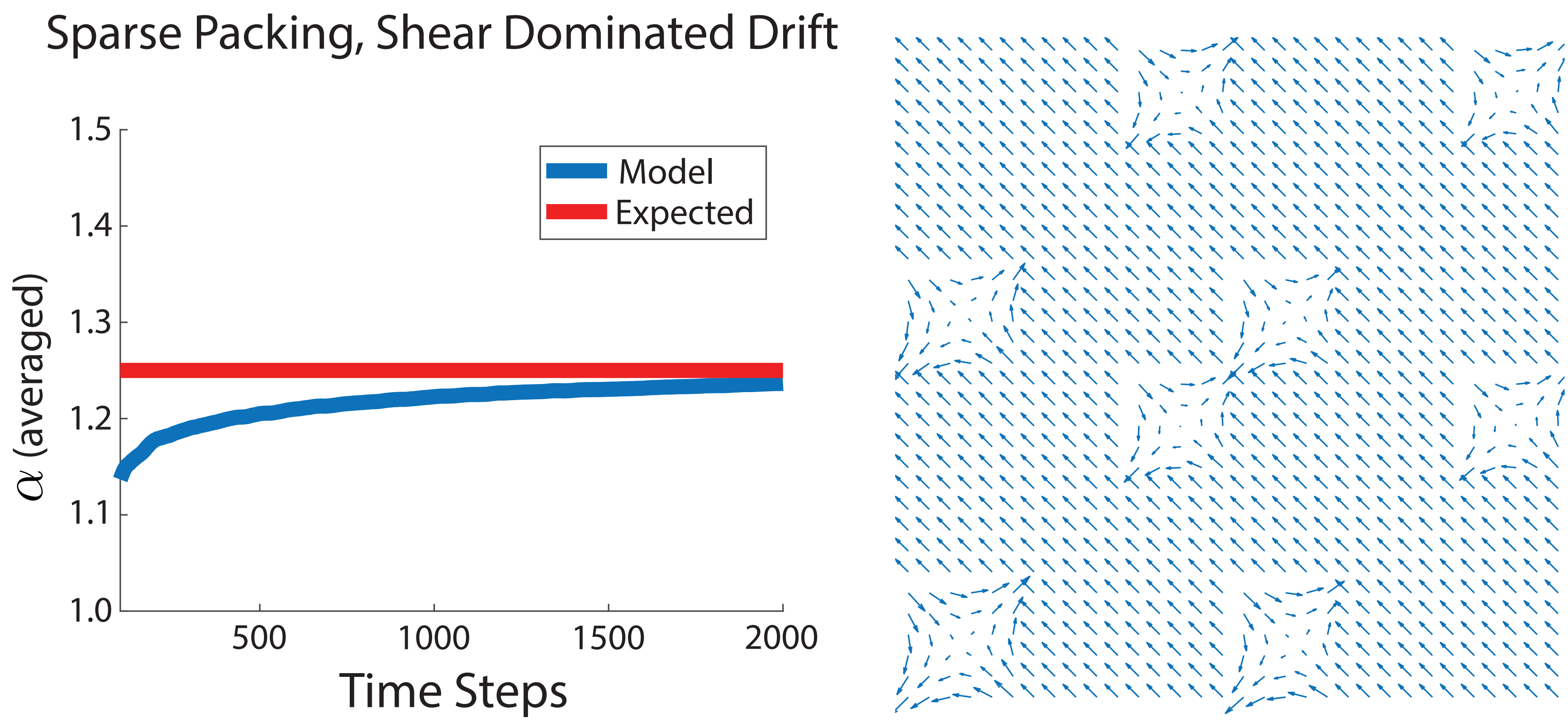

$$\text{Expected } \alpha = 5/4$$

k = 2.9 Concentration = 0.3